

# **The Upper Jurassic shallow marine siliciclastic-carbonate deposits in the North German Basin**

Dissertation

with the aim of achieving a doctoral degree

at the Faculty of Mathematics, Informatics and Natural Sciences

Department of Geology

of Universität Hamburg

submitted by

**Huaqing Bai**

from

China

Hamburg

2017



## **Eidesstattliche Versicherung**

### **Declaration on oath**

Hiermit erkläre ich an Eides statt, dass ich die vorliegende Dissertationsschrift selbst verfasst und keine anderen als die angegebenen Quellen und Hilfsmittel benutzt habe.

I hereby declare, on oath, that I have written the present dissertation by my own and have not used other than the acknowledged resources and aids.

Hamburg, den

Unterschrift

Day of oral defense: 17.10.2017

The following evaluators recommend the admission of the dissertation:

Prof. Dr. Christian Betzler

Prof. Dr. Gerhard Schmiedl



## Abstract

This thesis aims to establish the sequence stratigraphic framework of the Upper Jurassic deposits in the North German Basin, which makes a sequence stratigraphic correlation a possible supplement to the limited biostratigraphic correlation in this area. This study also aims to reveal the paleoclimate control on the evolution of the sequences, as well as to decipher how the diagenetic processes were affected by the sequence stratigraphy and facies evolution. To achieve these goals, the Eulenflucht-1 core drilled in Süntel Mountains and the Wendhausen-6 core drilled in Hildesheimer Wald were studied by core description, microfacies analysis, isotopic and element analysis, and cathodoluminescence imaging.

The Upper Jurassic deposits in the North German Basin consist of a mixture of siliciclastic and carbonate deposits. Thirteen facies were identified in the Eulenflucht-1 core and were interpreted to be deposited in a carbonate ramp ranging from the outer ramp into the restricted lagoon. Eight facies were identified in the Wendhausen-6 core and were considered to be deposited in a transition area between a delta setting and a carbonate ramp. Sequences of three different hierarchies were recognized both in the Eulenflucht-1 core and the Wendhausen-6 core. Small-scale sequences were delineated by the changes in grain size, variations in the amount of components, fluctuations of the matrix content, and the vertical facies stacking patterns. Medium-scale sequences were identified by the changes in facies combinations of the constituent small-scale sequences, and were confined by the distinctive hardgrounds or exposure surfaces, characterized by the occurrence of iron minerals or lowstand channel-fill sandstones. Sequence stratigraphic correlation across the North German Basin of the Korallenoolith Formation was achieved at the medium-scale sequence level, as some of the medium-scale sequence boundaries are basin-wide traceable. Large-scale sequences were differentiated by the facies proportion statistics in the distinct medium-scale sequences, which mirror the relative sea-level fluctuations. The shallowing trend in the Lower and Middle Oxfordian deposits is consistent with that of the global sea-level change during the Early and Middle Oxfordian age. But the continuous shallowing trend from the Late Oxfordian to the Tithonian age in the Eulenflucht-1 core, is in contrast with the global sea-level rise during that time, and is considered due to the local uplifting tectonic movement.

Specific facies are indicators of specific paleoclimate to some extent, e.g., ooid grainstone and coral boundstone are indicators of warm climate. Therefore, the large-scale sequences, documented by the facies statistic curves recording facies changes, were postulated to be

controlled by regional climate. The warm period during the Middle Oxfordian and Late Kimmeridgian was recorded by the development of the ooid grainstone and coral boundstone facies. This is also recorded by the carbon isotopic and the Mg/Ca data. The stable carbon isotope variations of the Eulenflucht-1 core were well correlated with those of the other European Basins, which were interpreted as a result of climate change during the Late Jurassic to Early Cretaceous. In-phase variations of the facies statistic curve and  $\delta^{13}\text{C}$  curve manifest the climate control on the large-scale sequences. The high paleotemperatures during the Middle Oxfordian and Late Kimmeridgian time were also documented by the positive excursion of the Mg/Ca curves detected from the well-preserved oyster shells, which also evidence the climate control on the deposits at that time.

Facies and sequence stratigraphy framework have a great control on the development of diagenesis processes. Diagenetic elements with different optical characteristics under polarized and cathodoluminescence microscopes were logged in the Eulenflucht-1 core. Cement with twin crystals or poikilotopic fabrics and non-luminescence implies late burial diagenesis. It is constrained in the facies with grain-supported texture, e.g., ooid grainstone and coral boundstone, which is resistant to compaction and can provide good water circulation for the formation of the deep burial cement. Micrite rims composed of microcrystalline calcite with dull luminescence represent the marine to early diagenetic products, whereas cement with equant or blocky morphologies and sub-bright to bright luminescence indicate meteoric phreatic or early burial diagenesis. These cement are observed throughout the Eulenflucht-1 core, and not constrained to any specific facies. Dolomite with euhedral to sub-euhedral morphologies and dull to no luminescence is of marine to deep burial diagenetic origin. The dolomite in wackestone or mudstone deposited under the storm wave base is related to bacterial induced sulfate reduction, whereas the dolomite constrained in the ooid grainstone and oyster-serpulid rudstone deposited around the fair weather wave base is precipitated from the mixture of meteoric and marine water in the vicinity of sequences boundaries. Another diagenetic element associated with sequence boundary is microkarst.

## Zusammenfassung

Die Aufgabe dieser Dissertation ist die Etablierung einer sequenzstratigrafischen Einordnung für die ober-jurassischen Ablagerungen des norddeutschen Beckens, welche eine mögliche Ergänzung zur limitierten biostratigrafischen Korrelation in diesem Gebiet darstellt. Die Studie zeigt die paläoklimatische Kontrolle auf die Sequenzevolution als auch wie die Sequenzstratigrafie und die Fazies-Evolution durch die diagenetische Prozesse beeinflusst wurden. Um diese Ziele zu erreichen, wurden die Kerne Eulenflucht-1 aus dem Süntel Gebirge und Wendhausen-6 aus dem Hildesheimer Wald mittels Kernansprache, Mikrofaziesanalyse, Isotopenanalyse, Elementanalyse und Kathodolumineszenz untersucht.

Die Ablagerungen des Oberjura im norddeutschen Becken bestehen aus siliziklastischen und karbonatischen Ablagerungen, gebildet auf einer flachmarinen Karbonatrampe, welche Ablagerungsräume von der äußeren Rampe bis zu einer hypersalinen Lagune umfasst. Dreizehn Fazies wurden in Eulenflucht-1 und acht in Wendhausen-6 definiert. Kleinskalige Sequenzen wurden durch Korngrößenwechsel, Änderungen im Komponentenverhältnis, Fluktuationen im Matrixgehalt und im vertikalen Fazies-Muster definiert. Autozyklische Prozesse verursachten Migration von Nebenarmen im Pro-Delta Bereich welche in die Entwicklung der kleinskaligen Sequenzen involviert sind. Mittelskalige Sequenzen wurden durch Änderungen in den Fazieskombinationen der einzelnen kleinskaligen Sequenzen definiert. Diese Sequenzen werden begrenzt durch Hartgründe und Freilegungsflächen, welche durch die Anreicherung mit Eisenmineralen oder die Rinnenfüllung charakterisiert sind. Die sequenzstratigraphische Korrelation des Korallenooliths im norddeutschen Becken gelang über die mittelskaligen Sequenzen und die beckenweite Verfolgung der Sequenzgrenzen. Großskalige Sequenzen wurden abgegrenzt durch die statistischen Faziesanteile in den mittelskaligen Sequenzen. Sie spiegeln die Fluktuationen des relativen Meeresspiegels wieder. Ein gefundener Meeresspiegelabfall in den untersuchten Ablagerungen des Unter- und Mitteloxfordiums folgt den Tendenzen des globalen Meeresspiegels. Allerdings, widerspricht der in Eulenflucht-1 gefunden Meeresspiegelabfall den Meeresspiegeldaten für den Zeitraum des Spät-Oxfordiums bis Tithonium und wird als lokale tektonische Hebung interpretiert.

Bestimmte Fazies sind Indikatoren für spezifische paläoklimatische Veränderungen, z.B. Ooid-grainstone und Korallen-Boundstone zeigen ein warmes Klima an. Somit, dokumentieren die Faziesstatistiken und Fazieswechsel der großskaligen Sequenzen das

regionale Klima. Warmphasen ereigneten sich während des Mittel-Oxfordiums und des späten Kimmeridgiums. Kaltphasen ereigneten sich vom Spät-Oxfordium bis zum frühen Kimmeridgium und vom späten Kimmeridgium bis zum Tithonium. Diese Interpretation wird gestützt durch die Karbonat-Isotopie und Mg/Ca Verhältnisse. Die stabilen Karbonat Isotopie im Kern Eulenflucht-1 korreliert sehr gut mit den Daten anderer europäischer Becken, die als Ergebnis klimatischer Veränderungen zwischen dem Spätjura und der Kreide interpretiert werden. Die Phasen-Variationen der Faziesstatistik-Kurven und der  $\delta^{13}\text{C}$  Kurve zeigen deutlich eine klimatische Kontrolle der großskaligen Sequenzen. Die hohen Temperaturen und die klimatische Kontrolle der Ablagerungen während des mittleren Oxfordiums und späten Kimmeridgiums werden auch durch die Mg/Ca Werte von Austernschalen bestätigt.

Die Entwicklung der Fazies und Sequenzstratigraphie kontrollierten die diagenetischen Prozesse. Diagenetische Elemente mit unterschiedlichen optischen Eigenschaften unter polarisiertem und Kathodolumineszenz wurden für den Kern Eulenflucht-1 analysiert. Verwilligte Zemente und poikiltopischen Strukturen und eine nicht vorhandene Lumineszenz weisen auf eine späte Versenkungsdiagenese hin. Grobe Zemente mit mittlerer oder heller Lumineszenz implizieren eine meteorisch/phreatische oder frühe Versenkungsdiagenese. Diese verschiedenen Zemente wurden im gesamten Kern Eulenflucht-1 gefunden und sind nicht an eine spezielle Fazies gebunden. Dolomit mit idiomorpher bis sub-idiomorpher Ausbildung und matter bis nicht vorhandene Lumineszenz ist ein Produkt der marinen bis späten Versenkungsdiagenese. Der Dolomit gefunden in Wackestone oder Mudstone wurde unterhalb der Sturmwellenbasis durch Sulfat-reduzierende Bakterien gebildet. Der Dolomit im Ooid-Grainstone und Austern-Serpulid-Rudstone wurde wahrscheinlich unterhalb der Schönwetterwellenbasis durch die Mischung von meteorischen und marinen Wässern in der Nähe der Sequenzgrenzen gebildet. Ein weiteres diagenetisches Element entlang der Sequenzgrenzen ist Mikrokarst.

## Acknowledgement

First of all, I would like to express my sincere gratitude to my supervisor Prof. Dr. Christian Betzler, who gave me the opportunity to pursue my PhD degree in Germany, an amazing country nearly ten thousand kilometers away from China. It was also him who brought me into the carbonate world. During my challenging PhD adventure, he always gave important and helpful suggestions about the research directions and push me forward, especially when I was confused and got stuck in my research. I also thank him for the heaps of times discussions about my text and figures, for his tolerance of the mistakes I made in my written English, and especially for his countless explanations about fossils beside the microscope. Furthermore, I would like to thank him for giving me the chance to participate the field cruise in Spain, where I got valuable experience in field works and shared a wonderful time with my German colleagues.

I sincerely thank Dr. Jochen Erbacher, who gave great support during the core description and the isotopic data collecting processes. He is thanked also for providing so many significant suggestions to my research, and especially for his patient revision and correction of the second chapter of this thesis. Thomas Wiese from LBEG Hannover is thanked for the help during the core description process.

I truly thank Dr. Sebastian Lindhorst, for his help about using softwares, for the smart suggestions about making figures, and especially for his patient explanations in the field trips in Spain and in the North Sea. I would also like to extend my special thanks to him for his help when I started my life in Hamburg.

I would like to extend my sincere thank to Prof. Dr. Wenhui Huang of China University of Geosciences (Beijing) for his great support for the in-situ elements measurement in Beijing. Thank you also for encouraging me to pursue my PhD degree abroad, and introduce my supervisor Prof. Dr. Christian Betzler to me.

My colleagues and friends in the Institute of Geology are thanked for their help from all aspects of my research and life. Dr. Jesus Reolid, I thank you for your help about the core description and facies analysis. Dr. Juliane Ludwig, my roommate and closest friend, thanks a lot for helping with all the issues associated with German language. With your accompany, life in the office was not boring, and in all the happy and tough days, I never feel alone. I will always remember the fascinating coffee smell came out of your various simple coffee

machines every noon. Marco Wunsch, I thank you for your help in German issues, especially for translating the abstract of this thesis into German. I also thank you for solving the software problems I met in the computer room. Khurram Shahyad, thank you for informing me many events in Piasta and always sharing with me the information about research and some other news in the life. Dr. Andrei Ernst, thank you for sharing so many amazing photos of Australia, I am impressed and enjoyed myself when I saw them. Feng Wu and Benjun Ma, my two colleges come from China, bring me a lot of happy time and ease my homesick. It was always happy with you two, no matter discuss science or eat and travel outside. Jesus, Marco, Khurram, and Feng Wu are thanked for the proof-reading of my thesis, and for all the discussions about the problems of my thesis.

Annemarie Gerhard is thanked for her help in lots of aspects when I started my life in Hamburg and for her support in lots of paper works during my PhD. Dirk Eggers are thanked for his help with the logistic works.

Dr. Martin Clark, I thank you for doing the English proof-reading of my paper and other text several times. I enjoy all the Sunday afternoons playing table tennis with you. Thank you for your accompany. Dr. Macr Theodor is thanked for the help in covering my thin sections with carbon.

Jutta Richarz and Eva Vinx are thanked for their contributions in the laboratory, including in the procedures of making thin sections, grinding samples, photographing thin sections, and measuring the carbonate contents. Thanks a lot for your help.

Fanfan Zuo of Leibniz Universität Hannover is thanked for the help during the description of the Wendhausen-6 core. She is also thanked for the delicious food provided in her home. The time we shared during the EGU meeting in Wien is impressive to me, thank you for your accompany.

I would like to say thank you to my mother. Thank you for your years of support in distance at home, and for coming to Germany to accompany me twice. I am proud of the great effort you made to learn English, in order to get used to the life in Germany. I love you!

Finally, I would like to thank the Chinese Scholarship Council to give the financial support for my PhD life.

# Table of Contents

<i>Abstract</i> .....	3
<i>Zusammenfassung</i> .....	5
<i>Acknowledgement</i> .....	7
<b>1. Chapter I Introduction</b> .....	<b>11</b>
1.1 Aim of this study .....	13
1.2 The study area .....	13
1.3 Outline of the thesis.....	15
<b>2. Chapter II Sequence stratigraphy of Upper Jurassic deposits in the North German Basin (Lower Saxony, Süntel Mountains)</b> .....	<b>17</b>
2.1 Introduction .....	18
2.2 Geological setting.....	19
2.3 Material and methods .....	21
2.4 Results .....	22
2.4.1 Facies description.....	22
2.4.2 Carbon isotopes .....	30
2.5 Discussion .....	31
2.5.1 Depositional environments interpretation .....	31
2.5.2 Sequence analysis.....	35
2.5.3 Stratigraphic correlation .....	39
2.5.4 Controlling factors of the large-scale sequence evolution.....	41
2.5 Conclusions .....	42
<b>3. Chapter III Sequence stratigraphy of the Upper Jurassic mixed siliciclastic-carbonate deposits in the North German Basin</b> .....	<b>45</b>
3.1 Introduction .....	46
3.2 Geological setting.....	47
3.3 Material and methods .....	49
3.4 Results .....	50
3.4.1 Facies description.....	50
3.4.2 Mg/Ca data .....	56
3.5 Discussion .....	57

3.5.1 Facies model interpretation .....	57
3.5.2 Sequence analysis.....	61
3.5.3 Climate control on the sequences evolution.....	64
3.5.4 Sequence stratigraphic correlation .....	65
3.6 Conclusion.....	68
<b>4. Chapter IV Diagenetic processes in the Upper Jurassic deposits in the North German Basin (Lower Saxony, Süntel Mountains).....</b>	<b>71</b>
4.1 Introduction .....	72
4.2 Geological setting.....	73
4.3 Methods .....	74
4.4 Results .....	76
4.5 Discussion .....	79
4.5.1 Diagenetic processes .....	79
4.5.2 Diagenetic zones.....	84
4.6 Conclusion.....	84
<b>5. Chapter V Conclusions .....</b>	<b>87</b>
<b>References .....</b>	<b>91</b>



# Chapter I

## **Introduction**

The North German Basin, as the most important basin for oil and gas production in Germany (Ferdani, 2006), is of great interest to sedimentologists, paleontologists, and petroleum geologists. The high-frequency sequence stratigraphy was applied in this area to characterize the hydrocarbon reservoirs in Zechstein Limestone, Upper Permian (Betzler and Pawellek, 2014; Füchtbauer, 1968; Richter-Bernburg, 1985; Strohenger and Strauss, 1996). The reconstruction of ancient sedimentary environments, understanding of processes controlling their evolution, and the correlation of the stratigraphic units play important role in predicting facies distribution and sequence development. As to the Upper Jurassic succession, facies and sequence stratigraphic analysis have been conducted, but are constrained in the Oxfordian and Lower Kimmeridgian deposits (Betzler et al., 2000; Cäsar, 2012; Kästner et al., 2010). Biostratigraphic analysis relied on ammonites, ostracods, dinoflagellate cysts, charophytes, and spores and pollen in the North German Basin (Gramann et al., 1997; Hardenbol et al., 1998; Schudack, 1994; Schulze, 1975; Weiss, 1995). However, these fossils are scarce in the Oxfordian deposits and the biostratigraphic correlation for the Oxfordian age is hindered. Therefore, the focus of this study is to establish a relatively complete sequence stratigraphic framework, which can serve as a correlation reference. This study also aims to prove the regional paleoclimate control on the development of the sequence stratigraphy, which provides a base to do the sequence stratigraphic correlation in a regional scale.

Successful sequence stratigraphic correlations for the Oxfordian and Kimmeridgian deposits were conducted in SW Germany, Switzerland, Spain, Scotland, and France. The recognized medium-scale sequences in these areas are proved to allow the comparison of facies evolution in regions that are up to 1000 km apart (Gygi, 2000; Gygi et al., 1998; Jank et al., 2006; Pittet and Strasser, 1998; Ruf et al., 2005a; Samankassou et al., 2003; Strasser et al., 1999, 2000). The sequence stratigraphy hierarchies of the Swiss Jura, Spain, and northeast France are asserted to be paleoclimate induced (Pittet and Strasser, 1998; Strasser et al., 2000). This proves the possibility and validity of using sequence stratigraphy to do regional correlations.

Paleoclimate variations during the Late Jurassic time are widely interpreted based on the oxygen isotopic data, the Mg/Ca data, the palynomorphs, and the sporomorphs (Abbink et al., 2001; Nunn and Price, 2010; Price and Rogov, 2009). For these methods, well-preserved foraminifer, brachiopods, palynomorphs, and sporomorphs are needed to be selected out of the bulk sediments. The development of the Laser Ablation Inductively-Coupled Plasma Mass Spectrometry (LA-ICP-MS) shed light on in-situ element analysis for the solid core samples (Christensen et al., 1995; Yang et al., 2009; 2014). In-situ analysis of the Mg/Ca

ratios on the well-preserved oyster shells, was proved to be an effective paleotemperature proxy (Bailey et al., 2003; Klein et al., 1996; Nunn and Price, 2010). Thus, the in-situ analyzed Mg/Ca ratio was used to figure out the paleoclimate variations during the Late Jurassic time in the North German Basin.

Facies, sequence stratigraphy, and paleoclimate conditions in deltaic, coastal, and shallow marine deposits, are reported to have an impact on early diagenesis (Ketzer, 2002; Morad et al., 2000; South and Talbot, 2000; Tucker, 1993; Worden and Morad, 2003). Relative sea-level changes can affect deep burial diagenesis via changing near-surface chemical conditions and the propagation of heat into the subsurface (Worden et al., 2000). In this way, recognized diagenetic products can help to interpret facies and sequence stratigraphic evolution. Thus, the attempt to analyze diagenetic processes in the Eulenflucht-1 core and to associate certain diagenesis product to a specific facies assemblage or a specific sequence stratigraphic position is conducted in this study.

### **1.1 Aim of this study**

The aim of this study is to establish a relatively complete sequence stratigraphic framework covering the deposits from the Oxfordian to the Tithonian age, and to make a sequences stratigraphic correlation possible. This sequence stratigraphic correlation is supposed to serve as a supplement to the biostratigraphic correlation, which is hindered by the scarcity of index fossils during the Oxfordian age. The factors controlling the evolution of the sequence stratigraphy are expected to be deciphered, such as paleoclimate and sea-level fluctuations. Another goal of this thesis is to clarify how the diagenesis was affected by the facies distribution and sequence stratigraphic evolution. The identified diagenetic products that linked to a certain facies assemblage and a specific sequence stratigraphic position can help sequence stratigraphic division in reverse.

### **1.2 The study area**

During the Late Jurassic, the North German Basin was bounded by the Ringkobing Fyn High to the north, and by the London Brabant, the Rhenish and the Bohemian Massifs to the south (Fig. 1.1). The target unit, Upper Jurassic succession, cropped out to the south of Hannover in the Wiehengebirge, Wesergebirge, Süntel Mountains, Ith Mountains, and in the Hildesheimer Wald. The researched Eulenflucht-1 core (52.18227418° N, 9.4002145° E) and Wendhausen-6 core (52.122721°N, 10.072847°E) located in the Süntel Mountains and the Hildesheimer Wald respectively (Fig. 1.2).

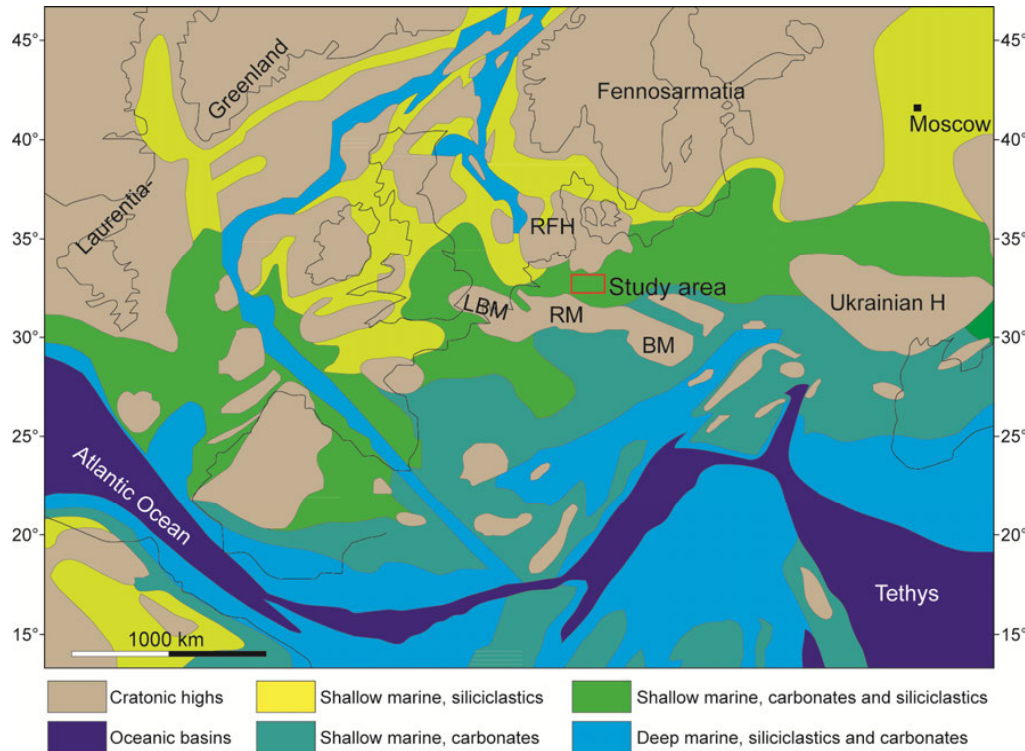


**Fig. 1.1** Late Jurassic paleogeography and main sediment associations in northern central Europe. LMB London-Brabant Massif, RM Rhenish Massif, BM Bohemian Massif, RFH Ringkobing Fyn High (modified from Ziegler, 1990; Thierry, 2000)

During the Late Jurassic time, the initial salt domes and pillows of the North German Basin reached their diapir stage (Mönnig, 2005), and the differential subsidence of the North German Basin controlled by syn-sedimentary faults began at that time (Betz et al. 1987; Gramann et al. 1997; Hoyer 1965). The basin was divided into a series of subdued relief structural highs and lows, and the thickness of the deposits varies by tens of meters over relatively short distance because of the differential subsidence (Hoyer, 1965).

The researched Upper Jurassic deposits covers the lithological units of the Upper Ornatenton Formation (Callovian), Heersumer and Korallenoolith Fms (Oxfordian), the Süntel Fm (Kimmeridgian), and the Holzen and Eimbeckhausen Fms (Tithonian). The Ornatenton Fm is composed of marls (Heunisch and Luppold, 2015). The Heersumer Fm consists of bioturbated marlstone rich in sponge spicules with part of the matrix dolomitized (Bai et al., 2017; Kästner et al., 2008). The Korallenoolith Fm is a diachronous unit encompassing oolite and coral buildups (Betzler et al., 2007; Cäsar, 2012; Helm, 1998, 2005; Helm et al., 2003; Helm and Schülke, 2006; Kästner et al., 2008; Schultz, 1975). The *Florigemma*-bank situated in the middle part of the Korallenoolith Fm contains species-rich coral associations. Its top boundary is an erosional unconformity that can be traced over a lateral extent of several hundred meters (Helm, 2005). To the northwest and west of the Lower Saxony Basin, the siliciclastic content of the deposits above the *Florigemma*-bank

increases (Kästner et al., 2008; Mönnig, 2005). Deposits of the Süntel Fm were described as alternations of glauconitic marl, limestone and sandstone (Klassen, 2003; Mönnig, 2005). The Holzen Fm consists of alternations of clay, marl and limestone, and the Eimbeckhausen Fm is dominated by gypsum and anhydrite (Heunisch and Luppold, 2015).

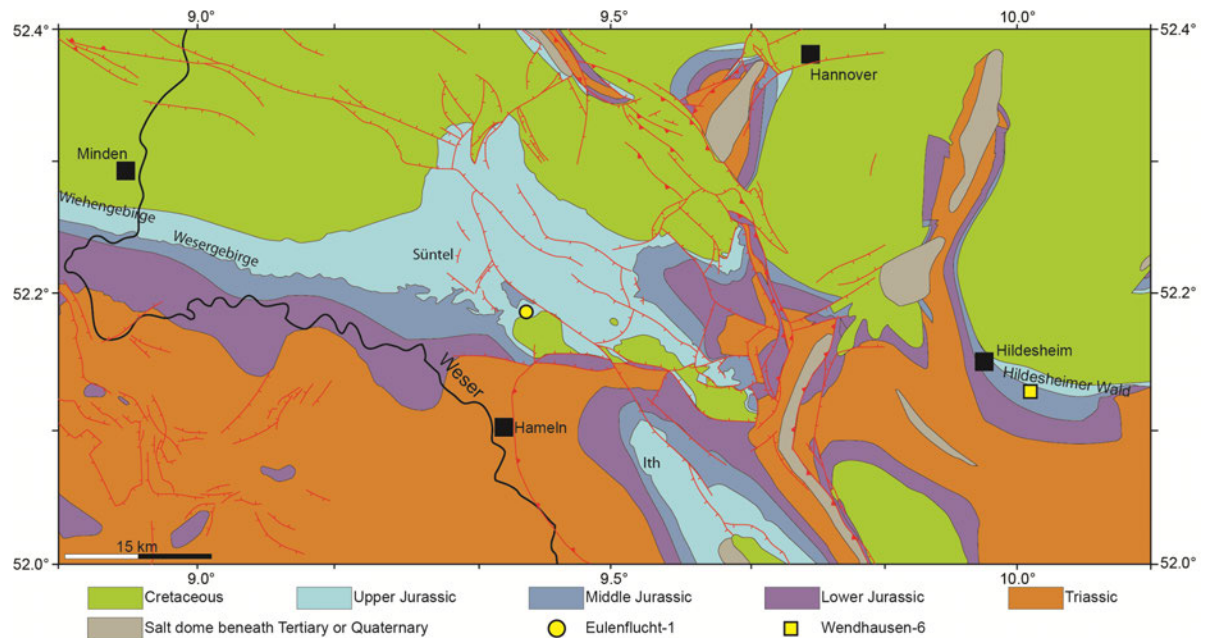


**Fig. 1.2** Geological map of the study area with the locations of the Eulenflucht-1 core and the Wendhausen-6 core (modified from Kockel et al., 1996)

### 1.3 Outline of the thesis

This thesis is subdivided into five chapters. Chapter I is the introduction of the thesis.

Chapter II focuses on the Upper Jurassic deposits of the Eulenflucht-1 core located in the Süntel Mountains. These deposits are considered to be deposited in a carbonate ramp ranging from the outer ramp into the restricted lagoon. A sequence stratigraphic framework of three hierarchies were constructed in this chapter. The climate control on the large-scale sequence stratigraphic evolution was clarified, and the decrease in the accommodation/sediment supply from the Oxfordian to Tithonian age was ascribed to the local uplift movement rather than sea-level fluctuations. This chapter was published as "Sequence stratigraphy of Upper Jurassic deposits in the North German Basin (Lower Saxony, Süntel Mountains)" in *Facies* (2017), volume 63.

Chapter III focuses on the Upper Jurassic deposits of the Wendhausen-6 core located in the Hildesheimer Wald. The Wendhausen-6 succession is supposed to be deposited in the transition area between a delta setting and a carbonate ramp. Sequence stratigraphy of three

hierarchies were also established. The climate control on the large-scale sequence evolution deciphered in chapter II was also unraveled in the Wendhausen-6 core, and is backed up by the paleoclimate variations reflected by the Mg/Ca data from both the Eulenflucht-1 core and the Wendhausen-6 core.

Chapter IV is about the impacts of the facies distribution and sequence stratigraphy evolution on the diagenetic processes. Facies with grain-supported texture, e.g., ooid grainstone and coral boundstone, favor the development of deep burial diagenetic cement. Dolomite in the ooid grainstone and oyster-serpulid rudstone, as well as microkarsts are the diagenetic products associated with sequence boundaries.

Chapter V presents the conclusions of this study.

## Chapter II

# Sequence stratigraphy of Upper Jurassic deposits in the North German Basin (Lower Saxony, Süntel Mountains)

### Abstract

A core recovered in the North German Basin at the locality of Eulenflucht in the Süntel Mountains, 30 km SW of Hannover, Germany, is interpreted in terms of Oxfordian to Kimmeridgian sequence stratigraphy of this basin. Thirteen different facies are recognized which record the evolution of an outer ramp into a restricted hypersaline lagoon. Changes in grain size, variations in the amount of components, fluctuations of the matrix content and of the microscopic texture, as well as vertical lithofacies stacking patterns, were integrated to define small-scale sequences. Medium-scale sequences were identified by changes in facies combinations of the constituent small-scale sequences. Large-scale sequences were differentiated by facies proportion statistics in the distinct medium-scale sequences. This allows the complete sequence stratigraphic subdivision of the Oxfordian and Kimmeridgian succession to be interpreted. The stable carbon isotopic composition of bulk samples enables a correlation with chemostratigraphic records found elsewhere. This result is supported by an ostracod biostratigraphy that allows a chronostratigraphic assignment of the succession. The large-scale sequences were controlled by climate and local tectonic movements. It is proposed that a long-term shallowing trend during the Kimmeridgian time was induced by regional uplift.

This chapter is based on **Bai, H.Q., Betzler, C., Erbacher, J., Reolid, J., Zuo, F.F.**, 2017. Sequence stratigraphy of Upper Jurassic deposits in the North German Basin (Lower Saxony, Süntel Mountains). *Facies*, 63. DOI 10.1007/s10347-017-0501-4

## 2.1 Introduction

The biostratigraphic correlation of Upper Jurassic deposits in the Lower Saxony Basin, a sub-basin of the North German Basin, is hindered by the scarcity of stratigraphic index fossils (Gramann et al., 1997). Therefore, sequence stratigraphy, in combination with other complementary methods, was used to correlate the succession investigated herein with other sections in North Germany, SW Germany, Switzerland, Spain, Scotland, and France. According to Pittet and Strasser (1998) and Strasser et al. (2000), sequence stratigraphy and cyclostratigraphy have proven to provide a good understanding of the paleoenvironmental changes which affected the area comprised of the Swiss Jura, Spain, and northeast France. Accordingly, medium-scale composite sequences that are related to the 100 and 400 ka eccentricity cycles allow the comparison of facies evolution in regions that are as much as 1000 km apart. In SW Germany, medium-scale sequences interpreted as recording a 400 ka Milankovitch signal were correlated on a basin-wide scale with help of gamma-ray logs, stable isotope records and palynofacies (Ruf et al., 2005a). A sequence stratigraphic framework, established by Gygi (2000) and Gygi et al. (1998), of the Oxfordian and Kimmeridgian stages in northern Switzerland and southern Germany, was correlated with that of other Late Jurassic sedimentary basins in Europe.

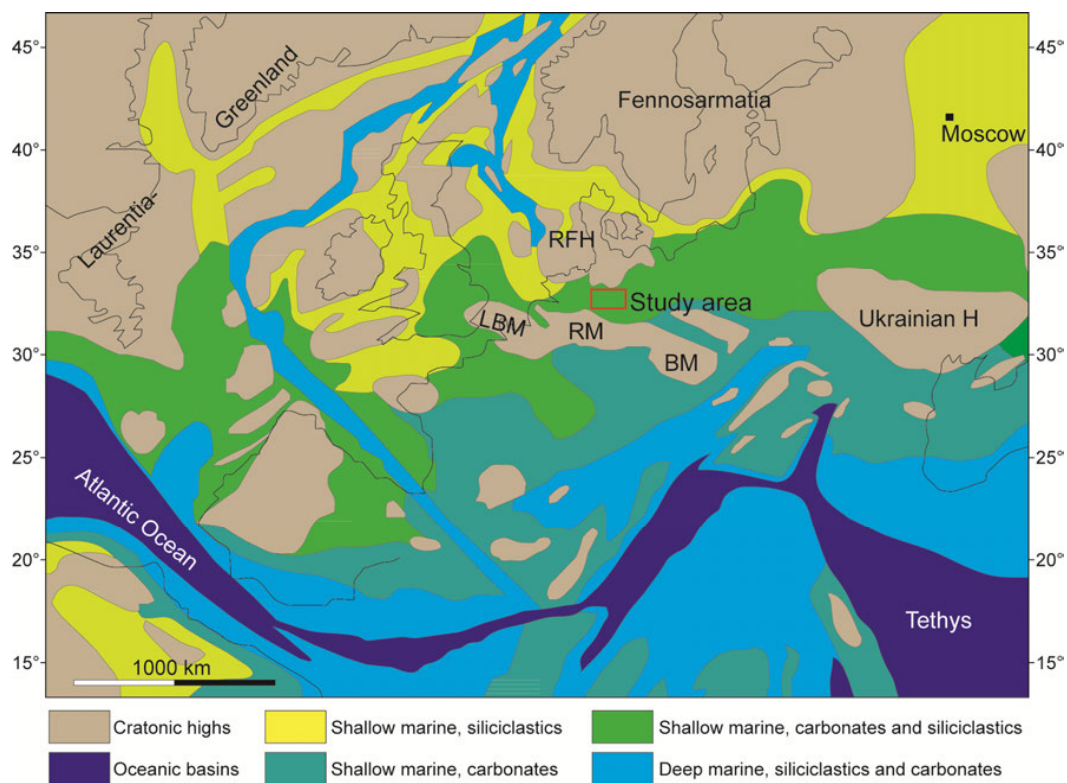


**Fig. 2.1** Late Jurassic paleogeography and main sediment associations in northern central Europe. LMB London-Brabant Massif, RM Rhenish Massif, BM Bohemian Massif, RFH Ringkobing Fyn High (modified from Ziegler, 1990; Thierry, 2000)



Applications of sequence stratigraphy to the Upper Jurassic in North Germany are, however, few and confined to the Oxfordian and Lower Kimmeridgian deposits (Betzler et al., 2007; Cäsar, 2012; Kästner et al., 2010).

The aim of this study is thus to develop a relatively complete sequence stratigraphic framework for the Oxfordian to Kimmeridgian deposits of the Lower Saxony Basin and to link this record to successions deposited in other European basins. Herein, the focus is on a core covering Oxfordian to Tithonian deposits from which a sequence stratigraphic scheme is devised based on facies analysis and vertical stacking patterns. Carbon isotopic data and ostracod biostratigraphy are integrated with sequence stratigraphic data. This integration results in an attempt to link this stratigraphic scheme with the chronostratigraphic chart established for the European Basins (Hardenbol et al., 1998; Ogg et al., 2012), and to decipher the potential factors controlling the observed facies development.

## 2.2 Geological setting

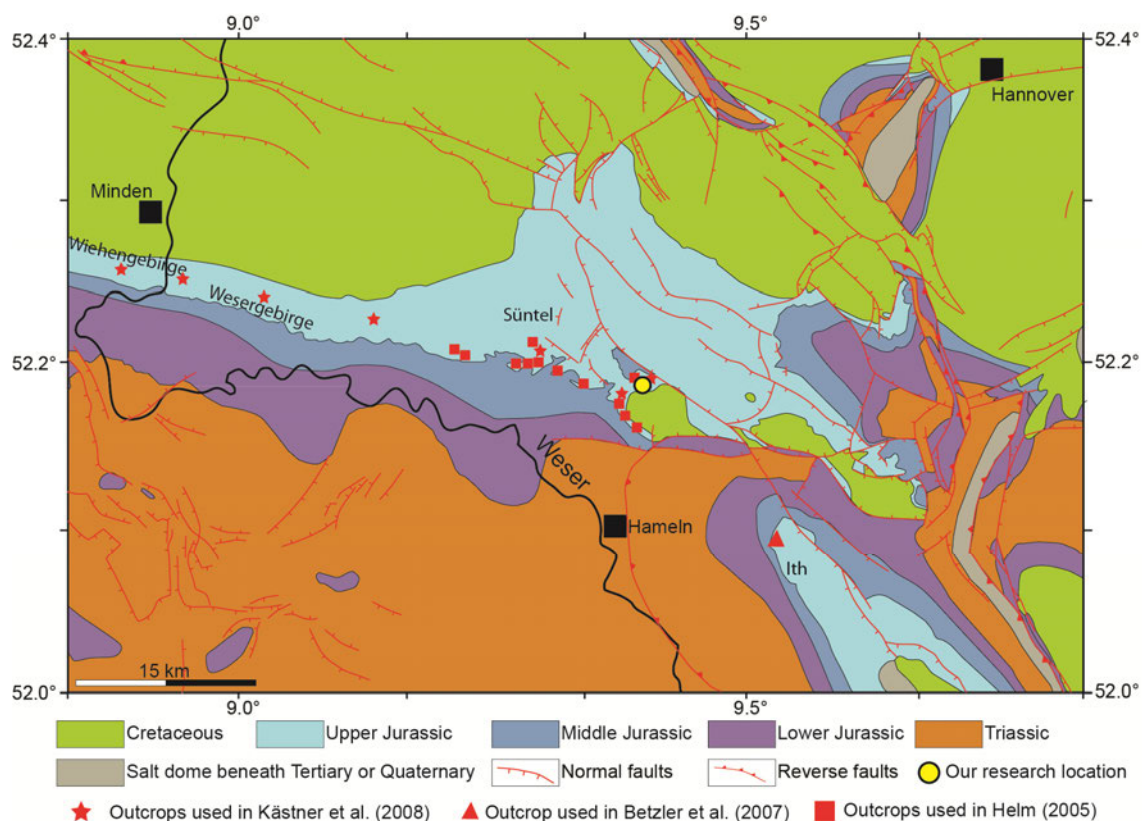


**Fig. 2.2** Geological map of the study area with the locations of the Eulenflucht-1 core and the other outcrops analyzed by Betzler et al. (2007), Helm (2005), and Kästner et al. (2008) (modified from Kockel et al., 1996)

During the Late Jurassic, the North German Basin was bounded by the Ringkobing Fyn High to the north, and by the London Brabant, the Rhenish and the Bohemian Massifs to the south (Fig. 2.1). The initial salt domes and pillows of the North German Basin reached the

diapir stage (Mönnig, 2005), and the differential subsidence of the Lower Saxony Basin controlled by syn-sedimentary faults began during the Late Jurassic (Betz et al., 1987; Gramann et al., 1997; Hoyer, 1965). The basin was divided into a series of subdued relief structural highs and lows, and the thickness of the deposits varies by tens of meters over relatively short distances because of the differential subsidence (Hoyer, 1965).

Serie	Stage	Lithostratigraphy Northwest Germany	Subboreal Ammonite zonation	Ostracod zonation	
Upper Jurassic	Tithonian	Eimbeckhausen Fm.	Zones not detectable in NW Germany	17	
		Holzen Fm.	<i>Elegans</i>	16	
	Kimmeridgian	Upper	Süntel Fm.	<i>Autissiodorensis</i>	15
				<i>Eudoxus</i>	14
		Middle	<i>Mutabilis</i>	13	
		Lower	Süntel Fm.	<i>Cymodoce</i>	12 - 9
				<i>Baylei</i>	8 7
		Oxfordian	Upper	Korallenoolith Fm.	<i>Pseudocordata</i>
	<i>Cautisnigrae</i>				5
	Middle		Korallenoolith Fm.	<i>Cautisnigrae</i>	4
	Lower			<i>Pumilus</i>	3
	Upper		Heersumer Fm.	<i>Plicatilis</i>	
Lower				<i>Cordatium</i>	
Middle Jurassic	Callovian	Ornatenton Fm.	<i>Mariae</i>	1	
			<i>Lamberti</i>		

**Fig. 2.3** Lithostratigraphic scheme of the Late Jurassic and their correlation with the standard zonation of the sub-boreal ammonite province (modified from Gramann et al., 1997; Hardenbol et al., 1998; Ogg et al., 2012; Schulze, 1975) and ostracod zonation (Schudack, 1994; Weiss, 1995)

Deposits of the Late Jurassic crop out in the mountain areas located to the southwest of Hannover (Fig. 2.2). The analyzed succession includes the Heersumer and Korallenoolith Fms (Oxfordian), the Süntel Fm (Kimmeridgian), and the Holzen and Eimbeckhausen Fms (Tithonian) (Fig. 2.3). The Heersumer Fm consists of bioturbated marlstone rich in sponge spicules (Kästner et al., 2008), whereas the Korallenoolith Fm encompasses oolite and coral buildups (Betzler et al., 2007; Cäsar, 2012; Helm, 1998, 2005; Helm et al., 2003; Helm and

Schülke, 2006; Kästner et al., 2008; Schultz, 1975). The *Florigemma*-bank situated in the middle part of the Korallenoolith Fm contains species-rich coral associations and its top is an erosional unconformity that can be traced over a lateral extent of several hundred meters (Helm, 2005). To the northwest and west of the Lower Saxony Basin, the siliciclastic contents of the deposits above the *Florigemma*-bank increase (Kästner et al., 2008; Mönnig, 2005). Deposits of the Süntel Fm were described as alternations of glauconitic marl, limestone and sandstone (Klassen, 2003; Mönnig, 2005). The Holzen Fm consists of alternations of clay, marl and limestone, whereas the Eimbeckhausen Fm is dominated by gypsum and anhydrite (Heunisch and Luppold, 2015).

A biostratigraphic division of the Upper Jurassic succession in Northern Germany was developed based on ammonites, ostracods, dinoflagellate cysts, charophytes and spores and pollen (Gramann et al., 1997; Hardenbol et al., 1998; Schudack, 1994; Schulze, 1975; Weiss, 1995) (Fig. 2.3). The Heersumer Fm covers the *Cordatum* and *Plicatilis* ammonite zones, whereas the Korallenoolith Fm covers the *Pumilus*, *Cautisnigrae*, and *Pseudocordata* zones. The Süntel Fm encompasses the *Baylei*, *Cymodoce*, *Mutabilis*, *Eudoxus*, and *Autissiodorensis* zones. The Holzen Fm is confined in the *Elegans* zone, while no ammonites have been found in the Eimbeckhausen Fm. Good biostratigraphic data exist only for the Heersumer Fm. The age diagnostic fossils in the analyzed core are limited to ostracods and palynomorphs in the Heersumer Fm and the formations in Kimmeridgian and Tithonian (Heunisch and Luppold, 2015).

### 2.3 Material and methods

The Eulenflucht-1 core (52.18227418° N, 9.4002145° E) is located in the Süntel Mountains (Fig. 2.2). The 340-m-long core covers the deposit from the Heersumer to the Deister Fms (Oxfordian to Berriasian) (Heunisch and Luppold, 2015). The core is stored at the BGR core repository in Grubenhagen. A total of 120 m of the core was described (Heersumer, Korallenoolith, Süntel, Holzen, and Eimbeckhausen Fm). A total of 80 samples was taken to produce thin-sections for microfacies analysis. To describe the texture of the sediments, the classification of Dunham (1962) with the modification by Embry and Klovan (1971) was used.

250 bulk rock samples were taken for carbon and oxygen stable isotope analysis. They were measured at the Leibniz Laboratory, University of Kiel with a Kiel 1 Finnigan MAT 251 mass spectrometer (reproducibility  $\pm 0.1\text{‰}$ ). The carbon isotope ratios are reported as delta values with reference to the international standard V-PDB (Brand and Veizer, 1981). The

biostratigraphic age assignment of the succession relies on the ostracod biostratigraphy for the Eulenflucht-1 core published by Heunisch and Luppold (2015).

## 2.4 Results

### 2.4.1 Facies description

Based on the differences in lithology, components and microscopic texture, thirteen lithofacies are identified (Table 2-1). The graphic log of the succession in the Eulenflucht-1 core with the distribution of these facies is shown in Fig. 2.4.

#### Facies 1: Bioturbated sponge spicule limestone

This facies consists of bioturbated packstone with sponge spicules and rhaxes, calcispheres and quartz as the main components (Fig. 2.5a). Other bioclasts are rare mollusc shells. The packstone has approximately 40% micrite. Burrows in this facies are up to 7 cm wide, and the burrow size decreases up-core to 323.80 m. This facies occurs from the base of the core to 323.78 m.

#### Facies 2: Bioturbated bioclastic wackestone

This facies contains rare to common bioclasts, including bivalves, sponge spicules and rhaxa, foraminifers and calcispheres. Abiotic components consist of common quartz and some pyrite. Burrows are distributed homogeneously and bioclasts are more densely packed in burrows. The micrite content is about 40%. The sediment is partially dolomitized, especially in the burrows (Fig. 2.5b). The degree of dolomitization decreases upwards. This facies occurs between 324.80 and 322.58 m, and is interbedded with the Bioturbated sponge spicule limestone facies (Facies 1).

#### Facies 3: Oyster-serpulid rudstone

Biotic components in this facies are common oysters, gastropods, serpulids and some echinoids. Abiotic components are common pyrite, some concentric ooids and quartz. Oyster shells and gastropods are up to 2 - 3 cm in length. Most of the serpulids encrust oysters (Fig. 2.5c). Geopetal textures occur in gastropods. The micrite matrix is partially dolomitized. This facies occurs in four intervals (323.60 - 323.77 m, 322.85 - 323.08 m, 322.29 - 322.59 m, and 321.74 - 322.00 m). This facies overlies the Bioturbated bioclastic wackestone facies (Facies 2) with a gradational contact.

**Table 2-1** Characteristics of Facies defined in core Eulenflucht 1

Facies	Components	Sedimentary structures	Interpretation
1. Bioturbated sponge spicule limestone	Some quartz, sponge spicules and rhaxes, calcispheres, rare mollusk shells	Massive with bioturbation	Outer ramp, below SWB
2. Bioturbated bioclastic wackestone	Some quartz, pyrite, bivalves, sponge spicules and rhaxes, foraminifers, calcispheres	Massive with bioturbation	Outer ramp, below SWB, shallower than Facies 1
3. Oyster-serpulid rudstone	Some pyrite, concentric ooids, quartz, common oysters, gastropods, serpulids, and some echinoids	Massive with bioturbation, geopetal structure	Middle ramp, below FWWB above SWB
4. Ooid packstone and grainstone	Rare quartz, abundant concentric ooids, some micritic ooids and compound ooids, some bivalves, echinoids, gastropods, rare serpulids, foraminifers	Cross-bedding	Inner ramp; above FWWB
5. Coral boundstone	Abundant coral casts, encrusting foraminifers, some coral debris, ooids, gastropods, bivalves, rare ostracods	Massive with hardground on the top	Middle ramp, deeper than Facies 3
6. Foraminifer wackestone and mudstone	Common foraminifers consisting of <i>Lenticulina spp.</i> , <i>Alveosepta jaccardi</i> , and <i>Textularia</i> , some serpulids, bivalves, echinoids, gastropods, rare ostracods	Massive	Outer ramp, below SWB, shallower than Facies 2
7. Radial ooid packstone and grainstone	Common radial ooids, some concentric ooids, echinoids, bivalves, gastropods, and foraminifers	Massive with hardground on the top	Inner ramp, open lagoon
8. Bioclastic floatstone and rudstone	Some glauconite, pyrite, ooids, common oysters, brachiopods, bivalves, echinoids, some serpulids, foraminifers, gastropods, rare ostracods	Massive with bioturbation, fining upward bedding	Inner ramp, semi-open lagoon
9. Bioclastic and peloid floatstone	Rare quartz, common to rare peloids, pyrite, common bivalves, gastropods, brachiopods, ostracods, foraminifers	Massive with bioturbation, fenestral structure	Inner ramp, restricted lagoon
10. Stromatolitic bindstone	Abundant quartz, Algae, some bioclasts	Horizontal bedding	Inner ramp, intertidal area
11. Evaporite	Common gypsum	Massive	Inner ramp, supratidal
12. Bioclastic wackestone and mudstone	Some quartz, bivalves, foraminifers	Massive with bioturbation	Inner ramp, intertidal area
13. Sandy limestone	Common quartz, bivalves, rare ooids, foraminifers, some glauconite	Massive with sharp base	Channel-fill, peritidal

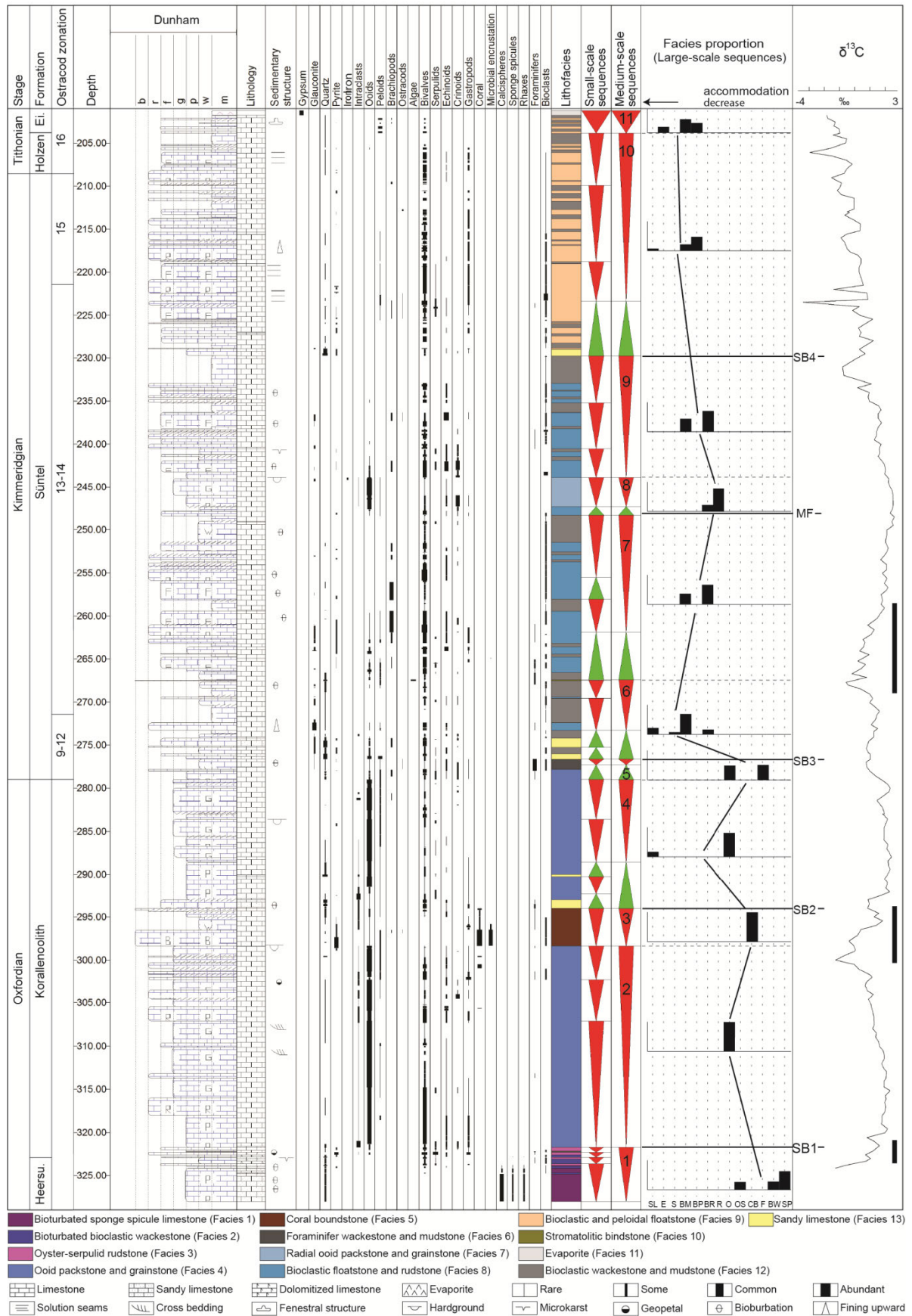


**Fig. 2.4** Lithostratigraphy of the Eulenflucht-1 core and abundance of components. Sequence division relies on components and textural changes, as well as facies superposition relationships. *SL* Sandy limestone, *E*

Evaporite, *S* Stromatolitic bindstone, *BM* Bioclastic wackestone and mudstone, *BP* Bioclastic and peloidal floatstone, *BR* Bioclastic floatstone and rudstone, *R* Radial ooid packstone and grainstone, *O* Ooid packstone and grainstone, *OS* Oyster-serpulid rudstone, *CB* Coral boundstone, *F* Foraminifer wackestone and mudstone, *BW* Bioturbated bioclastic wackestone, *SP* Bioturbated sponge spicule limestone. The *black bars* represent positive isotopic excursion intervals, and the height of the *vertical axis* of each *bar chart* in the facies proportion column represents 100%

#### Facies 4: Ooid packstone and grainstone

This facies contains abundant simple concentric ooids, micritic superficial ooids and some compound ooids with grain sizes less than 1 mm (Fig. 2.5d). Other components are minor to common bivalves, minor echinoids, gastropods, rare serpulids, foraminifers and quartz. Between 321.00 and 321.73 m, there are common intraclasts composed of abraded ooids, echinoids, serpulids and gastropods (Fig. 2.5e). The nuclei of the ooids are debris from bivalves, echinoids, gastropods, foraminifers and some quartz. Matrix is rare. Poikilotopic crystals fill the pore space between components. Between 307.00 and 309.00 m, the grainstone is cross bedded (Fig. 2.6a). This facies occurs in two intervals, at 321.00 - 298.40 m and 293.00 - 277.80 m.

#### Facies 5: Coral boundstone

This facies occurs between 294.00 and 298.40 m. Dendroid corals with foraminifer encrustations occupy 50% of its volume. The space between coral branches is occupied by wackestone. The components in the wackestone are poorly sorted, consisting of some coral debris, ooids, gastropods with geopetal structures, bivalves, foraminifers and rare ostracods (Fig. 2.5f). Coral branches are dissolved and molds filled by calcite cement and pyrite (Fig. 2.5g). The proportion of components decreases up-core in this facies as the micrite content increases. This facies overlies the Ooid packstone and grainstone facies (Facies 4) with a sharp contact.

#### Facies 6: Foraminifer wackestone and mudstone

This facies occurs between 277.80 and 276.65 m. It has the most common occurrence of foraminifers, including the calcareous benthic foraminifer *Lenticulina spp.* and the agglutinating foraminifer *Alveosepta jaccardi*, and *Textularia* (Fig. 2.5h). Other components are serpulids, bivalves, echinoids, gastropods, rare ostracods and other bioclasts that are too small to be identified. Some glauconite is present in this facies. Burrow density increases up-core. This facies has a sharp upper limit and is overlain by the Sandy limestone facies (Facies 13).



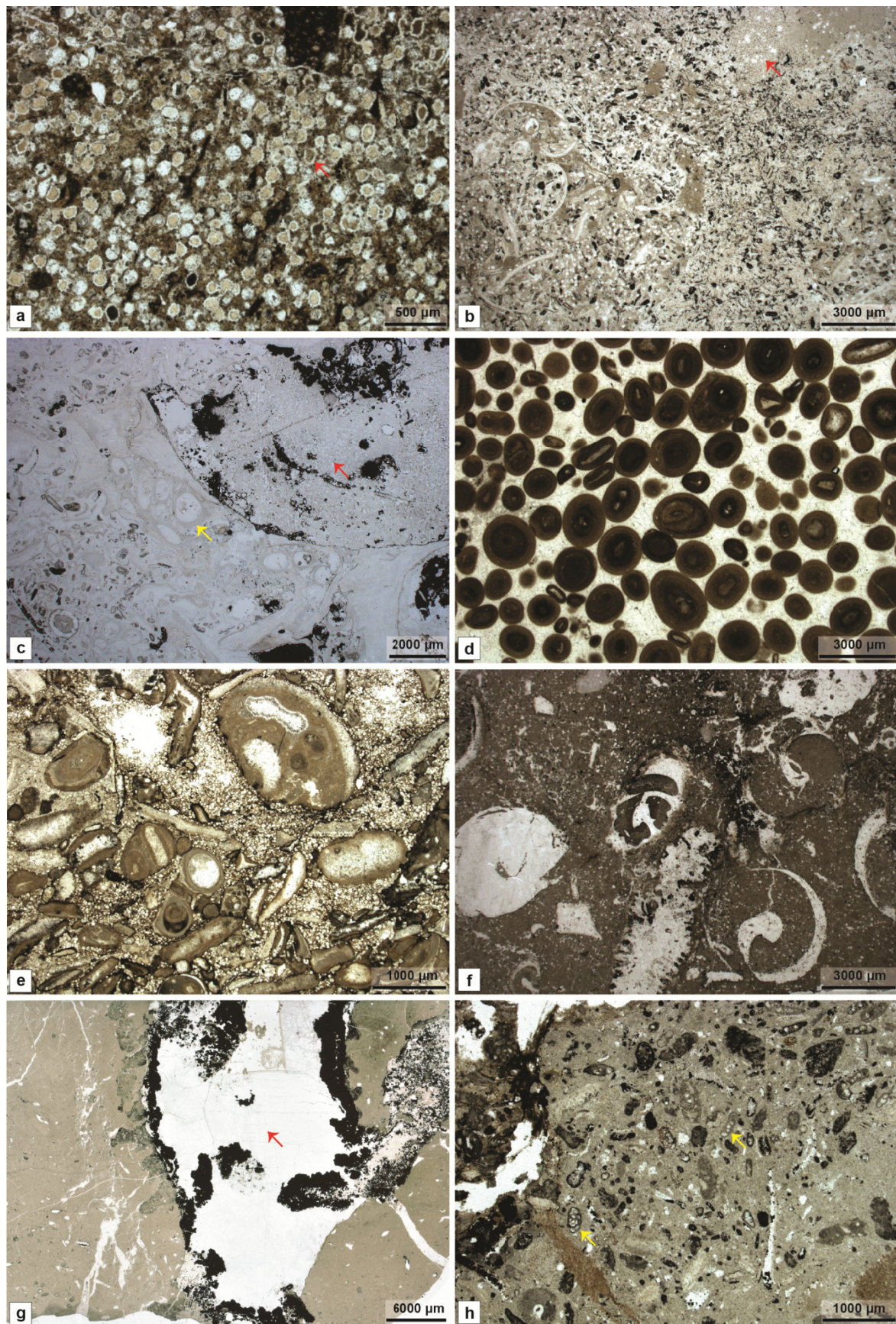


**Fig. 2.5** **a** Sponge spicules together with quartz and calcispheres in limestone. Central canals of sponge spicules filled with micrite (red arrow), at 327.05 m; **b** Bioclastic wackestone with partial dolomitization (red arrow), at 323.17 m; **c** Large oyster shells encrusted by serpulids (yellow arrow). Micrite is partially



dolomitized (red arrow). Sample from 322.48 m; **d** Ooid grainstone consists of concentric ooids and poikilotopic cement, at 310.20 m; **e** intraclasts in Ooid packstone and grainstone, at 321.74 m; **f** Coral debris and gastropods, at 295.86 m; **g** Microbial encrustations and mold of coral filled by pyrite and sparry calcite (red arrow), at 297.79 m; **h** Wackestone contains abundant foraminifers (yellow arrow), at 276.76 m

### Facies 7: Radial ooid packstone and grainstone

This facies contains radial ooids about 0.5 mm in diameter. Ooids either have only one lamina with a radial structure or have several concentric laminae with a fine radial inner structure (Fig. 2.7a). Other components are minor concentric ooids, echinoids, bivalves, gastropods and foraminifers. Poikilotopic crystals fill pore space between ooids. The grains have convex-concave contacts due to compaction. This facies occurs between 243.87 and 247.30 m. The top of the interval with this facies is an erosive surface. A well-cemented layer, about 2 mm thick, with high iron content occurs below this surface (Figs. 2.8a and 2.8b).

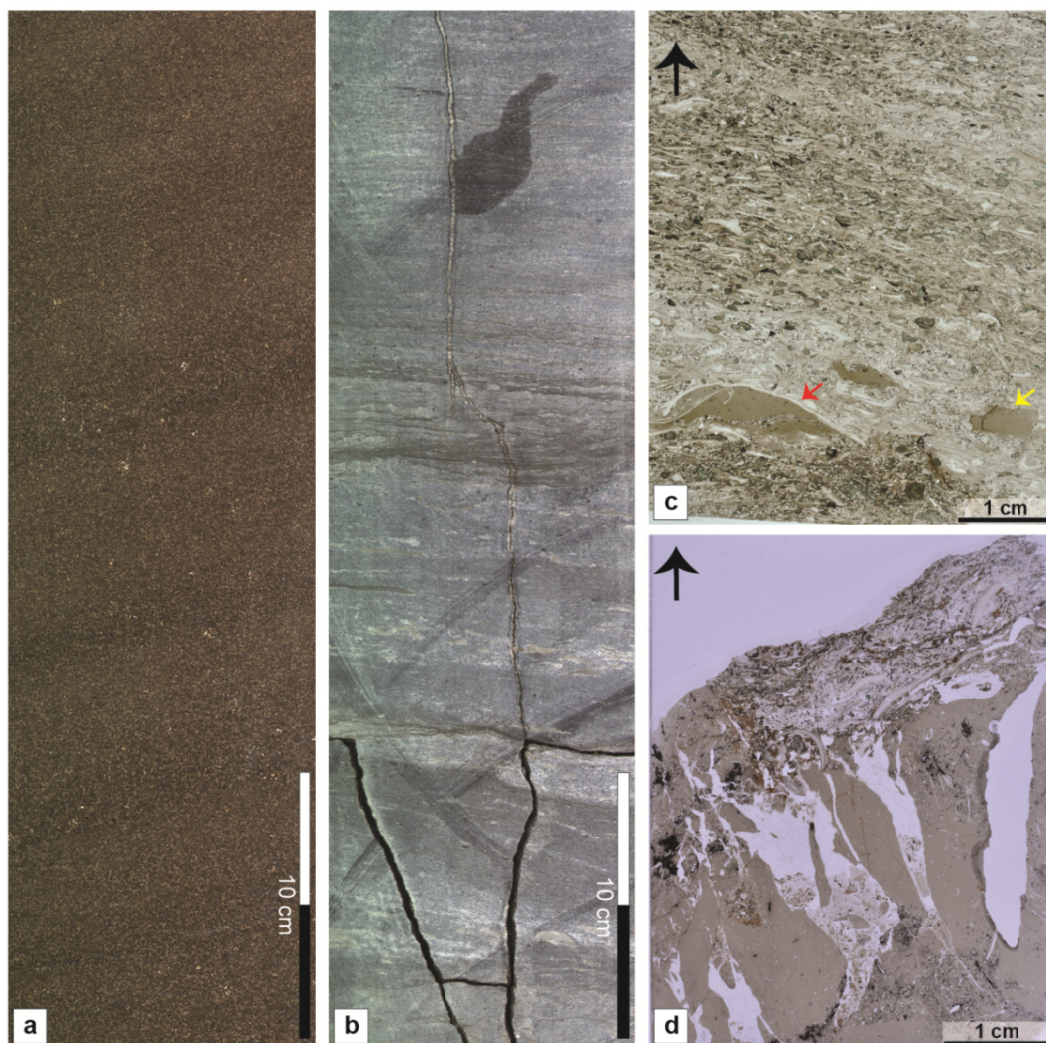


**Fig. 2.6** **a** Cross bedding in Ooid packstone and grainstone, 308.20– 308.70 m; **b** Fining upward succession with erosive base (yellow arrow) in Bioclastic floatstone and rudstone, 272.35–272.85 m; **c** Bioclastic rudstone



with concave-upward bivalve (red arrow) and mud clusters (yellow arrow), parallel structure shown by oriented bivalves. The black arrow points to the top of the thin-section, at 272.80 m; **d** Micro paleokarst in bioclastic wackestone, at 240.59 m. The black arrow points to the top of the thin-section

#### Facies 8: Bioclastic floatstone and rudstone

This facies occurs between 232.96 - 273.30 m (Fig. 2.4). It is subdivided by the Bioclastic wackestone and mudstone facies (Facies 12) into several units. The thickness of each unit varies from 10 cm to 4 - 6 m (e.g., the units are about 4 m thick at 253.71 - 258.00 m and 259.48 - 263.20 m). The large components are oyster fragments up to 2 cm long (Fig. 2.7b). Other components are common brachiopods, bivalves, echinoids, some serpulids, foraminifers, gastropods and rare ostracods. Glauconite, pyrite and some ooids are also present in this facies. In the interval between 272.40 and 273.30 m, four fining-upward successions were deposited. Each consists of a base with 2-cm-long, concave-upward bivalve fragments and 1-cm-large intraclasts followed by oriented bivalves, and a third layer with inclined bedding delineated by the alternating bioclastic packstone and wackestone. A layer of wackestone with horizontal lamination occurs at the top (Figs. 2.6b and 2.6c).

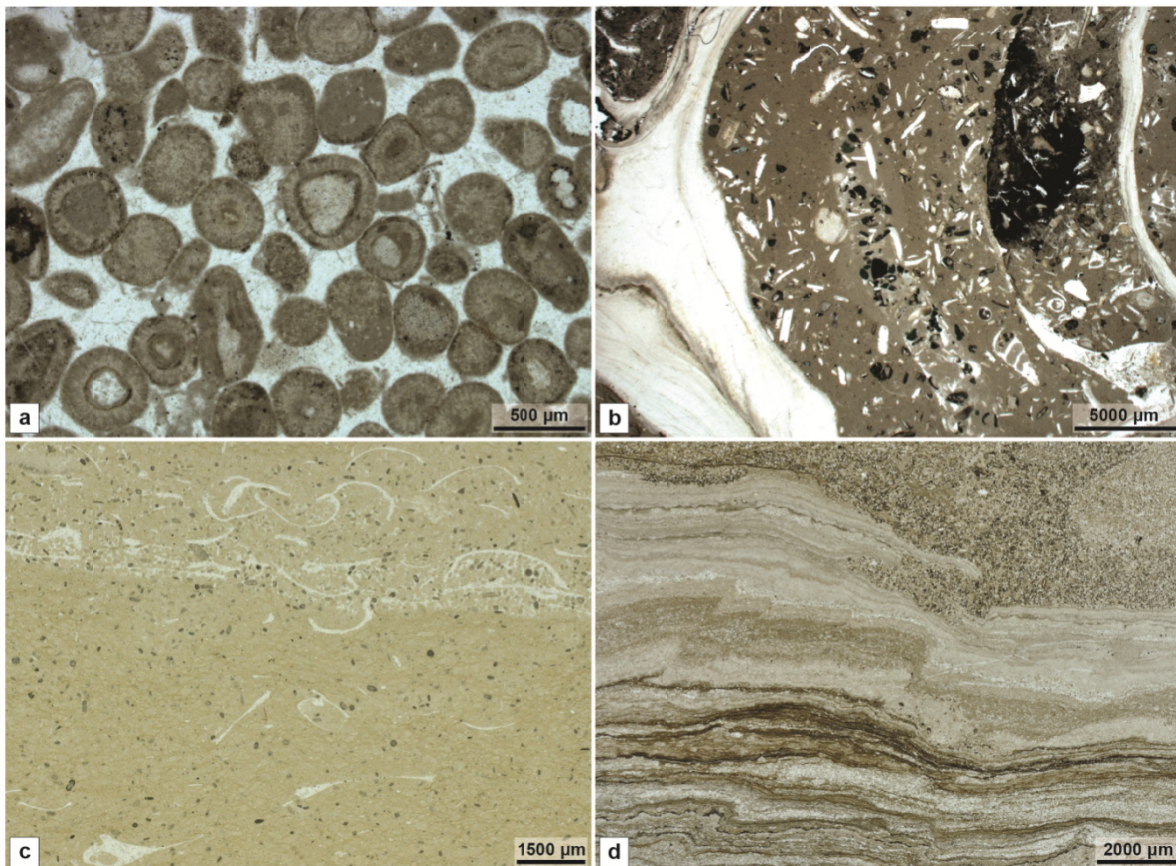


**Fig. 2.7** **a** Ooid with radial cortex, at 245.15 m; **b** Bioclastic rudstone with oyster fragments larger than 1 cm and glauconite, at 261.69 m; **c** Bioclastic and peloidal floatstone with thin shelled bivalves and peloids. Fenestral structures are included, at 203.34 m; **d** Stromatolitic bindstone, at 267.42 m

#### Facies 9: Bioclastic and peloidal floatstone



This facies occurs between 202.09 - 229.03 m and is interbedded with the Bioclastic wackestone and mudstone facies (Facies 12). Components are common bivalves, gastropods, rare echinoids, brachiopods, ostracods and foraminifers. The abiogenic components are common to rare peloids, rare quartz and pyrite. Fossil diversity decreases from the base of this facies interval to the top, whereas the micrite content increases and reaches a maximum of 70% at the top. In the uppermost part of this interval, there are fenestral structures, and only thin-shelled bivalves and peloids are included (Fig. 2.7c). Dissolution seams are common in this facies.

#### Facies 10: Stromatolitic bindstone

This facies occurs between 267.57 and 267.43 m. It is a bindstone with abundant quartz, algae and some bioclasts. Parts of the horizontal laminae are disrupted (Fig. 2.7d). The bindstone is overlain by packstone with peloids, quartz and foraminifers. Both the base and top surfaces of this facies are sharp.

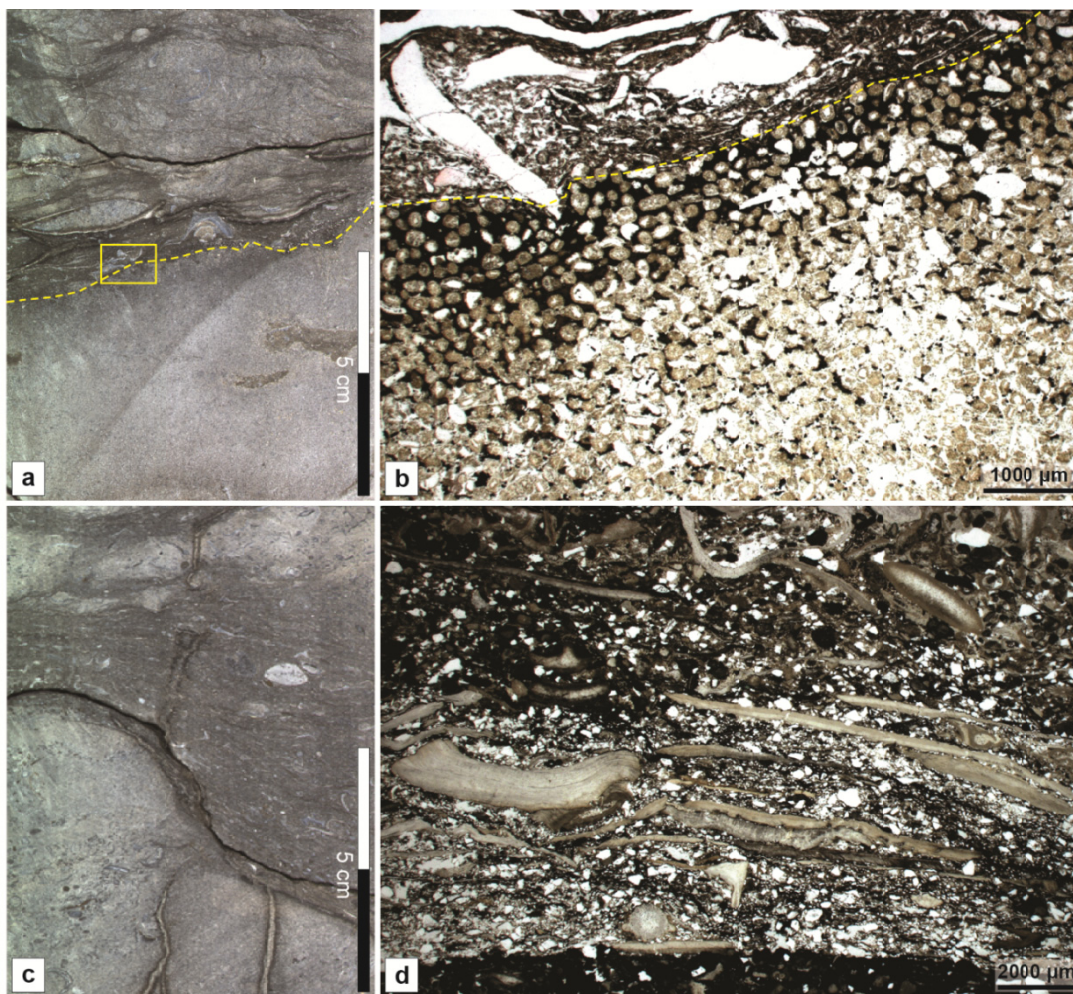


**Fig. 2.8** **a** Contact between radial ooid grainstone and bioclastic floatstone in a hand specimen (yellow dashed line), 243.85–243.95 m; **b** Well-cemented thin layer with iron content under the contact surface shown in the previous photo, sample taken from the yellow square shown in the previous photo; **c** Erosive surface corresponding to the main disconformity across the Lower Saxony Basin. Sandy limestone with burrows

overlies this surface. 293.75–294 m; **d** Sandy limestone with angular quartz and poorly sorted bioclasts, at 293.08 m

#### Facies 11: Evaporite

Evaporites occur in the uppermost part of the measured core, above 201.78 m. Deposits consist of laminated gypsum interbedded with mudstone. The thickness of each single gypsum layer increases upwards, from less than 10 cm to more than 1 m.

#### Facies 12: Bioclastic wackestone and mudstone.

This facies occurs from 201.78 to 276.00 m, interbedded with the Bioclastic floatstone and rudstone facies (Facies 8), Bioclastic and peloidal floatstone facies (Facies 9) and the Stromatolitic bindstone facies (Facies 10). The thickness of each single interval increases from 276.00 m upwards and reaches its maximum of 3.18 m at 229.78 - 232.96 m, after which the interval thickness decreases again. Dark mudstone is well laminated, whereas grey wackestone is bioturbated and contains microkarst structures (*sensu* Freytet and Plaziat 1982, Fig. 2.6d). There are some bivalves, foraminifers, rare echinoids and some quartz in the wackestone parts. This facies is overlain by the Evaporite Facies (Facies 11).

#### Facies 13: Sandy limestone

This facies occurs in three units (293.00 - 294.00 m, 274.23 - 276.65 m and 229.00 - 229.80 m), all of which have a sharp base. For example, the irregular base of the sandy limestone between 293.00 and 294.00 m cuts into the underlying layers (Fig. 2.8c). The components of this facies are common detrital quartz grains, bivalves, rare ooids, foraminifers and some glauconite. Quartz grains occupy about 50% of the rock in thin-section and are subrounded (Fig. 2.8d). Burrows are common.

### 2.4.2 Carbon isotopes

The carbon isotopic values of the bulk samples from the Eulenflucht-1 core vary between -4‰ and +3‰ (Fig. 2.4). Three intervals with positive excursions are recorded. The lowest one is from the bottom of the core to 315.14 m, with a carbon isotopic value increase from -1.27‰ to +2.20‰. This interval covers the facies changing from the Bioturbated sponge spicule limestone facies (Facies 1) to the Ooid packstone and grainstone facies (Facies 4). The second interval is between 300.00 and 287.95 m, with carbon isotopic values between -1.26‰ and +2.16‰. This interval coincides with the position of the Coral boundstone facies (Facies 5) package. The third interval is from 267.62 to 248.47 m, with carbon isotopic values increasing from -0.61‰ to +2.47‰. This interval corresponds to the succession changing from the Stromatolitic bindstone facies (Facies 10) to the Bioclastic floatstone and rudstone facies (Facies 8). Negative excursions of the carbon isotopic values are located at

315.14 - 300.00 m and 287.95 - 267.62 m. Above 248.47 m, carbon isotope values gradually decrease towards the top of the succession

## 2.5 Discussion

### 2.5.1 Depositional environments interpretation

The proposed facies model is based on the interpretation of sedimentary structures, dominating components and micrite content variations of each facies. Sediment deposited below the fair weather wave base (FWWB) is characterized by small grain sizes, high micrite content, lack of wave-induced sedimentary structures, and the inclusion of pyrite, which forms in a reducing environment. Sediments deposited above the FWWB have cross bedding and are rich in ooids. The decrease in fossil diversity, lack of stenohaline marine organisms such as echinoids, and the occurrence of gypsum, indicate a depositional regime which switched from an open-marine setting to a restricted lagoonal setting.

Facies 1 is interpreted as being deposited below the storm wave base (SWB). According to Kästner et al. (2008), the sponge spicules and rhaxa in the Heersumer Fm are from siliceous sponges that thrived in open-marine conditions with low-medium water energy (Haslett, 1992; Townson, 1975) and a certain oxygen deficiency (Reid, 1968). Similar to the sponge-spicule rich deposits of the Terrain à Chailles Fm of Early Oxfordian age in the eastern Paris Basin (Carpentier et al., 2007), the scarcity of marine organisms, lack of sedimentary structures and well-developed burrows indicate that this facies was formed in a tranquil marine setting with low hydrodynamic energy below SWB.

Facies 2 has a higher amount and diversity of bioclastic components than Facies 1. This shows a switching from a tranquil marine setting to a relatively shallower area with better oxygenation conditions. The decrease in burrow size and increase in burrow intensity from Facies 1 to Facies 2 reflects the increased water energy. The gradual contact between these two facies indicates that they were adjacent at the time of deposition. The absence of sedimentary structures and the presence of pyrite support the assignment of this facies to a zone below SWB, but in a shallower area than Facies 1.

In Facies 3, the occurrence of pyrite indicates an oxygen-deficient depositional environment (Fig. 2.4). The micro-encruster association encrusting the oyster shells shows a low diversity and contains almost only serpulids, comparable with the *Terebella-Tubiphytes* association defined by Schmid (1996) in the Swiss Jura Mountains that formed in an environment with low to moderate water energy. The presence of large oyster and gastropod

shells and some ooids shows that the water energy switched from low to moderate. This helps to locate this regime with moderate water energy above SWB, but below FWWB.

Facies 4 is interpreted as a deposit that formed above the FWWB. Minor micrite content and well-winnowed ooids about 0.5mm in diameter (Fig. 2.5d) indicate a medium to high hydrodynamic environment (Strasser, 1986). The tangential structure of ooids suggests sufficient water energy to rotate the grains and keep frequent abrasion of the original radial arrangement of calcite crystals in each cortex (Medwedeff and Wilkinson, 1983). Large-scale cross bedding (Fig. 2.6a) induced by strong water movement is a evidence of sediment deposition above FWWB (Betzler et al., 2007). Facies 4 is located below low-tide level and above FWWB, which is similar to the oolites deposited in Lauensteiner Pass in North Germany, as described by Betzler et al. (2007).

Coral reefs (Facies 5) were widely recorded in the French Jura, NE France and North Germany and are interpreted as being deposited below FWWB with low or low-moderate water energy, regardless of their morphology and taxa (Betzler et al., 2007; Carpentier et al., 2007; Helm, 2005; Helm et al., 2003; Lathuiliere et al., 2005; Schmid, 1996). In the Upper Jurassic, microbial crusts were deposited in low-energy and oxygen-deficient settings during phases of reduced background sedimentation (Leinfelder et al., 1993), which is also a setting favorable for the formation of pyrite encrustations. Wackestone deposited between the coral skeletons also implies that the hydrodynamic power was not sufficient to winnow the lime mud (Carpentier et al., 2007). Large coral and gastropod debris in the wackestone are the result of episodically raised water energy induced by storms that broke coral colonies. Some scattered ooids indicate that the facies formed not far from the higher water energy settings where Facies 4 was deposited. Therefore, this facies is interpreted to have been deposited between FWWB and SWB.

Facies 6 was deposited below SWB. The agglutinating foraminifer *Alveosepta jaccardi*, which is abundant in this facies, thrived below FWWB in open-marine, unrestricted regimes (Dupraz and Strasser, 2002; Hughes, 2004). The occurrence of glauconite reflects periods of low sedimentation rates and low current velocities (O'Brien et al., 2011). A micrite content of 70%, the small sizes of components and horizontal burrows all support a quiet water regime below SWB.

Facies 7 is assumed to have been deposited in an open-lagoon setting. Ooids with radial cortical fabrics can be compared with ooid types 4 and 5 defined by Strasser (1986), which formed in calm brackish restricted-marine settings with intermittent high energy (Davies et al., 1978; Suess and Fütterer, 1972). The lack of matrix and the occurrence of some

concentric ooids attest that this facies was formed within a setting with intermittent high water energy conditions, adjacent to Facies 4.

A gradual contact between Facies 8 and Facies 7 shows that they were formed in adjacent depositional settings. High fossil diversity and the occurrence of echinoids, brachiopods and serpulids indicate a normal-marine salinity setting. The presence of glauconite suggests a low sedimentation rate during periods of high sea-level and low current velocity (O'Brien et al., 2011). A high matrix content reflects an environment of low water energy. This facies is thus interpreted to have been deposited in the open lagoon next to Facies 7 with a marine water circulation but low water energy. The less than 40 cm thick fining-upward successions in this facies are assumed to reflect tempestite deposits. Erosive bases and coarse concave-upward bioclastic fragments were formed during peak storm conditions (Kreisa and Bambach, 1982). Inclined bedding indicates the existence of wave oscillation generated by storm waves. The fining-upward grain-size shows flow-waning conditions.

A restricted lagoon regime with high salinity is proposed for the formation of Facies 9 because of its low fossil diversity, the absence of echinoids, which have a very limited range of salinity tolerance (Roller and Stickle, 1985; Scholle and Ulmer-Scholle, 2003), and the occurrence of peloids, which are abundant in hypersaline lagoons (Scholle and Ulmer-Scholle, 2003). The fenestral structure at 202.24 m (Fig. 2.7c) indicates an intertidal depositional setting. Within this facies interval, from base to the top, changes of the deposits with bioclastic components into the deposits with fenestral structures and the restricted biota of thin-shelled bivalves and gastropods represent an environment changing from subtidal to intertidal (Pomoni-Papaioannou, 2008). Thus, this facies is interpreted as the subtidal and intertidal deposits of a restricted lagoon with high salinity.

The Stromatolitic bindstone (Facies 10) is interpreted as deposited in the intertidal environment of a protected lagoon with restricted water circulation (Hofmann, 1976; Hyam and Kamal, 2010; Wilson, 1975). The common incorporation of quartz grains indicates formation near the coastline.

Facies 11 was formed in the supratidal environment of a protected lagoon with extremely high water salinity and high evaporation rates to form the gypsum.

Facies 12 is considered to be deposited in the upper intertidal area, not only because it is interbedded with the subtidal to intertidal Facies 9 and the intertidal Facies 10, but also because of the absence of the stenohaline marine echinoids and the presence of quartz. As

the grain-size is much finer and the micrite content is much higher in this facies than in Facies 9, it is assigned to the upper part of the intertidal zone, shallower than Facies 9.

In Facies 13, incorporation of quartz grains with poor sorting indicates a short transport distance. The erosive contact of this facies with underlying deposits at 294.00 m is interpreted to correspond to a regionally traceable disconformity surface, known as the “Hauptdiskontinuität” (Helm, 1998, 2005) and “Hauptemersion” (Schulze, 1975). Iron ooids, karst features and palaeosoil, which are signs of a low sea-level position, are recorded together with this surface in outcrop sections northwest of Eulenflucht (Helm, 2005). Thus, with the common quartz grains, Facies 13 is interpreted as a shoreline deposit, perhaps a channel-fill deposit where its base is erosive.

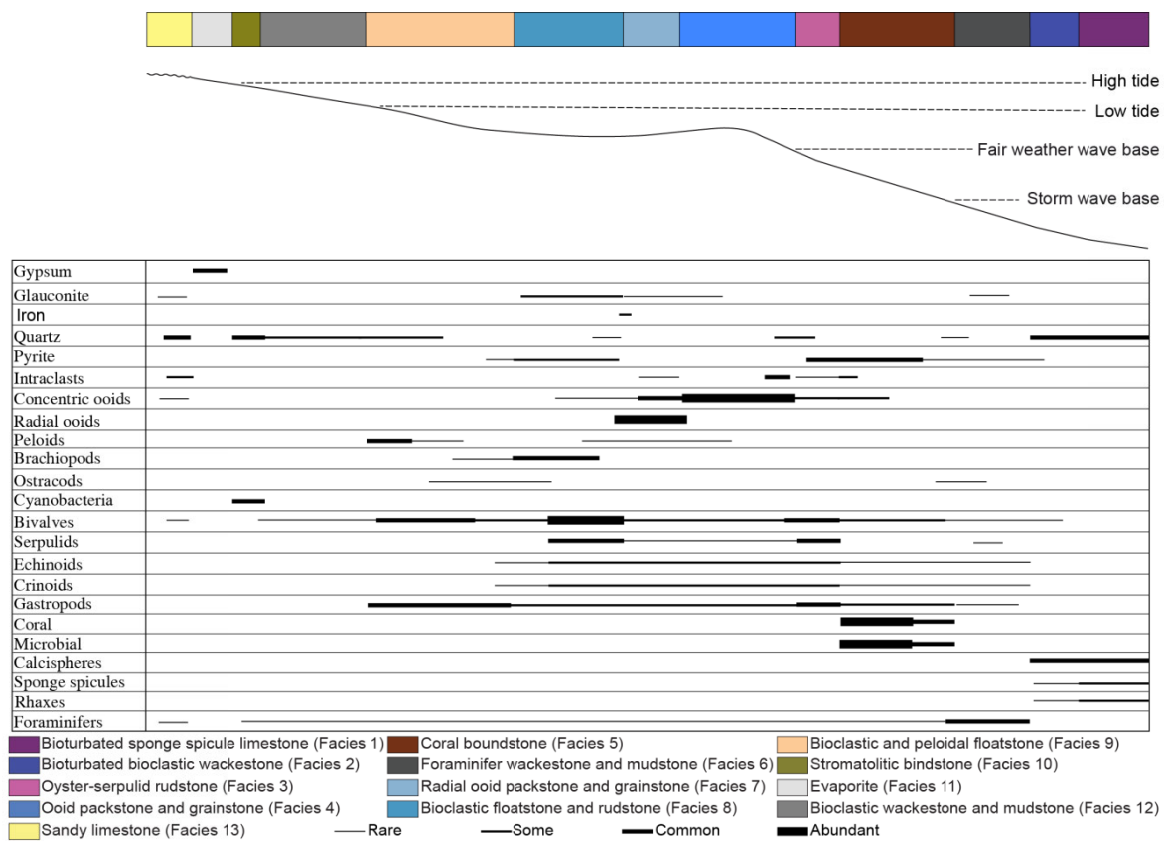


Fig. 2.9 Facies model of the Eulenflucht-1 core from the Heersumer Formation to Eimbeckhausen Formation

### Depositional Model

Based on the facies interpretation, a carbonate platform ramp is inferred to be the depositional environment for the succession of the Eulenflucht core (Fig. 2.9). A similar depositional environment for the Korallenoolith Fm was suggested by Betzler et al. (2007) and Kästner et al. (2008). The 13 lithofacies are assigned to different packages with respect to the effects of fair weather and storm waves, tides and the protection provided by a ooid



barrier. Facies deposited below SWB are characterized by a large amount of matrix, fine grain-size, and a lack of sedimentary structures. Facies deposited above SWB and around FWWB typically show the presence of ooids, large oyster and coral fragments, in-situ coral boundstone, and cross bedding induced by wave movement. Facies deposited in an open lagoon behind an ooid shoal are characterized by diverse normal-marine fossils, large component size, and the occurrence of radial ooids. Peritidal deposits are featured by the occurrence of peloids, stromatolitic bindstone, gypsum, a low fossil diversity and a lack of stenohaline marine organisms. These interpretations result in a facies model ranging from tidal flat to lagoon, to outer ramp (Fig. 2.9).

### 2.5.2 Sequence analysis

Three types of sequence are identified in the succession. These are small-scale sequences 1 - 5 m thick, medium-scale sequences 2.5 - 26 m thick, and large-scale sequences 17 - 37 m thick.

There are 25 small-scale sequences defined by changes in grain content, grain-size, sedimentary structures and vertical facies superposition relationships (Fig. 2.4). An increase in grain-size and amount, and facies deposited in deeper water without sedimentary structures overlain by shallower facies with cross bedding, microkarst or fenestrae indicate a shallowing-up trend, and the reverse succession indicates a deepening-up trend.

There are 11 medium-scale sequences defined and marked as Sequence 1 - 11 from bottom to the top (Fig. 2.4). The medium-scale sequences are composed of 1 - 4 small-scale sequences containing the same facies combination. Sequence boundaries are identified by the presence of hardgrounds, and the changes in facies combinations of their constituent small-scale sequences. The bases of the Sandy limestone facies (Facies 13) are also treated as sequence boundaries, because they are assumed to be unconformity surfaces marking the end of the highstand systems tract (HST) deposits, and this assumption has been proved by the existence of 'Hauptdiskontinuität' (Helm, 2005; Kästner et al., 2010). As no stacking pattern can be recognized in the core data, assignment of Facies 13 into an early or late lower systems tract, is not straightforward. The concept of accommodation to sediment supply cycles (Cross et al., 1993; Cross and Lessenger, 1998; Homewood et al., 2000) is used to express each sequence.

Large-scale sequences are defined by the facies proportion statistics of each medium-scale sequence. According to the method described by Kerans and Tinker (1997), the curve made

by facies proportion statistics per medium-scale cycle reflects the large-scale cycles superimposed on the medium-scale cycles.

### Medium-scale sequences

Sequence 1 is a shallowing-up hemicycle from the bottom of the core to 321.71 m. It contains four shallowing-up small-scale sequences. The shallowing-up trend of each small-scale sequence is reflected by an increase in grain-size from small spicules, rhaxes and calcispheres to large oysters, and by facies changing from Facies 1 to 2 to 3 (Fig. 2.4). The thickness of each small-scale sequence decreases up-core. The boundary between Sequence 1 and 2 is based on the facies changing from Facies 3 to 4. The same facies superposition was used in the Hildesheim area, which is about 45 km east of the Eulenflucht-1 core site, to define an unconformity (Helm et al., 2003; Pienkowski et al., 2008).

Sequence 2 is also a shallowing-up hemicycle with three small-scale sequences. The division of these three small-scale sequences relies on the repeated trends of changes from micritic ooid packstone or rudstone to concentric ooid grainstone, and on the increase in the amount of ooids. A reduction in accommodation/sediment supply (A/S) ratio in the lowest small-scale sequences in Sequence 2 can be inferred by the development of cross-bedding in concentric ooid grainstone at about 307.10 m (Fig. 2.4).

Sequence 3 encompasses Facies 5 with one small-scale sequence. The boundary between Sequence 2 and 3 is a hardground with an irregular relief. This surface corresponds to the base of the '*Florigemma*-bank' and marks a major flooding surface with considerable amplitude (Helm and Schülke, 2006). An abrupt increase in accommodation is reflected by Facies 5 overlying Facies 4. The overlying shallowing-up trend is characterized by an increase in the amount of ooids and in the size of coral debris in the wackestone filling the spaces between coral branches (Fig. 2.4).

The boundary between Sequence 3 and 4 is an erosive surface at the base of Facies 13, which corresponds to a regional traceable disconformity ("Hauptemersion" or "Hauptdiskontinuität") above the '*Florigemma*-bank' that divides the Korallenoolith Fm into two parts (Helm, 1998, 2005; Kästner et al., 2010; Schulze, 1975;). Sequence 4 contains a deepening-up hemicycle indicated by a decrease in the amount of quartz grains. A 2-cm-thick mudstone at 288.56 m is interpreted as the deposit formed during the highest sea-level stand in this sequence (Fig. 2.10). An increase in abundance of ooids and a decrease in micrite matrix in Facies 4 form the shallowing-up hemicycle of Sequence 4. Three small-scale sequences are detected in Sequence 4. The deepening-up hemicycle of the first and

second small-scale sequences is reflected by facies changing from the lowstand Facies 13 to Facies 4, and a decreasing amount of quartz. The following increase in ooids and the change in sediment texture from packstone to grainstone define their shallowing-up hemicycles. The boundary of these two small-scale sequences is defined at 290.26 m. The boundary between the second and third small-scale sequences is marked by a hardground that indicates a flooding event with a low amplitude of accommodation increase at 283.62 m. The third small-scale sequence is defined by an increase in ooids and the sediment texture changing from packstone to grainstone (Fig. 2.4). The top of Sequence 4 is defined by an abrupt decrease in the amount of ooids.

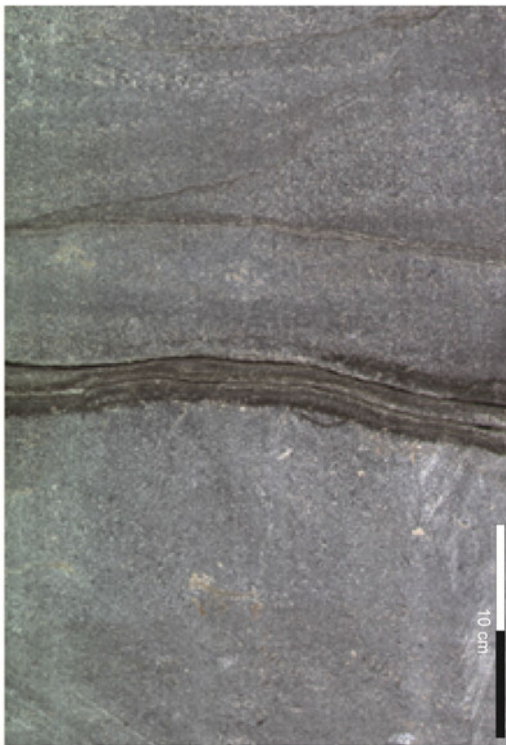


**Fig. 2.10** 2-cm-thick mudstone layer around 288.56 m

The decrease in ooid content and a change from Facies 4 to 6 define the deepening hemicycle of Sequence 5. This horizon also marks the lithostratigraphic boundary between the Korallenoolith and the Süntel Fm (Heunisch and Luppold, 2015). Most of the sequence reflects a deepening-up trend. A slight shallowing-up trend is indicated by an increase in bioclastic components and a decrease in the size of burrows.

The base of Sequence 6 is defined by the appearance of Facies 13 with an irregular erosive base. The deepening hemicycle of Sequence 6 consists of two deepening-up small-scale elements defined by the facies changing from Facies 13 to 12. The maximum A/S ratio is inferred by an occurrence of Facies 8 with abundant large oyster shells and glauconite. The shallowing hemicycle of Sequence 6 has two shallowing-up small-scale elements

characterized by the facies changing from Facies 8 to 12, and by a considerable decrease in grain-size and amount. The top of Facies 10 with abundant quartz and desiccation structures, resulting from intermittent subaerial exposure, marks the top of Sequence 6.

Sequence 7 has two small-scale sequences. The deepening-up trend of the two small-scale sequences is defined by an increase in grain-size, an increase in the number of bivalves, and a textural change from mudstone to rudstone. Successions with Facies 12 overlying Facies 8 form the shallowing-up hemicycle of the two small-scale sequences. The maximum flooding surface of Sequence 7 is indicated by the development of a thick bioclastic rudstone with large oyster shells and the occurrence of glauconite at around 261.92 m. The boundary between Sequence 7 and 8 is poorly defined and is located at the top of a thick layer of intertidal Facies 12.

Sequence 8 is an asymmetrical sequence with one small-scale sequence. An increase in echinoids, crinoids and radial ooids indicates an increase of accommodation space. The texture of the radial ooid deposit changes from packstone to grainstone, reflecting the shallowing-up trend of this sequence. A well-cemented iron-stained hardground is interpreted as a flooding surface and marks the top of Sequence 8 (Figs. 2.8a and 2.8b).

Sequence 9 has three shallowing-up small-scale hemi-sequences that are characterized by Facies 12 overlying Facies 8. The top of each of these short sequences is marked by microkarst structures (for example at 240.54 m) (Fig. 2.6d), indicating an exposure surface. The occurrence of glauconite overlying these surfaces shows a flooding event that resulted in a considerable increase in accommodation space initiating the formation of the following small-scale sequence. An increase in thickness of the intertidal Facies 12 in each of the small-scale sequences suggests that Sequence 9 is a shallowing hemi-sequence.

The boundary between Sequence 9 and 10 is set at the irregular base of the lowstand Facies 13 at 229.80 m, which is interpreted to be an exposure surface. The initial deepening trend of Sequence 10 is recorded by an increase in grain-size, a textural change from mudstone to rudstone, the superposition of Facies 13 by Facies 12 and 9, and the increase in thickness of layers representing Facies 9. Again, a shallowing hemi-sequence follows the deepening, as indicated by repeated occurrences of Facies 9, each overlain by Facies 12. Relatively frequent facies changes and an increase in mudstone thickness above 218.76 m are interpreted to result from a change of subtidal to intertidal conditions.

The boundary between Sequence 10 and 11 is based on the occurrence of Facies 11 in the constituent small-scale sequences in Sequence 11. This level also marks the lower boundary

of the Eimbeckhausen Fm (Heunisch and Luppold, 2015). Above 203.88 m, the thickness of the Facies 9 interval drops considerably. Fenestral structures within Facies 12 in this interval indicate an upper intertidal environment. Facies 11 overlying Facies 12 underlines the shallowing-up trend of Sequence 11 from upper intertidal to supratidal.

### Large-scale sequences

Five large-scale sequences, based on the variations of the facies proportion in each medium-scale sequence, are differentiated (Fig. 2.4). The sequence boundary of the lowest large-scale sequence is set at the top of Sequence 1. Above this surface, the shallowing-up trend from Sequence 1 to 2 shown on the facies statistic curve is replaced by the deepening-up trend from Sequence 2 to 3. In the second large-scale sequence, the palaeobathymetric trend of deepening-up is reflected by the facies proportion of Facies 5, deeper than Facies 4, increasing from Sequence 2 to 3. In this large-scale sequence a regressive trend abruptly follows the deepening trend and results in the formation of the sequence boundary at around 294.00 m, marked by the Sandy limestone facies lying on this boundary. Similarly, the third large-scale sequence is also dominated by a deepening-up trend succeeded by a sudden regression leading to the formation of the sequence boundary at 276.65 m, marked by the occurrence of the Sandy limestone facies above this boundary. Above 276.65 m, a deepening-uptrend is reflected by an increase in the proportion of the relatively deep Facies 7 from Sequence 6 to 8. The maximum flooding surface of the fourth large-scale sequence is taken to be around 247.35 m at the position of Facies 7. The sequence boundary of the fourth large-scale sequence is again marked by the base of the Sandy limestone facies at 229.80 m. Above this boundary, a shallowing-up trend is indicated by the onset of evaporite deposition in Sequence 11.

### 2.5.3 Stratigraphic correlation

Heunisch and Luppold (2015) developed a biostratigraphic framework for the Eulenflucht-1 core based on ostracods and palynology. Following these authors, the biostratigraphic information is constrained to the interval above 278.00 m, belonging to the Early Kimmeridgian to Early Tithonian. It is noteworthy, however, that these zones reflect biozones defined for the North German Basin, and that these zones are only poorly correlated to the global chronostratigraphy. Nevertheless, a stratigraphic correlation of the results here to sections elsewhere has to rely on this biostratigraphic zonation. Stable carbon isotope curves were used as a tool for regional correlation in the Upper Jurassic deposits of the Swabian Alb (SW Germany) by Ruf et al. (2005a, b). The high-resolution  $\delta^{13}\text{C}$  curve here, although poorly constrained by biostratigraphy, is used as a tool to correlate

chemostratigraphically the Eulenflucht-1 core to sections elsewhere. It shows similar variation trends with the  $\delta^{13}\text{C}$  curves from Scotland (Nunn and Price, 2010; Nunn et al., 2009; Wierzbowski, 2004; Wierzbowski et al., 2006), Russia (Podlaha et al., 1998; Price and Rogov, 2009; Riboulleau et al., 1998; Wierzbowski et al., 2013), Poland (Wierzbowski, 2002, 2004), the Northern Alps and the Swiss Jura Mountains (Padden et al., 2001; Rais et al., 2007; Weissert, 2011; Weissert and Mohr, 1996), SW Germany (Bartolini et al., 2003; Ruf et al., 2005a; Wierzbowski, 2004), and North Germany (Kästner et al., 2010) (Fig. 2.11).

There are 6 pronounced carbon isotope shifts used for correlation. The broad positive excursion between 320.00 and 315.14 m, followed by the negative excursion until 300.00 m of the core is correlated to a similar succession in the Middle Oxfordian, documented elsewhere. The broad positive excursion between 300 and 287.95 m correlates to similar excursions described for the Late Oxfordian (Fig. 2.11). The following negative excursion until 275.43 m, which is within ostracod zones 9-12 (coeval with the *Baylei* ammonite zone), is comparable to the negative trend measured from the Late Oxfordian to Early Kimmeridgian elsewhere. The most positive  $\delta^{13}\text{C}$  values around depth 248.47 m fit with the positive excursion in the Late Kimmeridgian described by Rais et al. (2007), Weissert (2011), and Weissert and Mohr (1996), and is succeeded by a distinct, large-scale shift towards negative values during Latest Kimmeridgian to Early Tithonian (Fig. 2.11). The good stratigraphic correlation of the carbon isotope curve here with the sections elsewhere is striking. Especially if one takes into account the facies variations in the Eulenflucht-1 core and the related depositional environments. Nevertheless, the observed similarities infer that the diagenetic overprint of our carbon isotope values, although obvious (Bruckschen et al., 1992), may have changed the original carbon isotope signatures but not the overall stratigraphic trend.

As to sequence stratigraphy, the top boundary of Sequence 3 is correlated to the top surface of '*Florigemma*-bank', which is a major unconformity surface overlain by sandstone in the North German Basin. It is regarded as the base of the Ox6 boundary surface.

All these correlations, with the support by the published ostracod zonation (Heunisch and Luppold, 2015), allow for a rather specific chronostratigraphic assignment of the Eulenflucht-1 core (Fig. 2.11). However, the poorly constrained age information hinders the comparison of our sequence stratigraphic hierarchy to the 3rd- and 2nd-order sequence stratigraphic hierarchy of Hardenbol et al. (1998).

#### 2.5.4 Controlling factors of the large-scale sequence evolution

Marine ooids are grains forming in warm and shallow waters, and are therefore considered an important paleoenvironmental indicator for such environments (Opdyke and Wilkinson, 1990; O'Reilly et al., 2017). The Ooid packstone and grainstone facies between 321.00 and 277.80 m and the Radial ooid packstone and grainstone facies around 247.00 m reflect a warm climate period during the Middle Oxfordian and Late Kimmeridgian. Cessation of ooid formation between 277.78 and 247.30 m, and above 243.87 m, could be interpreted as the record of a cooling trend from the Latest Oxfordian to Early Kimmeridgian, and from the Latest Kimmeridgian to the Tithonian. The evaporites deposited above 202.00 m are considered to be the result of a persistent arid climate. This climatic evolution fits very well with the climates of the Late Jurassic time deciphered by Abbink et al. (2001). Since these facies changes are documented in the facies statistic curves reflecting the development of the large-scale sequences, the large-scale sequences are considered to be controlled by regional climate changes causing variations in depositional conditions and so facies. From the geochemical aspect, this assumption is endorsed by the in-phase variations of the facies proportion curve and  $\delta^{13}\text{C}$  curve (Fig. 2.4). There are great similarities in the  $\delta^{13}\text{C}$  trends noted here and those of other areas, where the  $\delta^{13}\text{C}$  variations were interpreted as the results of climate change during the Late Jurassic to Earliest Cretaceous (Nunn and Price., 2010; Weissert and Mohr, 1996). Therefore, the facies statistic curve varying in-phase with the  $\delta^{13}\text{C}$  curve supports the postulated climate control on the development of the large-scale sequences.

The shallowing-up trend throughout the Kimmeridgian shown in the facies statistic curve, however, is in conflict with the record of the 100 to 150 m sea-level rise from the Oxfordian to Kimmeridgian recorded in other European Basins (Hardenbol et al., 1998), and also with the deepening-up trend reflected by the  $\delta^{18}\text{O}$  curve from the Upper Oxfordian to Upper Kimmeridgian in southwest Germany (Ruf et al., 2005a). Since the analyzed core was located on the upthrow side of a syn-sedimentary fault active during Late Jurassic time (Gramann et al., 1997) (Fig. 2.2), this can be reconciled by postulating that the area was affected by local tectonic uplift caused by salt diapirism (Mönnig, 2005). Therefore, it is suggested that the development of the large-scale sequences in the Eulenflucht-1 core is controlled by both climate change and local tectonic movements.

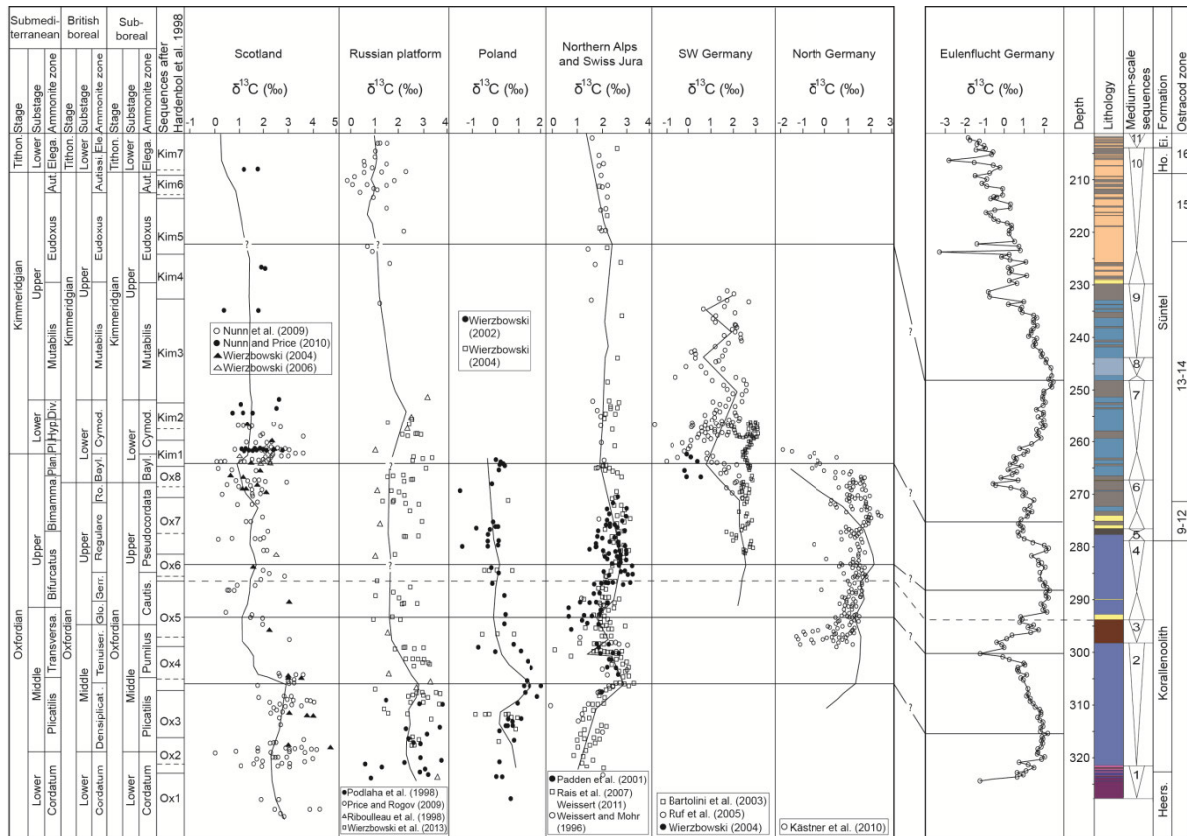


**Fig. 2.11** Compilation of carbon isotopic curves from Scotland (Nunn et al., 2009; Nunn and Price, 2010; Wierzbowski, 2004; Wierzbowski et al., 2006), Russian (Podlaha et al., 1998; Price and Rogov, 2009; Riboulleau et al., 1998; Wierzbowski et al., 2013), Poland (Wierzbowski, 2002, 2004), Northern Alps and Swiss Jura Mountains (Padden et al., 2001; Rais et al., 2007; Weissert, 2011; Weissert and Mohr, 1996), Southwest Germany (Bartolini et al., 2003; Ruf et al., 2005a; Wierzbowski, 2004), North Germany (Kästner et al., 2010), and the Eulenflucht-1 core. Dashed lines are the sequence stratigraphic correlated surfaces. Straight lines are the chemostratigraphic correlated surfaces

**2.6 Conclusions**

The Eulenflucht-1 core, consisting of Oxfordian to Kimmeridgian sediments, represents a succession formed in an outer ramp to restricted hypersaline lagoonal setting. Thirteen facies are identified based on their lithology, components and microscopic texture.

Depositional sequences at three different scales are identified. Small-scale sequences are defined by changes in grain-size, variations in the amount of components, fluctuations of the matrix content, the microscopic texture, and the vertical lithofacies stacking patterns. Medium-scale sequences are delimited by changes of facies combinations and the bundling of small-scale sequences. Large-scale sequences, which are differentiated by facies proportion statistics, are controlled by climate change and local tectonic movements. A shallowing-up trend during the Kimmeridgian was induced by regional tectonic uplift. This is the first sequence stratigraphic framework that covers the succession of the Oxfordian and



Kimmeridgian in the Lower Saxony Basin, and it can be used as a reference section for the Lower Saxony Basin.

Sequence stratigraphic, biostratigraphic and chemostratigraphic correlation helped to assign a chronostratigraphy to the succession analyzed, and demonstrates that using sequence stratigraphy and chemostratigraphy is a valid and practical approach for regional correlation in the North German Basin, especially in the Korallenoolith Fm, where age-diagnostic fossils are scarce.



## Chapter III

# **Sequence stratigraphy of the Upper Jurassic mixed siliciclastic-carbonate deposits in the North German Basin**

### **Abstract**

The Wendhausen-6 core, located in the Hildesheimer Wald, 30 km SE of Hannover, provides an insight into the Oxfordian deposits consisting of the Ornatenton, Heersumer, and Korallenoolith Formations. Eight facies are recognized based on the different fossil combinations, sedimentary structures, and the carbonate content variations. They are interpreted to be deposited in a transition area between a delta system and a carbonate ramp. Sequences of different hierarchies are delimited. Small-scale sequences are defined by the changes in components, grain size, and the vertical facies stacking patterns. Medium-scale sequences are bounded by distinctive exposure surfaces. These surfaces are characterized either by the enrichment of iron minerals or by the lowstand channel-fill sandstones overlying on them. Large-scale sequences are derived from the facies proportion statistics of each medium-scale sequence. Sequence stratigraphic correlation was achieved at the medium-scale sequence level, and three surfaces of the Oxfordian age were correlated across the North German Basin. The similar variation trend between the global sea-level curve and the facies statistic curve implies that sea-level fluctuations have a great control on the large-scale sequence evolution during the Oxfordian age. Covariation between the paleoclimate changes deciphered by the facies development and the paleotemperature changes reflected by Mg/Ca ratio, prove that the paleoclimate is another controlling factor of the facies development. The consistent paleotemperature fluctuation trends among Scotland, Russian platform, and the North German Basin during the Late Jurassic suggest that they are intimately connected at that time.

### 3.1 Introduction

Because of the scarcity of stratigraphic index fossils in the Upper Jurassic deposit in North Germany, the biostratigraphic correlation in this area is hindered (Gramann et al., 1997). Sequence stratigraphic analysis have been done in the Oxfordian and Kimmeridgian deposits in Switzerland, Spain, Scotland, and France, and the recognized medium-scale sequences are proved to allow the comparison of facies evolution in regions that are as much as 1000 km apart (Jank et al., 2006; Pittet and Strasser, 1998; Samankassou et al., 2003; Strasser et al., 1999, 2000). The sequence stratigraphic framework established by Gygi (2000) and Gygi et al. (1998) in northern Switzerland and southern Germany were even correlated with that of other European Basins. In Southwest Germany, sequence stratigraphic division has been achieved based on the facies variations, gamma-ray logs, carbon- and oxygen-isotopes, and palynofacies (Ruf et al., 2005a). In North Germany, sequence stratigraphy is also considered as a tool to provide a robust and testable high-resolution correlation (Betzler et al., 2007). Helm (2005) described the facies of the *Florigemma*-bank belonging to Korallenoolith Fm in detail and the main disconformity above *Florigemma*-bank was recorded across Süntel Mountains in North Germany. Sequence stratigraphic frameworks for the Oxfordian, Kimmeridgian, and the base of the Tithonian deposits have been established by Bai et al. (2017), Betzler et al. (2007), Cäsar (2012), and Kästner et al. (2010) in North Germany. However, detailed data referring to the Heersumer Formation belonging to the early Oxfordian is rare.

Climate influence and sea-level controls on the sequence stratigraphic development have been reported in some European Basins. According to Pittet and Strasser (1998) and Strasser et al. (2000), sequence stratigraphy and cyclostratigraphy are proven to be a good tool to understand paleoenvironmental changes affecting the areas comprised of the Swiss Jura, Spain, and northeast France. The control of the eccentricity induced sea-level fluctuations on the medium-scale sequence development in SW Germany was reported by Ruf et al. (2005a), while the sea-level impact on the sequence stratigraphy evolution in North Germany was recorded by Betzler et al. (2007). Bai et al. (2017) decipher the climate control on the sequence stratigraphic evolution based on the facies and carbon isotopic correlation data. However, no proxies that directly reflect the paleoclimate conditions have been recorded in North Germany.

The aim of this study is to establish a detailed sequence stratigraphic framework for the Heersumer and Korallenoolith Fms, in order to supplement the scarcity of the deposit information of the Heersumer Fm in the North German Basin, and to decipher the probable

controlling factors on these deposits. Herein, we focus on the Wendhausen-6 core with half of the core covering the deposits of the Heersumer Fm. In-situ analysis of the Mg/Ca ratios on the well-preserved oyster shells, which can be used as a paleotemperature proxy (Bailey et al., 2003; Klein et al., 1996; Nunn and Price, 2010), provides an insight into the paleoclimate variations during the Oxfordian time. A tentative basinwide sequence stratigraphic correlation for the Upper Jurassic deposits is achieved based on the existing data.

### 3.2 Geological setting

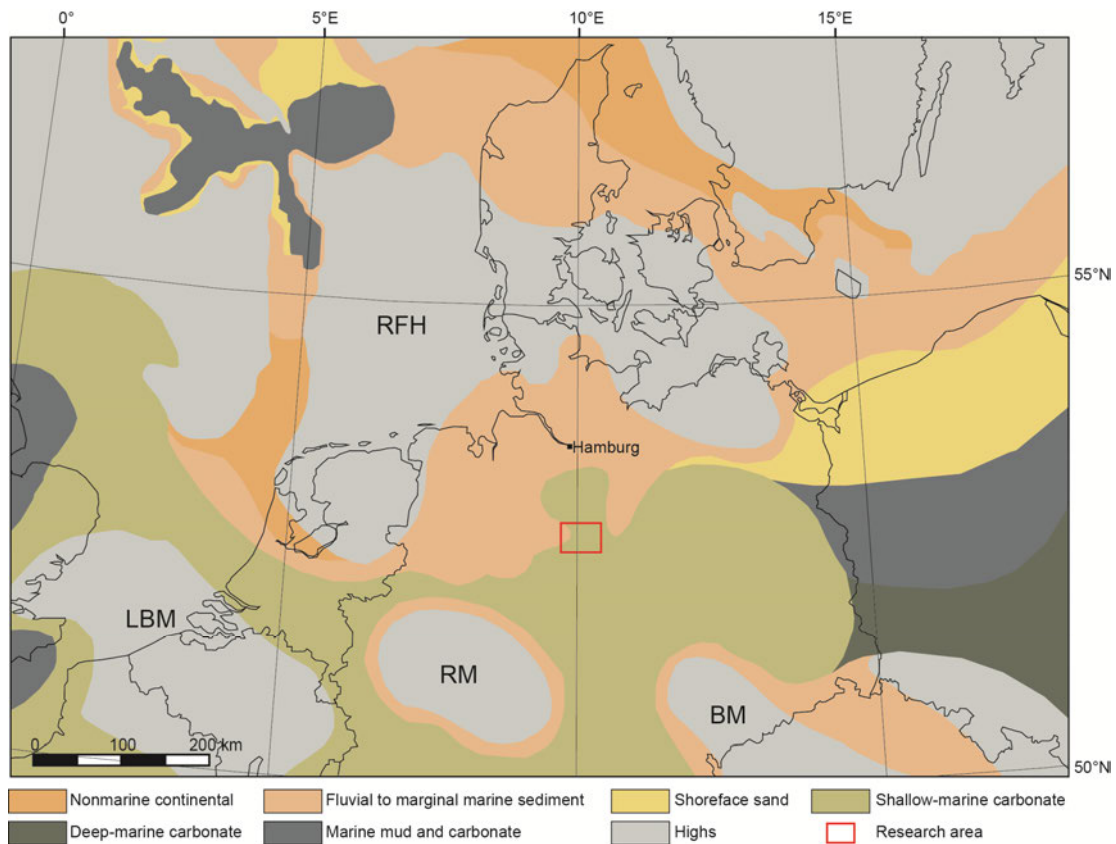


**Fig. 3.1** Oxfordian paleogeography and main sediment associations in northern central Europe. LBM: London-Brabant Massif; RM: Rhenish Massif; BM: Bohemian Massif; RFH: Ringkøbing Fyn High (modified from Ziegler, 1990; Thierry, 2000)

During the Late Jurassic, the North German Basin was bounded by the Ringkøbing Fyn High to the north, and by the London Brabant, the Rhenish and the Bohemian Massifs to the south (Fig. 3.1). Intense crustal extension across the Arctic-North Atlantic rift system and large-scale thermal uplift in the North Sea area started in the Middle Jurassic. Synsedimentary fault activities led to the subdivision of the North German Basin into small depressions with differential subsidence during the Late Jurassic (Gramann et al., 1997),

resulting in variations in the thickness of the deposits by tens of meters over relatively short distances (Hoyer, 1965).

Outcrops consisting of the Upper Jurassic deposits in Süntel, Wesergebirge, and Ith Mountains are well recorded (Fig. 3.2). The Korallenoolith Fm is a diachronous unit dominated by oolite and coral buildups (Bai et al., 2017; Betzler et al., 2007; Cäsar, 2012; Gramann et al., 1997; Kästner et al., 2008). The coral reefs, constrained in the *Florigemmbank*, comprised species-rich coral associations and microbialite according to Helm (2005). The Heersumer Fm is composed of marlstone rich in sponge spicules and rhaxes (Bai et al., 2017; Kästner et al., 2008). The analyzed succession, located in Hildesheimer Wald, contains the Korallenoolith, Heersumer, and the Ornatenton Fms. The Korallenoolith Fm is dominated by ooid and sandstone, while the Heersumer Fm is a mixture of spicules-rich calcareous-sandstone and ooid-rich limestone. The Ornatenton Fm consists of marls (Heunisch and Luppold, 2015).

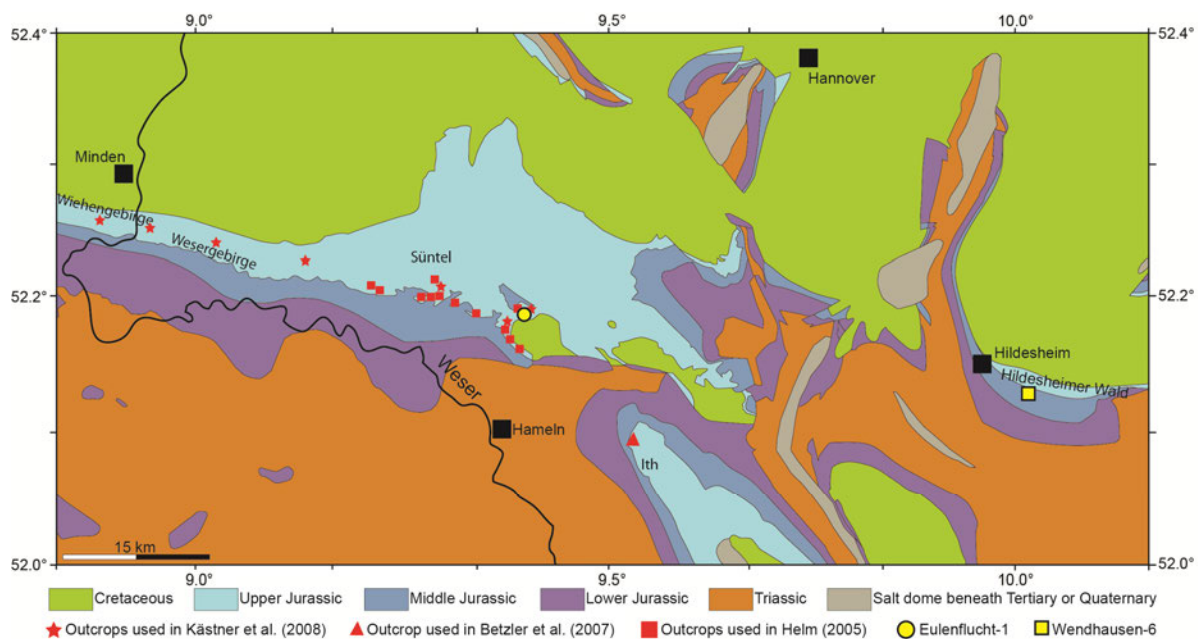


**Fig. 3.2** Geological map of the North German Basin with the location of Wendhausen-6 core, the Eulenflucht-1 core, and outcrops with the Upper Jurassic deposits analyzed by Bai et al. (2017), Betzler et al. (2007), Helm (2005), and Kästner et al. (2008) (modified from Kockel et al., 1996)

Because the scarcity of ammonites, a biostratigraphic division of the Upper Jurassic deposits in North Germany is based on ostracods, dinoflagellate cysts, charophytes, and spores and pollens (Gramann et al., 1997; Hardenbol et al., 1998; Schudack, 1994; Schulze, 1975; Weiss, 1995) (Fig. 3.3). As to the Wendhausen-6 core, ostracods and foraminifers are used as biostratigraphic fossil index. The foraminifer species *Vaginulinopsis pasquetae* and *Paleogaudryina heersumensis* are considered as the index marker of Upper Heersumer Fm.

Serie	Stage	Lithostratigraphy Northwest Germany	Subboreal Ammonite zonation	Ostracod zonation
Upper Jurassic	Kimm.	Korallenoolith Fm.	<i>Baylei</i>	7
			<i>Pseudocordata</i>	6
	Oxfordian	Heersumer Fm.	<i>Cautisnigrae</i>	5
			<i>Pumilus</i>	4
			<i>Plicatilis</i>	3
	Callovia	Ornatenton Fm.	<i>Cordatum</i>	2
			<i>Mariae</i>	1
Middle Jurassic	Callovia		<i>Lamberti</i>	

**Fig. 3.3** Lithostratigraphy scheme of the Middle and Upper Jurassic and their corresponding sub-boreal ammonite zonations and ostracod zonations (Gramann et al., 1997; Hardenbol et al., 1998; Ogg et al., 2012; Schudack, 1994; Weiss, 1995)

### 3.3 Material and methods

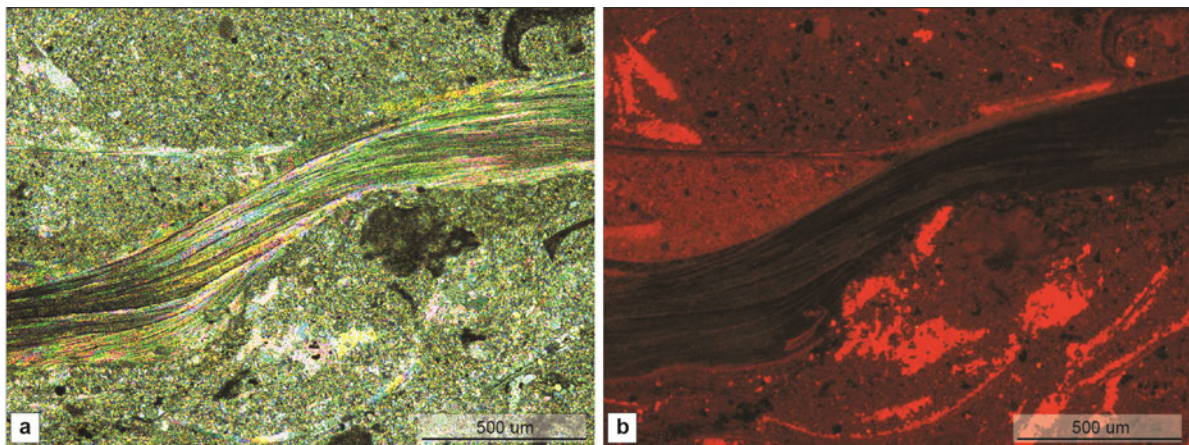


**Fig. 3.4 a** Oyster shell fragment with the well preserved intra-shell structure under cross-polarized microscope; **b** the same area as shown in **a** under cathodoluminescence microscope

The Wendhausen-6 core (52.122721°N, 10.072847°E) is located in the Hildesheimer Wald Mountains (Fig. 3.2). The 60-m-long core covers the deposit of the Upper Ornatenton Formation, the Heersumer Formation, and the Lower Korallenoolith Fm. The core is stored at the BGR core repository in Grubenhagen. A total of 57 samples were taken to produce

thin-sections for microfacies analysis, and for the measurement of the carbonate content. The carbonate content was measured in the Laboratory of the Institut für Geologie, Universität Hamburg, using the LECO SC-14DR analysis equipment with the temperature of 1350°C. To describe the texture of the sediments, the classification of Dunham (1962) with the modification by Embry and Klovan (1971) was used.

Six thin-sections from the Eulenflucht-1 core and 7 thin-sections from the Wendhausen-6 core with well-preserved oyster shells were chosen for in-situ Mg and Ca content measurement, using the Laser Ablation Inductively-Coupled Plasma Mass Spectrometry (LA-ICP-MS). They were measured in the School of Scientific Research Laboratory of China University of Geosciences (Beijing), using the Up193ss laser from NewWave company with a wave length of 193 nm. Carrier gas is helium with a flowing velocity of 0.94 L/min. Diameter of the laser spot is 100 µm. Laser frequency is 10 Hz. Pre-ablation time is 5 seconds and the ablation time is 45 seconds. The ICP-MS system is the Agilent Serie 7500a. Auxiliary gas is argon with a speed of 1.13 L/min. Power of Radio Frequency Generator is 1350 W. The element result is reported by ppm. The preservation of oyster shells was identified by the non-luminescent to dull-luminescent features under cathodoluminescence microscope and by the well observed original intra-shell structure under cross-polarized microscope (Fig. 3.4) (Aguirre-Urreta et al., 2008; Boggs and Krinsley, 2006; Hönig et al., 2017). Two to four points of the chosen oyster shells were measured on each thin-section.

### **3.4 Results**

#### **3.4.1 Facies description**

Based on the differences in lithology, carbonate content, components, and texture, eight lithofacies are identified. The graphic log of the Wendhausen-6 core is shown in Fig. 3.5.

##### **Facies 1: Marls**

This facies contains 30% - 50% carbonate content. Abiotic components encompass some quartz, pyrite, and rare ooids. Bioclasts include some calcispheres, foraminifers, bivalves, spicules, echinoids, rare serpulids, and gastropods. Deposits are poorly cemented and burrows can be observed (Fig. 3.6a). This facies alternates with Bioclastic ooid wackestone facies from base to 22.57 m. Between 15.10 and 20.13 m, this facies is interbedded with Bioclastic rudstone facies and Bioclastic wackestone and floatstone facies.

##### **Facies 2: Bioclastic ooid wackestone and packstone**



In this facies, abiotic components are common to some ooids, peloids, quartz, pyrite, and rare intraclasts. Bioclastic components include some bivalves, serpulids, echinoids, foraminifers, ostracods, calcispheres, and rare gastropods (Fig. 3.7a). Ooids have diverse nuclei such as bivalves, echinoids, and foraminifers, and its amount increases downwards from 20.94 to 30.71 m. Burrows are common in this facies, and bivalves are bored and refilled by anhydrite. Parts of its micrite matrix is dolomitized. The carbonate content more is than 70%.

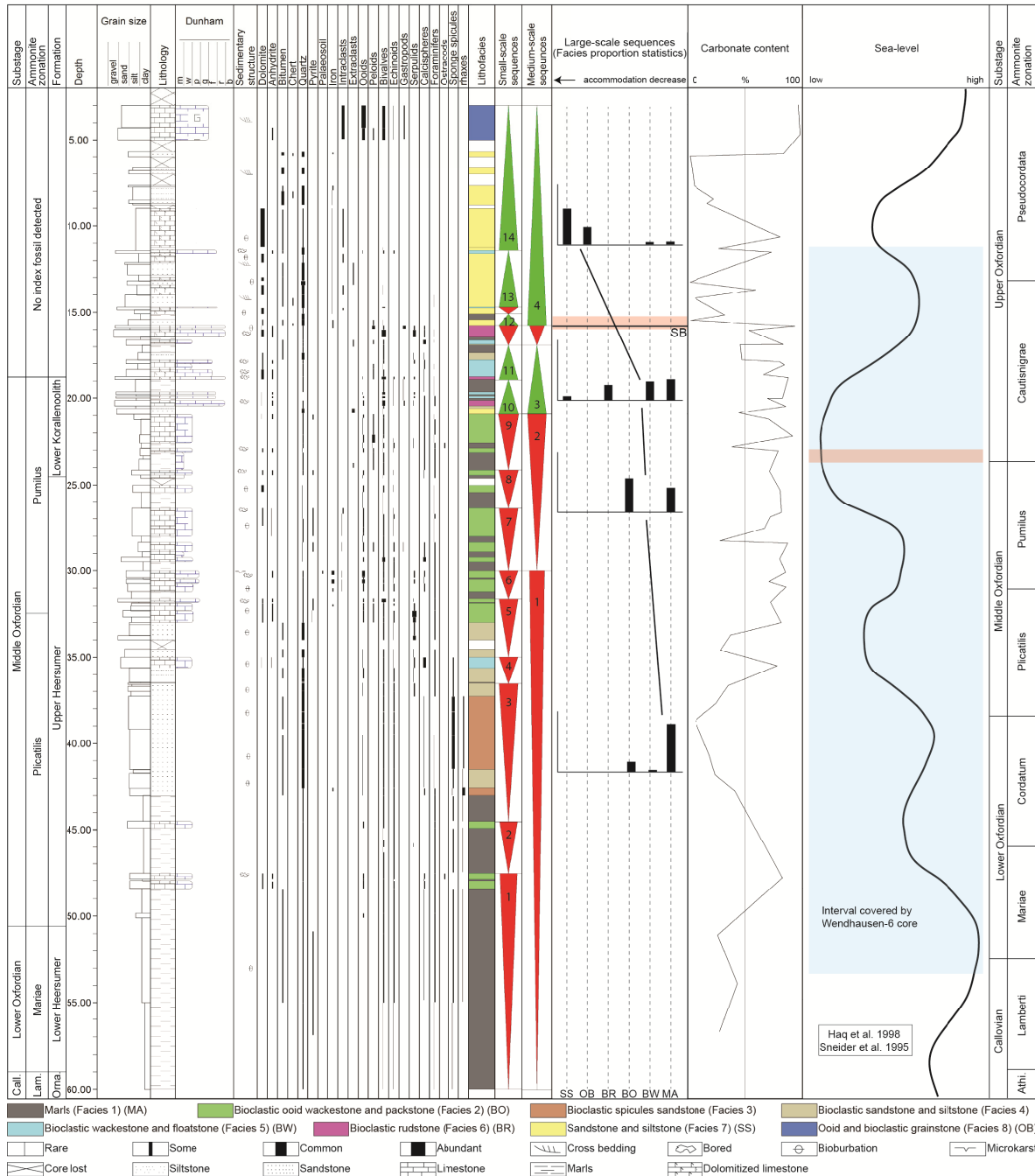


**Fig. 3.5** Lithostratigraphy of the Wendhausen-6 core with the abundance of components. Sequence stratigraphy division is based on components and texture changes, as well as facies superposition relationships.

Global sea-level fluctuations of the Middle to Late Jurassic time is from Haq et al. (1987) and Sneider et al. (1995)

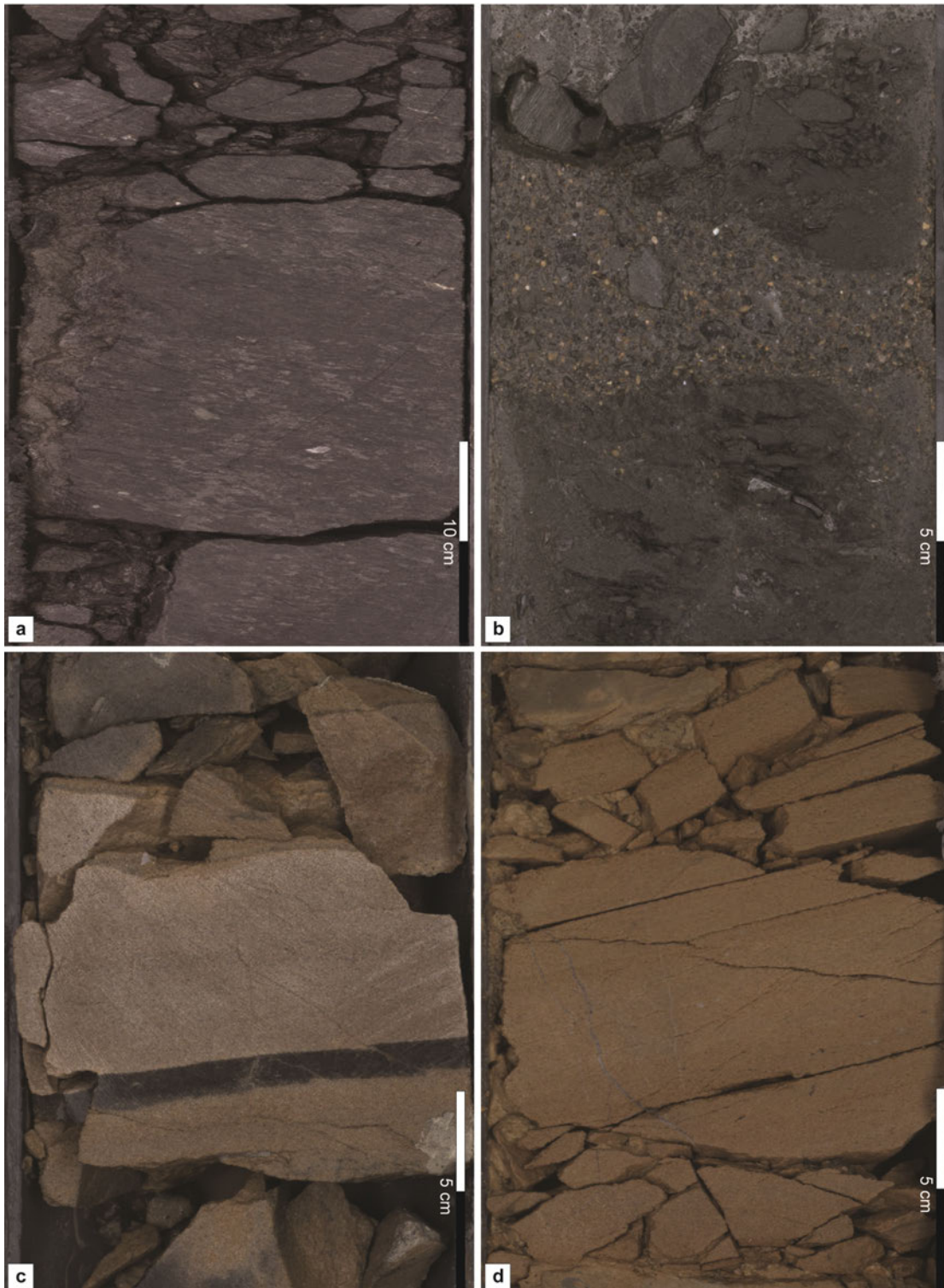


**Fig. 3.6** **a** Marls with burrows, 54.40 - 54.70 m; **b** Sandstone with large extraclasts overlying on an erosive surface, 20.63 - 20.78 m; **c** Black chert belt embedded in sandstone, 14.52 - 14.68 m; **d** Cross bedding developed in sandstone, 12.10 - 12.27 m

Facies 3: Bioclastic spicules sandstone



Main components of this facies are sponge spicules, rhaxes, and quartz (Fig. 3.7b). Other components are some bivalves, echinoids, foraminifers, and calcispheres. This facies occurs between 37.30 and 42.97 m with a carbonate content of less than 40% (Fig. 3.5). It is moderately cemented and impregnated by bitumen. This facies is interbedded with Bioclastic sandstone and siltstone facies.

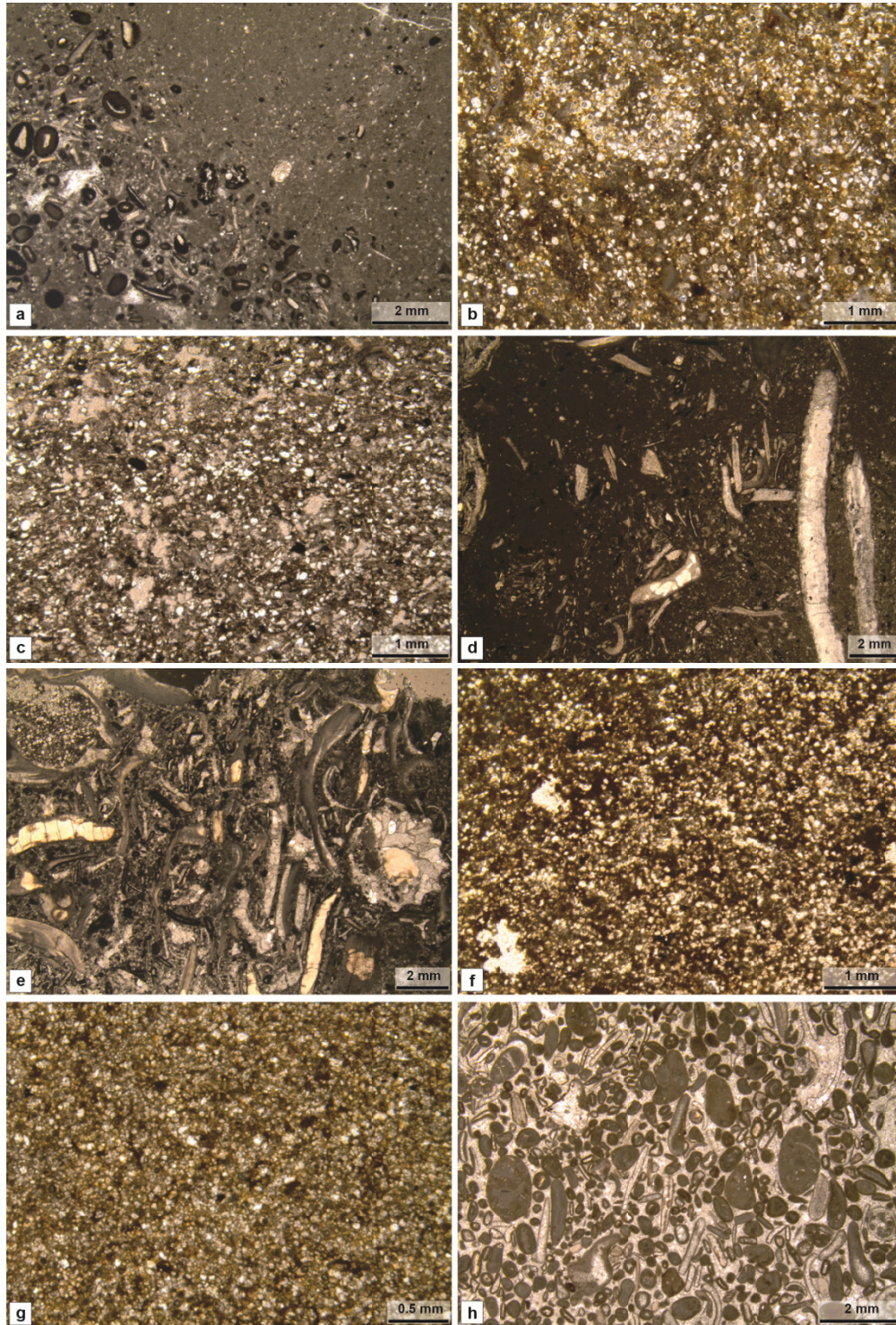


**Fig. 3.7** a Bioclastic ooid wackestone and packstone, at 30.91 m; b Bioclastic spicules sandstone with both transverse and longitudinal sections of sponge spicules, at 37.67 m; c Bioclastic sandstone to siltstone with

bioclastic fragments and common quartz components, at 36.64 m; **d** Large bivalve shells scattered in Bioclastic wackestone and floatstone, at 19.98 m; **e** Large shells supported Bioclastic rudstone, at 18.79 m; **f** Sandstone and siltstone with abundant quartz, at 7.70 m; **g** Crystalline dolomite with sub-euhedral dolomite rhombs, at 10.64 m; **h** Ooid and bioclastic grainstone with common ooids and bioclastic fragments and rare matrix, at 3.00 m

### Facies 4: Bioclastic sandstone to siltstone

Main component in this facies is quartz (Fig. 3.7c). Other components are some bivalves, echinoids, serpulids, foraminifers, and spicules, as well as rare ooids, calcispheres, and rhaxes. Burrows are common in this facies with mud clusters of 1 - 2 cm long included (Fig. 3.8a). Fining upward succession is shown, e.g., between 33.02 and 34.02 m. This yellowish facies are very poorly cemented with a carbonate content varying from 25% to 38% (Fig. 3.5). Bitumen impregnation is also observed. It occurs in two intervals (17.35 - 17.77 m, 33.00 - 42.53 m), and the matrix was partially dolomitized between 17.35 and 17.77 m.

### Facies 5: Bioclastic wackestone and floatstone

This facies contains some bivalve shells, echinoids, gastropods, and serpulids up to 2 - 4 mm large. Shells are bored and refilled by anhydrite (Fig. 3.7d). Other components are common to some quartz, peloids, calcispheres, rare foraminifers, and ooids (Fig. 3.5). Burrows are common and the matrix is partially dolomitized. This facies is well cemented with a carbonate content of 70% - 93%. It occurs in two intervals (14.69 - 20.01 m, 34.99 - 35.61 m), and is interbedded with Bioclastic rudstone facies and Marls facies between 15.77 and 20.01 m with gradual contact.

### Facies 6: Bioclastic rudstone

Large components in this facies are abundant oyster shells, common serpulids, and some gastropods larger than 2 mm. Other components are some echinoids, calcispheres, bivalve fragments, quartz, and some peloids. Oyster shells are bored, and borrows are refilled with anhydrite. In the interval 20.13 - 20.45 m, there are some foraminifers and ooids. This facies is well cemented with a dark gray color, and the matrix is partially dolomitized (Fig. 3.7e). Carbonate content in this facies is about 80% (Fig. 3.5). It occurs between 15.99 and 20.45 m, and is interbedded with the Marls facies and Bioclastic wackestone and floatstone facies.

### Facies 7: Sandstone and siltstone

Most of this brownish facies is impregnated by bitumen, and quartz is the main component (Fig. 3.7f). Between 20.60 and 20.91 m, there are common extraclasts 2 mm - 2 cm large,



and an erosive surface developed at the base of this interval (Fig. 3.6b). Black chert belts are embedded in this facies (Fig. 3.6c). Cross beddings accompanied by high rock porosity occur at intervals of 6.80 - 7.00 m, 12.10 - 12.80 m, and 14.06 - 14.16m (Fig. 3.6d). This facies is poorly cemented with parts of the interval between 9.00 and 15.11 m severely dolomitized (Fig. 3.7g). Carbonate content in this facies is below 7% with exceptions of values of 60% - 80% in the dolomitized parts. This facies occurs in two intervals (5.71 - 15.78 m, 20.60 - 20.91 m).

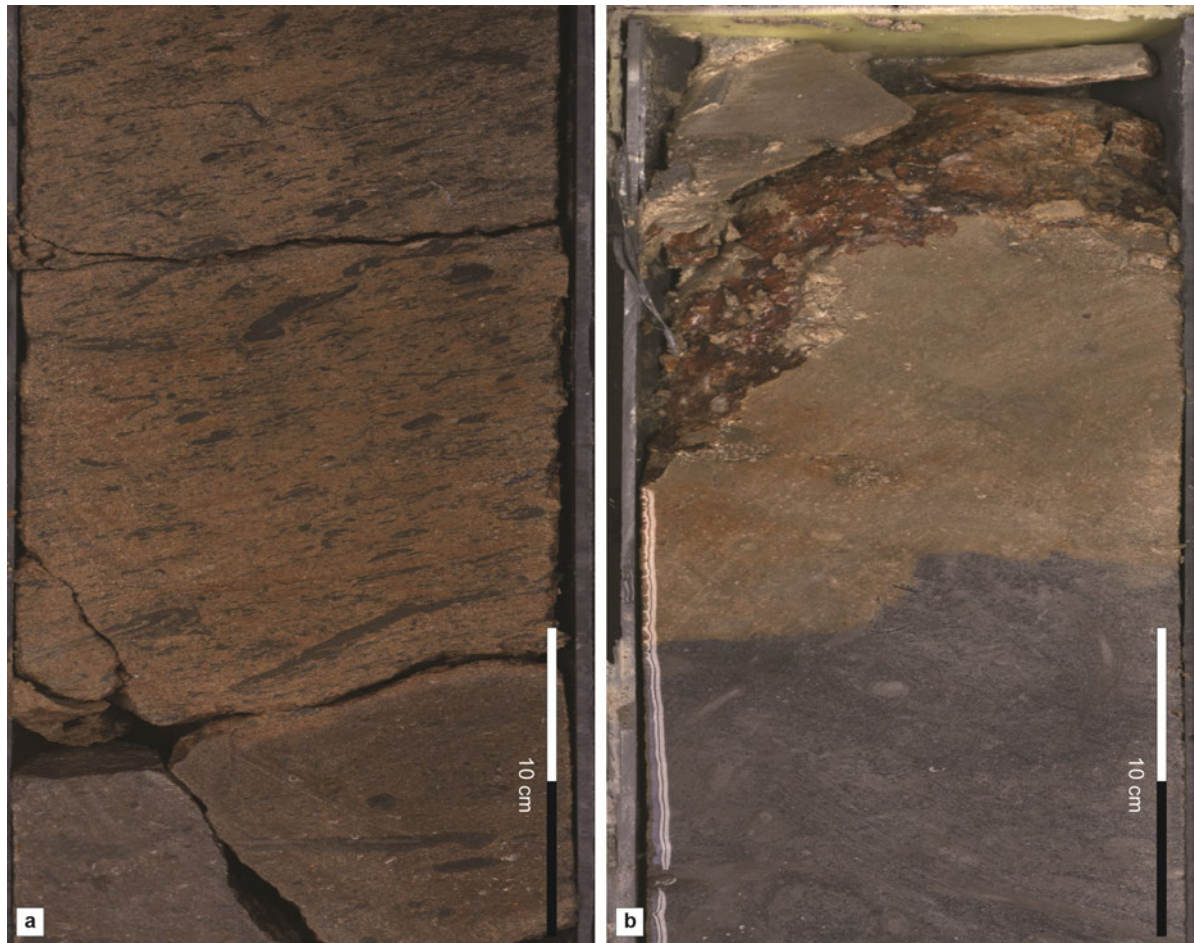


**Fig. 3.8** **a** Sandstone section with a sharp irregular base and the inclusion of large mud clusters in it, 33.50 - 33.80 m; **b** The exposure surface indicated by the occurrence of iron mineral, 30.00 - 30.30 m

#### Facies 8: Ooid and bioclastic grainstone

This facies is composed of common ooids, bivalves, intraclasts, some gastropods, peloids, and rare echinoids (Fig. 3.7h). Bivalves are about 2 mm large, and some of them are bored and refilled with anhydrite. Most of the ooids are micritic ooids, whereas few of them has concentric cortical fabric. Nuclei of ooids contain gastropods, intraclasts, and some other bioclasts. This facies is grain supported without micrite matrix, and occurs between 3.00

and 5.00 m with cross bedding developed between 3.80 and 3.90 m. Some solution seams appears in this interval.

### 3.4.2 Mg/Ca data

The Mg/Ca ratios of the well preserved oyster shells are presented in Table 3-1. The Mg/Ca ratios of the Eulenflucht-1 core samples are between 1.84 and 11.27, with the average values of samples at each depth varying between 2.71 and 8.59 and displaying an increase from 307.03 to 240.59 m. The Mg/Ca ratios of the Wendhausen-6 core samples are between 1.96 and 10.17, with the average values of samples at each depth varying between 2.25 and 5.71 and the highest value at 16.05 m.

**Table 3-1** Mg/Ca data of the well-preserved oyster shells from the Eulenflucht-1 and Wendhausen-6 core

Eulenflucht-1		Wendhausen-6	
Depth (m)	Mg/Ca (mM/M)	Depth (m)	Mg/Ca (mM/M)
228.95	2.91	4.67	6.35
228.95	4.14	4.67	6.51
228.95	10.68	4.67	4.04
240.59	11.27	4.67	3.88
240.59	5.91	11.5	5.55
261.63	4.66	11.5	4.36
261.63	3.11	11.5	2.87
261.63	9.17	11.5	2.37
261.63	10.70	16.05	3.58
293.08	5.62	16.05	3.39
293.08	4.82	16.05	10.17
307.03	2.62	17.87	1.96
307.03	3.68	17.87	8.62
307.03	1.84	20.45	4.20
318.6	9.81	20.45	4.15
318.6	2.87	20.45	5.85
		33.67	2.43
		33.67	2.06
		34.57	3.02

### 3.5 Discussion

#### 3.5.1 Facies model interpretation

Establishment of a facies model for Wendhausen-6 core is derived from the depositional environment interpretation of each facies based on their different fossil combinations, sedimentary structures, and carbonate content. Facies with rare marine fossils and a carbonate content less than 40% are thought to be associated with a deltaic system fed by terrestrial supply. The abundant dolomite encompassed in the sandstones is regarded as diagenesis product, thus is not used for the original environment interpretation. On the contrary, the facies containing grain supported ooid deposits with cross bedding, rare matrix content, and a carbonate content of more than 50%, signal the high water energy regime above fair weather wave base (FWWB) in a normal marine setting. Increase in the matrix content and the texture change from grain supported to matrix supported hints the transfer from a high water energy setting to a low water energy setting below FWFB.

Facies 1 is assigned in the tranquil water environment under the storm wave base (SWB). A large proportion of matrix composed of micrite and clay, and the small size of the diverse fauna components such as stenohaline echinoids, foraminifers, and sponge spicules and rhaxas in this facies indicate the normal marine regime with low water energy that allows the deposit of fine grain sediments. According to Kästner et al. (2008) and Bai et al. (2017), deposits with sponge spicules and rhaxas in the Heersumer Fm was formed below SWB with low water energy and a certain oxygen deficiency. The presence of pyrite and the dark grey color of this facies both endorse the assignment of this facies in the reducing ambience under SWB with few water oscillation.

Facies 2 is interpreted as a deposit that formed under the FWFB. According to Medwedeff and Wilkinson (1983), ooids with concentric cortexes suggest sufficient water energy rotating the grains and keeping the frequent abrasion of the original radial calcite crystals in each cortex. Inclusion of some ooids in this facies thus indicates a medium to high hydrodynamic environment (Strasser, 1986). However, large proportion of matrix in this facies help to assign it to an environment with medium water energy, which is not high enough to winnow much of the matrix. A carbonate content of more than 70% implies the little influence of the terrestrial influx on it. Therefore, this facies is interpreted to be deposited under FWFB in normal open marine environment adjacent to the places where the ooid grainstone can be formed.

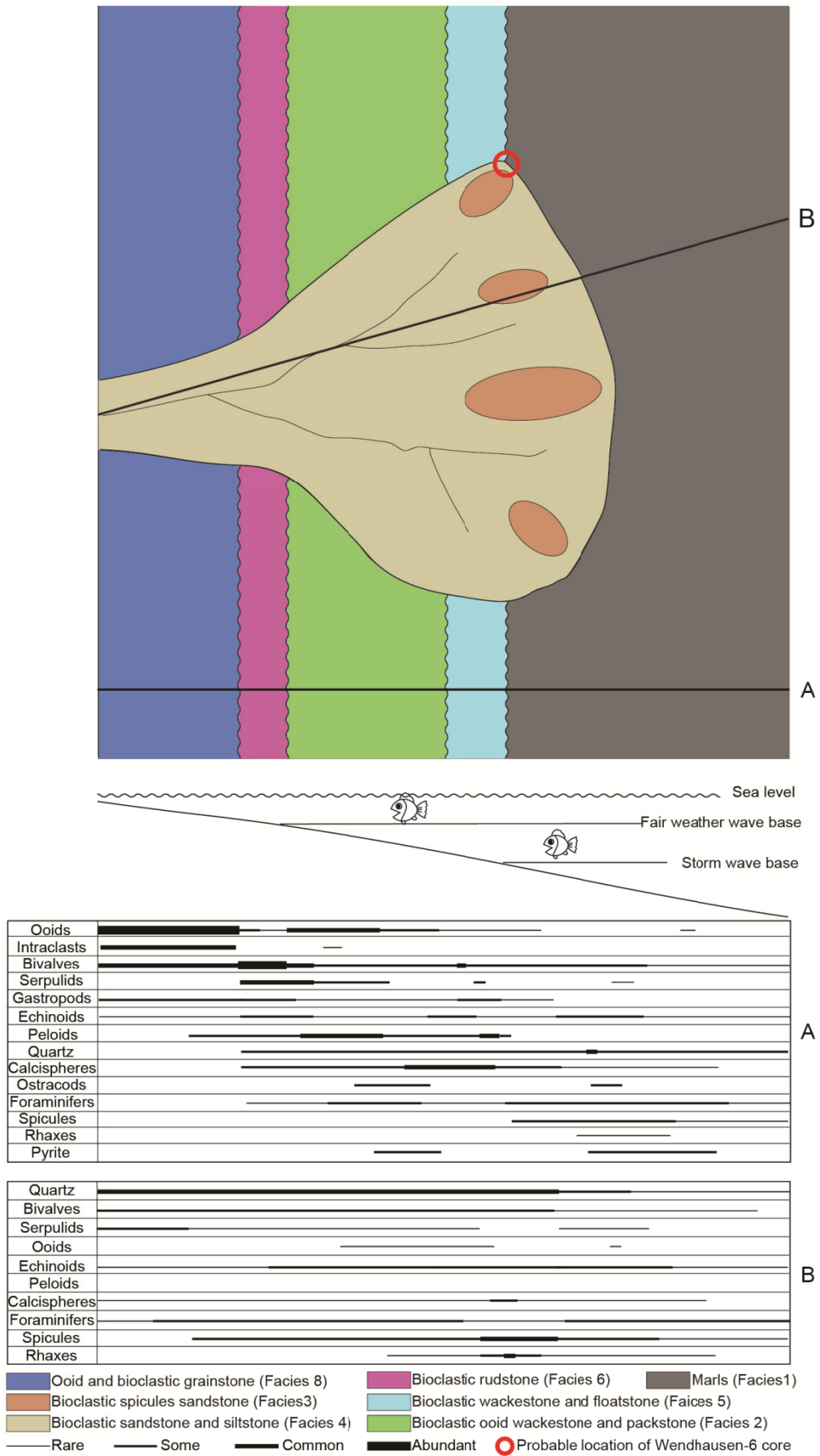


Fig. 3.9 Facies model of Wendhausen-6 core



Facies 3 is regarded as deep water deposit below and around SWB. The occurrence of abundant sponge spicules indicates a depositional environment in quiet water. According to Pisera (1997), the Oxfordian assemblage is dominated by *hexactinellid* sponge, which could tolerate the extreme settings below the zones of coral facies and mixed 'lithistid'-*hexactinellid* growth in deep water (Leinfelder et al., 1996). The interbed of sponge reefs and marl layers identified between 33.00 and 44.50 m was also recorded in south Germany and Spain by Pittet et al. (2000) as deep-shelf deposit. Sponge spicules derived from sponge reefs in the North German Basin and eastern Paris Basin were interpreted as deposits under SWB (Bai et al., 2017; Carpentier, 2007; Kästner et al., 2008). But the incorporation of common quartz component and the carbonate content of less than 40% with a minimum of 7% in interval 37.30 - 41.50 m indicate an association of Facies 3 with deltaic deposit. Sponges developed in the interdistributary bay on the proximal prodelta facies was reported in the Lengwu Formation in South China by Shen and Kawamura (2001). Therefore, the large amount of spicules and quartz help to locate this facies not far from this area, in the interdistributary bay of the proximal prodelta below and around SWB.

Facies 4 is ascribed to deltaic deposit because of the dominance of sub-angular to sub-round quartz component and the carbonate content of 25% - 38%. Fining upward sandstone to siltstone successions found in intervals of 33.02 - 35.02 m, 35.60 - 37.02 m, and 41.52 - 41.48 m, and inclusion of mud cluster, as well as the sharp base of the sandstone sections (Fig. 3.8a), indicate that this facies is deposited in distributary channels. The superposition of Facies 4 on Facies 3 shows they are deposited in adjacent areas. Therefore, Facies 4 is supposed to be deposited in the distributary channels which enclose the interdistributary bay where Facies 3 was deposited.

With a carbonate content of more than 70%, Facies 5 is supposed to be deposited on a carbonate ramp. A high percentage of micrite matrix indicates a low hydrodynamic condition, while the presence of some large bivalve fragments indicates a depositional setting above SWB where intermittent high energy waves make the deposit of large components possible.

Facies 6 is interpreted to be deposited above FWFB. Abundant components larger than 2 mm composed of oyster fragments, serpulids, and gastropods, and the large grain supported texture both show a high hydrodynamic condition. This facies is comparable to the Oyster-serpulid rudstone facies defined in the Eulenflucht-1 core by Bai et al. (2017), which is formed below and around FWFB. However, features of the deposits indicating low to moderate water energy described by Bai et al. (2017), e.g., the occurrence of pyrite and the

*Terebella-Tubiphytes* micro-encrust association, in the Oyster-serpulid rudstone facies are absent in Wendhausen-6 core. Therefore, this facies is considered as high water energy deposit above and around FWWB.

In Facies 7, abundant quartz components, and a carbonate content less than 7% both indicates a terrestrial origin of this facies. The occurrence of cross bedding (Fig. 3.6d) shows the existence of current movement. The erosive base of this facies (Fig. 3.6b), as well as the large size of the grains lying on the erosive base help to assign this facies as a channel deposit. The lack of fossil debris signifies a not fully marine environment. Therefore, this facies is interpreted as a channel-fill deposit on delta front.

Facies 8 is interpreted as a deposit that formed above FWWB. Biogenic components and intraclasts about 2 mm large, and the concentric ooids about 0.5 mm in diameter (Fig. 3.7h), which is similar to the ooids described by Strasser (1986), indicate a high water energy environment. Rare micrite content and the tangential structure of ooids are evidences for a hydrodynamic condition that is high enough to keep winnowing the fine matrix and rotating the grains to form the concentric cortices. Cross bedding result from strong water movement is a sign of deposit above FWWB (Betzler et al., 2007). This facies is comparable to the Ooid packstone and grainstone facies and the oolites facies described by Bai et al. (2017) and Betzler et al. (2007) respectively, both of which are deposits above FWWB.

Based on the facies interpretation, a transition area between a deltaic deposit system and a normal marine carbonate ramp is inferred to be the depositional environment for the Wendhausen-6 core (Fig. 3.9). Facies with carbonate content less than 40% are assigned to the deltaic system, while the others to a normal carbonate ramp. This interpretation is endorsed by the foraminifer assemblages discovered in Wendhausen-6 core. Arenaceous foraminifer assemblage composed of genera *Trochammina*, *Textularia*, *Ammobaculites*, and *Haplophragmium*, and the calcareous assemblage composed of genera *Lenticulina*, *Rectoglandulina*, *Frondicularia*, *Dentalina*, *Nodosaria*, *Astacolus*, *Eoguttulina*, and *Citharina* described by Nagy et al. (1984) were found in Wendhausen-6 core. According to Nagy et al. (1984, 2010), arenaceous foraminifer assemblage is ascribed to a delta-influenced area. Calcareous assemblages, although dominating the modern delta environment (Adegoke et al., 1976; Lutze and Wolf, 1976), were thought not well adapted to delta-dominated environment during the Jurassic and thus represent normal marine environment (Barnard et al., 1981; Nagy et al., 2010). Deltaic deposits of Callovian and Oxfordian age were also widely recorded in other European Basins such as Terschelling Basin and Dutch Central Graben (Abbink et al., 2006; Wong, 2007).

### 3.5.2 Sequence analysis

Sequences of three hierarchies are recognized. They are small-, medium-, and large-scale sequences. 14 small-scale sequences of 1 - 12 m thick are defined by changes of their grain components, variations of grain size, and the superposition of the constituent facies (Fig. 3.5). An increase in grain size and abundance, and the superposition of shallower facies overlying deeper facies all are indicators of a shallowing-up trend, and the reverse succession represents the deepening trend. 4 medium-scale sequences of 5 - 30 m thick are identified. Small-scale sequences with the same constituent facies make up a medium-scale sequence. Boundaries of the medium-scale sequences are defined by the exposure surface indicated by the occurrences of iron mineral and the lowstand channel-fill sandstones which are considered as formed during sea-level fall. Large-scale sequences are derived from the facies proportion statistics of each medium-scale sequence. Kerans and Tinker (1997) described that facies proportion statistics per medium-scale cycle reflect the large-scale cycles superimposed on the medium-scale sequence. Abrupt shallowing trend reflected by the facies proportion statistic curve is considered as the sign of relative sea-level fall and is supposed to represent the large-scale sequence boundary.

Small-scale sequences are marked as SS 1 - 14, and medium-scale sequences are marked as S 1 - 4. The concept of accommodation to sediment supply (A/S) cycles (Cross et al., 1993; Cross and Lessenger, 1998; Homewood et al., 2000) is used to describe each sequence.

#### Small-scale sequences

SS 1 - 2 are shallowing-up hemicycles defined by the increase in ooid component and the increase in grain size from the Facies 1 formed below SWB to the overlying Facies 2 formed above SWB. Their top limits are identified by the occurrences of Marls representing flooding surfaces.

SS 3 is also a shallowing-up sequence reflected by the increase in grain size upcore. The superposition of Facies 3 and 4 representing prodelta deposits on the Facies 1 representing under SWB deposits is considered as a result of the delta seaward progradation during reduction of A/S ratio. The repeated facies changing rhythm of Facies 4 overlying Facies 3 is considered as autocyclic deposits probably caused by the migration of distributary channel and not a response to A/S ration change. A flooding surface reflected by the occurrence of the 10 cm thick Marls at around 36.50 m marks the top boundary of SS 3.

SS 4 is another shallowing-up hemicycle, reflected by the increase in grain size and the facies shift from Facies 1 to 5.

The shallowing-up SS 5 is determined by the increase in ooid and large serpulid components, and by the Facies 2, representing deposit around FWWB, overlying the Facies 4, representing the prodelta facies around SWB.

The shallowing-up SS 6 - 9 display the same facies superposition rhythm of Facies 2 overlying Facies 1. Marls overlying the thick ooid packstone points to the flooding events that record the base of a shallowing hemicycle.

SS 10 is a deepening-up hemicycle. The base of SS 10 is reflected by the occurrence of lowstand Facies 7. The erosive base of Facies 7 around 21.00 m and large extraclasts (Fig. 3.6b) both show this is an unconformity surface caused by sea-level fall. The deepening trend is reflected by the decrease in grain size and by the facies shift from Facies 7 via Facies 6, which is deposited above FWWB, to Facies 5 and 1 that formed around and below SWB.

The following fining upward succession with the facies changing from Facies 6 via Facies 5 to Facies 1 composed the deepening hemicycle of SS 11, while the reverse shift of facies from Facies 1 to 6 formed the shallowing hemicycle of SS 11. The occurrence of the 0.5 m thick marls shows the place with highest A/S ratio in this small-scale sequence.

SS 12 is also a complete sequence. The base of this sequence is again indicated by the occurrence of the lowstand Facies 7. The deepening hemicycle is defined in the fining upward succession, while the coarsening upward succession denotes the shallowing hemicycle. Severely dolomitized intervals were not considered during sequence stratigraphy analysis, as they are diagenetic products.

SS 13 and 14 both are deepening hemicycle with the base marked by the occurrence of the lowstand Facies 7. Their deepening trend is reflected by the facies changing from Facies 7 to Facies 5 formed above SWB, and to Facies 8 formed above FWWB, respectively. The top boundary of SS 14 is not detected here limited by the length of the core date.

#### Medium-scale sequences

S 1 is a shallowing-up hemi-sequence composed of 6 small-scale sequences. Three of the constituent small-scale sequences (SS 1, 2, and 6) have the same facies combination consisting of Facies 1 and Facies 2, while the other three small-scale sequences (SS 3, 4,

and 5) have prodeltaic facies. The absence of these prodelta deposits in SS1 and 2, their incorporation in SS 3, 4, and 5, and its retreat from the SS 6 are regarded as a result of the lateral migration of a delta system, and not taken into account during medium-sequence division. The Wendhausen-6 core is thus inferred to be located on the edge of the delta lobe, at the transition area of a delta system and a carbonate ramp (Fig. 3.9), responding sensitively to the delta lateral migration. The shallowing trend of S 1 is reflected by the decrease of the small-scale sequence thickness upwards. The large thickness of SS 3, which deviates this trend could be caused by the fast accumulation of the influx of deltaic deposit. The top limit of this facies is set on an exposure surface, indicated by the presence of abundant iron mineral and pedogenic grains (Fig. 3.8b).

S 2 is a shallowing-up hemi-sequence consisting of three small-scale sequences (SS 7 - 9) with the same facies stacking pattern and the same A/S reducing trend. Boundary between S 2 and 3 is set at the base of the lowstand Facies 7 which signifies the initiation of a sea-level fall.

S 3 is a complete sequence, composed of two small-scale sequences (SS 10 and 11). The deepening hemi-sequence is featured by the facies switching from the lowstand Facies 7 via Facies 6 formed in shoreface area to Facies 5, 4 and 1 formed in offshore transition area and offshore area, respectively. The increase in the thickness of Facies 5 and 1 also implies the increase in A/S ration. Maximum flooding surface is indicated by the occurrence of Marls at around 16.90 m with the finest grain size in this sequence. The shallowing-up hemicycle of SS 11 composed the shallowing hemi-sequence of S 3.

The boundary between S 3 and 4 is another irregular base of the lowstand Facies 7. The occurrence of the Sandstone and siltstone of 10 m thick above this surface is comparable to the quartz-rich facies described by Bai et al. (2017) and Kästner et al. (2010) in Eulenflucht-1 core and the outcrops in Süntel Mountains respectively. This boundary is thus thought to be the main unconformity (“Hauptemersion” or “Hauptdiskontinuität”) located on the top of the *Florigma*-bank, which can be correlated across the Lower Saxony Basin (Helm, 2005; Helm and Schülke, 2006). Three small-scale sequences (SS 12 - 14) are included in S 4. They compose a deepening hemi-sequence, because the increase in the thickness of each small-scale sequence upcore and the incorporation of the Facies 8 in SS 14. The top boundary of S 4 is not detected because of the limit of the core data.

Large-scale sequences

Two large-scale sequences are differentiated based on the facies proportion statistic curve. The sequence boundary is set at the top of S 3, defined by the abrupt considerable decrease in the accommodation space at this point. The large-scale sequence below this boundary, consisting of S 1, 2, and 3, is a shallowing-up sequence with a slight decrease in accommodation. The large-scale sequence above this boundary is not fully recorded due to the limit of the core data.

The sea-level fluctuations for NW Europe deciphered by Haq et al. (1987) and Sneider et al. (1995) showed a decreasing trend from Late Callovian to Middle Oxfordian. The lowest sea-level point during the Upper Jurassic time was recorded at the boundary between the Middle and Upper Oxfordian substage, which can be comparable to our large-scale boundary located on the top of S 3. The covariation of the facies proportion curve and the sea-level fluctuations shows a great potential of the sea-level control on the large-scale sequence evolution (Fig. 3.5).

### 3.5.3 Climate control on the sequences evolution

Marine ooids are grains forming in warm and shallow waters (Opdyke and Wilkinson, 1990; O'Reilly et al., 2017). Therefore, ooids are considered as an important paleoenvironmental indicator for such environments. The increase in the thickness of the Bioclastic ooid wackestone and packstone facies (Facies 2) and the ooid component from 60.00 to 20.94 m reflects a warming climate period from the Late Callovian to the Middle Oxfordian (Fig. 3.5). The occurrence of coral debris between 19.65 and 20.00 m recorded by Heunisch and Luppold (2015) is another signal of warm climate during the Middle Oxfordian substage. The Ooid and bioclastic grainstone facies (Facies 8) between 3.00 and 5.00 m indicates another warm period.

The aforementioned climate change is echoed by the variations in paleotemperature index: ratio of Mg/Ca in well-preserved oyster shells. Mg/Ca ratio in biogenic calcite, e.g., in foraminifers, belemnites, and oysters, were proved to covary with ambient water temperature (Bailey et al., 2003; Bougeois et al., 2016; Klein et al., 1996; Mouchi et al., 2013; Nunn and Price, 2010). The relationship between Mg/Ca ratio and paleotemperature is best described by an exponential curve  $(Mg/Ca)_{\text{calcite}} = Be^{AT}$ , where A specifies the Mg/Ca dependence on temperature, T is the calcification temperature, and B is the species-specific pre-exponential constant (Bailey et al., 2003; Lear et al., 2002). The Mg/Ca ratio of the well-preserved foraminifers and belemnites were proved to be a reliable and valuable proxy for calculating the paleotemperature of Middle-Upper Jurassic (Nunn and Price, 2010; Wierzbowski et al., 2013). As the parameter B in the equation mentioned above is species-

specific constant, the equations used for foraminifers and belemnites need to be calibrated before applied here for oyster shells. But based on the general equation, no matter what value should be assigned to parameter B, it is pronounced that the in-phase changing relationship between paleotemperature and the Mg/Ca ratio of oyster shells will remain. Therefore, since no equation calibration for oyster shells has been done, absolute paleotemperature calculation is not straightforward. Instead, variations in original Mg/Ca values are used to reflect the paleotemperature changing trend. Intervals with high values of Mg/Ca ratio represent warm periods, while those with low values of Mg/Ca ratio represent cool periods. Two warming trends in Wendhausen-6 core are recorded from 35.00 to 15.00 m and from 10.00 to 5.00 m (Fig. 3.10). The warm period with the Mg/Ca about 6 mMol/Mol around the *Florigemma*-bank is comparable to the warm interval in Eulenflucht-1 core around the *Florigemma*-bank, which also has a relatively high Mg/Ca value of 6 mMol/Mol. Furthermore, this warm interval is able to be correlated with the warm period during the late Middle Oxfordian recorded in Scotland (Fig. 3.10). The warmest period recorded in Eulenflucht-1 core in *Eudoxus* ammonite zonation with the Mg/Ca value of 8 mMol/Mol is comparable to the warmest period recorded in Scotland and Russian (Fig. 3.10) (Nunn and Price., 2010; Price and Rogov, 2009). The above climate variation is also consistent with the climate record of the Late Jurassic time deciphered by Abbink et al. (2001).

Facies changes are documented in the facies statistic curves reflecting the development of large-scale sequences, and secular paleotemperature variations are deciphered by the Mg/Ca data. Coincident variations between the climate inferred by the development of facies, and by the values of paleotemperature proxy, prove that the climate has a great impact on the deposits, as suggested by Bai et al. (2017) in Eulenflucht-1 core.

#### 3.5.4 Sequence stratigraphic correlation

Detailed sequence stratigraphic framework with three hierarchies have been established for the deposits in Korallenoolith Formation in Lauensteiner Pass (Betzler et al., 2007) and for the deposits from Heersumer to Eimbeckhausen Formations in Eulenflucht-1 core (Bai et al., 2017) in the Lower Saxony Basin. These published data together with the sequence stratigraphy established in Wendhausen-6 core make a tentative sequence stratigraphic correlation across the Lower Saxony Basin possible.

Small-scale sequences are thought to be easily affected by autocyclic process such as distributary channel swinging in Wendhausen-6 core. Involvement of the autocyclic processes in the oolithe shoal successions are also recorded in the short-term cycles in the



Lauensteiner Pass and in Swiss Jura Mountains (Betzler et al., 2007; Samankassou et al., 2003). Therefore, the sequence stratigraphic correlation is based on the medium-scale sequences. Deposits of the Heersumer and Lower Korallenoolith Formations in Wendhausen-6 core and deposits in the Korallenoolith Formation in Lauensteiner Pass are considered to be controlled by the sea-level fluctuations (Betzler et al., 2007). The decrease in the accommodation space in Kimmeridgian is attributed to the local uplift tectonic movement outpaced the sea-level rise (Bai et al., 2017). Thus, sequence stratigraphic correlation in Kimmeridgian deposits should be cautious with consideration of local tectonics, while sequence stratigraphic correlation in Korallenoolith Formation is much more testable in North Germany as proposed by Betzler et al. (2007). Also limited by the existing data, the sequence stratigraphic correlation in this paper focuses on the deposits of Heersumer and Korallenoolith Formations with three surfaces correlated (Fig. 3.11).

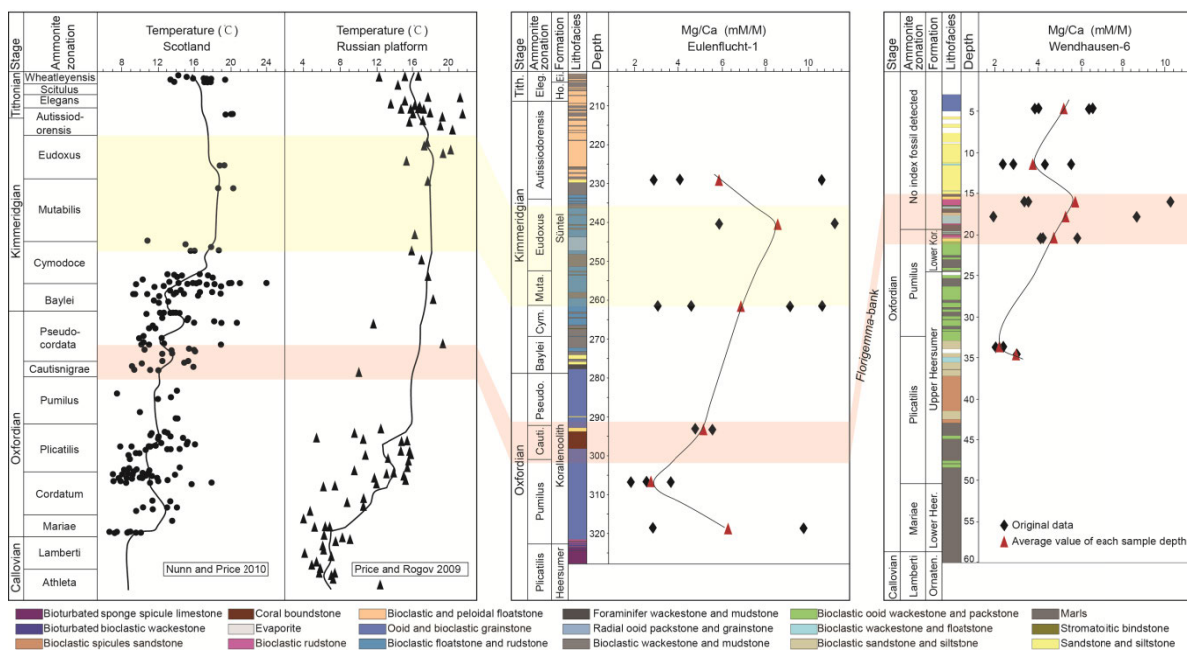


**Fig. 3.10** Paleotemperature variation trends reflected by the Mg/Ca ratio of the well preserved oyster shells from the Eulenflucht-1 core and Wendhausen-6 core, and their correlation with the paleotemperature variations of Scotland and Russian platform (Nunn and Price, 2010; Price and Rogov, 2009). Yellow area marks the warm period during the Late Kimmeridgian time. Pink area marks the warm period during the transition from the Middle to Late Oxfordian time. Facies division of the Eulenflucht-1 core is from Bai et al. (2017)

The top correlated surface is the main unconformity surface setting on top of the *Florigemma*-bank. It corresponds to the top boundary of the medium-scale sequence 3 of Wendhausen-6 core and Eulenflucht-1 core, and to the top boundary of the medium-scale sequence 4 of Lauensteiner Pass.

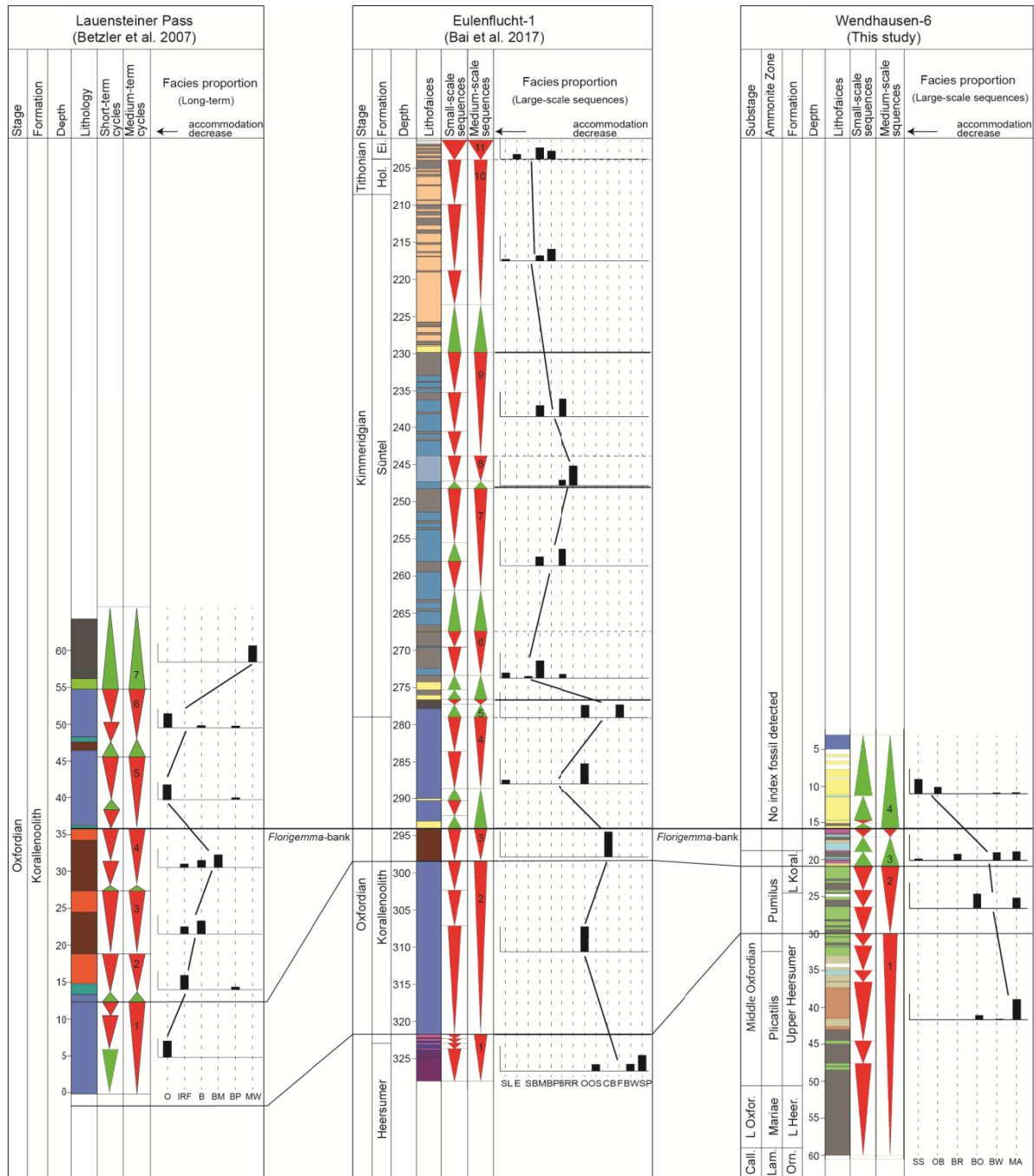


**Fig. 3.11** Sequence stratigraphic correlation of the Oxfordian deposits across the North German Basin at the medium-scale sequence level

The middle correlated surface corresponds to the top boundary of the medium-scale sequence 2 of the Wendhausen-6 core and the Eulenflucht-1 core, and to the top boundary of the medium-scale sequence 1 of Lauensteiner Pass. Above this surface, deposits are dominated by corals. An increase in accommodation space is reflected by the facies proportion statistic curves from the part under this surface to the part above this surface. This increase in the accommodation space is not so obvious in the Wendhausen-6 core. Above the middle correlated surface, corals in the Wendhausen-6 core are also not

dominating (Heunisch and Luppold, 2015). These two phenomena may be caused by the abundant supply of sediments, as deposits in Wendhausen-6 core is delta influenced.

The base correlated surface corresponds to the top boundary of the medium-scale sequence 1 of Wendhausen-6 core and Eulenflucht-1 core, and to the lower part of the base of Lauensteiner Pass outcrop. Above this surface, deposits are dominated by ooids and a decrease in accommodation space is recorded from the part under this surface to the part above this surface in both Wendhausen-6 core and Eulenflucht-1 core.

Because the lack of specific age control, the correlation of these sequence stratigraphic frameworks with that of the other European Basins and the third-order depositional sequences established by Jacquin et al. (1998) is not straightforward.

### **3.6 Conclusions**

A detailed lithologic and sequence stratigraphic description of the Heersumer Fm is firstly described in the North German Basin based on the Wendhausen-6 core data covering the deposits of the Ornatenton, Heersumer and Korallenoolith Fms. According to the different fossil combinations and sedimentary structures, as well as the carbonate content variations, eight facies are recognized and are assigned to a transition area between a deltaic deposit system and a normal marine carbonate ramp.

Three sequence hierarchies are identified. 14 small-scale sequences are defined by changes of their grain components, variations of grain size, and the stacking patterns of the constituent facies. 4 medium-scale sequences are bounded by the exposure surfaces indicated by the occurrence of iron mineral and the lowstand channel-fill sandstones. Medium-scale sequences are composed of the small-scale sequences with the same constituent facies. 2 large-scale sequences are derived from the facies proportion statistics of each medium-scale sequence. With the supplement of the Heersumer Fm sequence stratigraphy established in this paper, a sequence stratigraphic correlation of the Oxfordian deposits across the North German Basin was achieved on a medium-scale sequences level. Correlation of the small-scale sequences are hindered because of the interference of the autocyclic processes.

Both Sea-level fluctuations and climate variations are proved to play important roles in the sequence stratigraphic evolution of the Wendhausen-6 core. Covariation between the paleoclimate changes deciphered by the facies development and by the paleotemperature, reflected by ratio of Mg/Ca, endorses the climate control on the deposits of the

Wendhausen-6 core. The consistent paleotemperature fluctuation trends during the Late Jurassic between Scotland, Russian platform, and the North German Basin suggests that they are intimately connected at that time.



## Chapter IV

# **Diagenetic processes in the Upper Jurassic deposits in the North German Basin (Lower Saxony, Süntel Mountains)**

### **Abstract**

Facies and sequence stratigraphy evolution are believed to have great impacts on the development of diagenetic processes. Thus diagenetic processes in the Eulenflucht-1 core were analyzed. Several diagenetic elements are recognized and assigned into different facies. They are solution seams and stylolites due to physical or chemical compactions, moldic pores and microkarsts resulting from dissolution, dolomite formed by dolomitization, and types of cement formed by precipitation, recrystallization, and syntaxial overgrowth. Cement types are differentiated by their morphology and cathodoluminescence characteristics. Cement composed of microcrystalline calcite with dull luminescent represent the products of marine to early diagenesis. Cement with equant or blocky morphologies and sub-bright to bright luminescence indicate meteoric phreatic to early burial diagenesis. Cement with twin crystals or poikilotopic fabrics and non-luminescence are signs of the late burial diagenesis. Deep burial diagenesis products are constrained in facies deposited near shoal area, such as ooid grainstone and coral boundstone. They have grain-supported texture that resistant to compaction and can provide good water circulation for the formation of deep burial cement. Wackestone or mudstone deposited under storm wave base are favorable for the formation of dolomite related to bacterial induced sulfate reduction. Dolomite in the ooid grainstone and oyster-serpulid rudstone, and microkarsts are the diagenetic elements associated with sequence boundaries.

## 4.1 Introduction

Diagenetic processes play an important role in modifying the porosity and permeability of sedimentary rocks. A complex array of parameters from tectonic setting to depositional facies and paleoclimate conditions are recognized to have impact on diagenesis (Ketzer, 2002; Morad et al., 2000, 2012). Facies distribution, providing information on the sorting and grain size of sediments, influences diagenesis via controlling the pore fluid flow conditions. Early diagenetic process can be linked to sequence stratigraphy in deltaic, coastal, and shallow marine deposits, as they are sensitive to relative sea-level changes (Morad et al., 2000; South and Talbot, 2000; Tucker, 1993; Worden and Morad, 2003). Relative sea-level changes can also affect shallow and deep burial diagenesis by changing near-surface chemical conditions and the propagation of heat into the subsurface (Worden et al., 2000). All these imply that associating certain diagenesis products to a specific facies assemblage or a specific sequence stratigraphic position is possible.

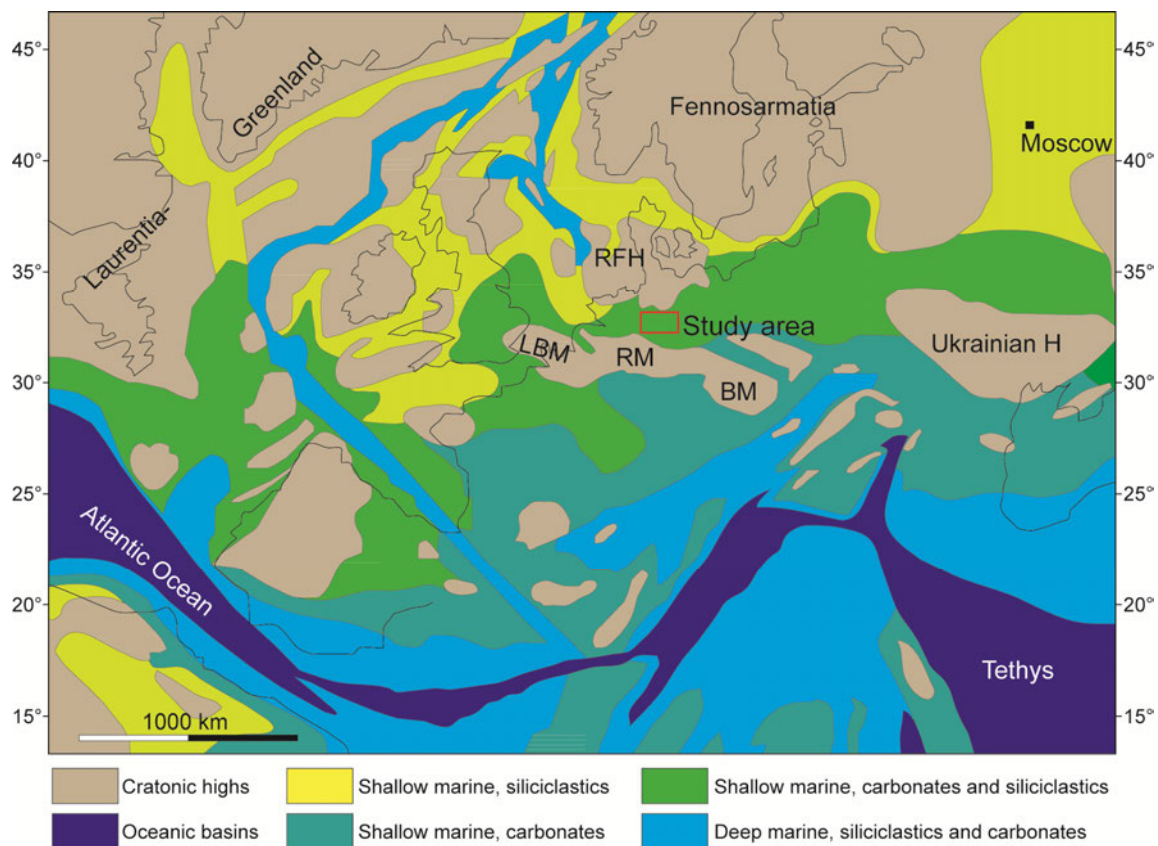


**Fig. 4.1** Late Jurassic paleogeography and main sediment associations in northern central Europe. LBM London-Brabant Massif, RM Rhenish Massif, BM Bohemian Massif, RFH Ringkobing Fyn High (modified from Ziegler, 1990; Thierry, 2000)

Diagenetic processes occurred in various environments result in cement with different morphologies (Scholle and Ulmer-Scholle, 2003). Cement from marine diagenesis always



have microcrystalline or fibrous fabric, whereas cement with equant or blocky fabric are always formed during meteoric or burial diagenesis (James and Choquette, 1984). But in some cases it is not enough to assign a type of cement to a specific diagenetic process only with morphology features. Different cathodoluminescence (CL) characteristics reflect the variations in the incorporated content of Mn and Fe during cement growth, which can not be observed with polarized microscope. They are used to trace the changes in pore fluid trace element concentrations and the changes in redox conditions during burial diagenesis (Meyer, 1974; Frank et al., 1996, Swart, 2015).  $Mn^{2+}$  is the luminescence activator and  $Fe^{2+}$  is quencher. When  $Mn^{2+}$  content is constant, CL intensity is inversely proportional to  $Fe^{2+}$  content, while when  $Fe^{2+}$  content is under a certain concentration, CL intensity is positively proportional to  $Mn^{2+}$  content (Gillhaus, 2001). Practice of using CL to analysis cement and diagenetic processes of the Upper Jurassic deposits in the North German Basin has been carried out by Bruckschen et al. (1992), However, they focused mainly on the timing of different cement generations in the Korallenoolith Fm.

Aim of this study is to discriminate the various cement types resulting from different diagenetic processes, and to evaluate how the diagenetic alteration was constrained within the context of facies and sequence stratigraphy framework.

#### **4.2 Geological setting**

The North German Basin, where the Eulenflucht -1 core is located, was bounded by the Ringkobing Fyn High to the north, and by the London Brabant, the Rhenish and the Bohemian Massifs to the south (Fig. 4.1). Synsedimentary tectonics and salt dome diapirs were active during the Late Jurassic age. Thickness of deposits varies by tens of meters between structural highs and lows resulting from the differential subsidence (Mönnig, 2005; Neuser, 1988).

In the Süntel Mountains, SW Hannover, deposits of the Jurassic period crop out (Fig. 4.2). The Upper Jurassic deposits are composed of Heersumer and Korallenoolith Fms (Oxfordian), the Süntel Fm (Kimmeridgian), and the Holzen and Eimbeckhausen Fms (Tithonian). The Heersumer Fm is partially dolomitized and consists of bioturbated marlstone enriched with sponge spicules. The Korallenoolith Fm is dominated by grain-supported ooid grainstone and coral boundstone. It is also partially dolomitized and have intercalations of sandy limestones (Bai et al., 2017; Betzler et al., 2007; Neuser, 1988). Deposits of the Süntel Fm are alternations of glauconitic marl, limestone and sandstone (Klassen, 2003; Mönnig, 2005), whereas the Holzen Fm consists of alternations of clay,

marl and limestone. Matrix-supported texture is dominating in these two formations. The Eimbeckhausen Fm is dominated by gypsum and anhydrite (Bai et al., 2017; Heunisch and Luppold, 2015). Burial depth of the Upper Jurassic deposits has reached 3000 - 4000 m with temperature of 90° - 120°, according to the thermometry of the fluid inclusion (Vackiner and Kukla, 2013).

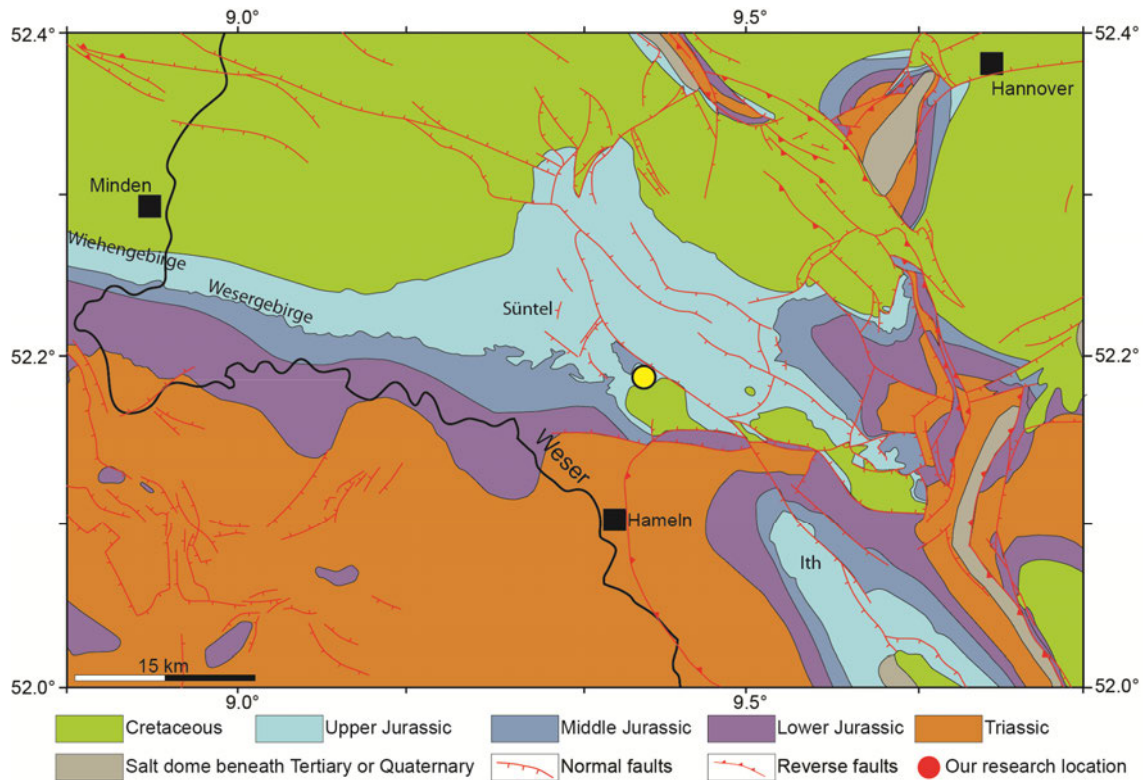


**Fig. 4.2** Geological map of the North German Basin with the location of the Eulenflucht-1 core (modified from Kockel et al., 1996)

### 4.3 Methods

A total of 80 samples were taken to make thin-sections from the Eulenflucht-1 (52.18227418°N, 9.4002145°E) core within the depth range between 201.00 and 328.00 m covering the deposits of Heersumer, Korallenoolith, Süntel, Holzen, and Eimbeckhausen Fms (Fig. 4.3). The core is stored at the BGR core repository in Grubenhagen.

Cement morphologies and structures results from diagenetic processes are observed under the plane-polarized microscope. 20 thin-sections were selected for CL observations. They were polished and coated with carbon in order to neutralize any charge build-up. The CL examinations were carried out in the Laboratory of the Institut für Geologie, Universität Hamburg. A CL microscope HC5-LM with the following setup was used: beam energy 6-7 KV, beam current 0.02mA.

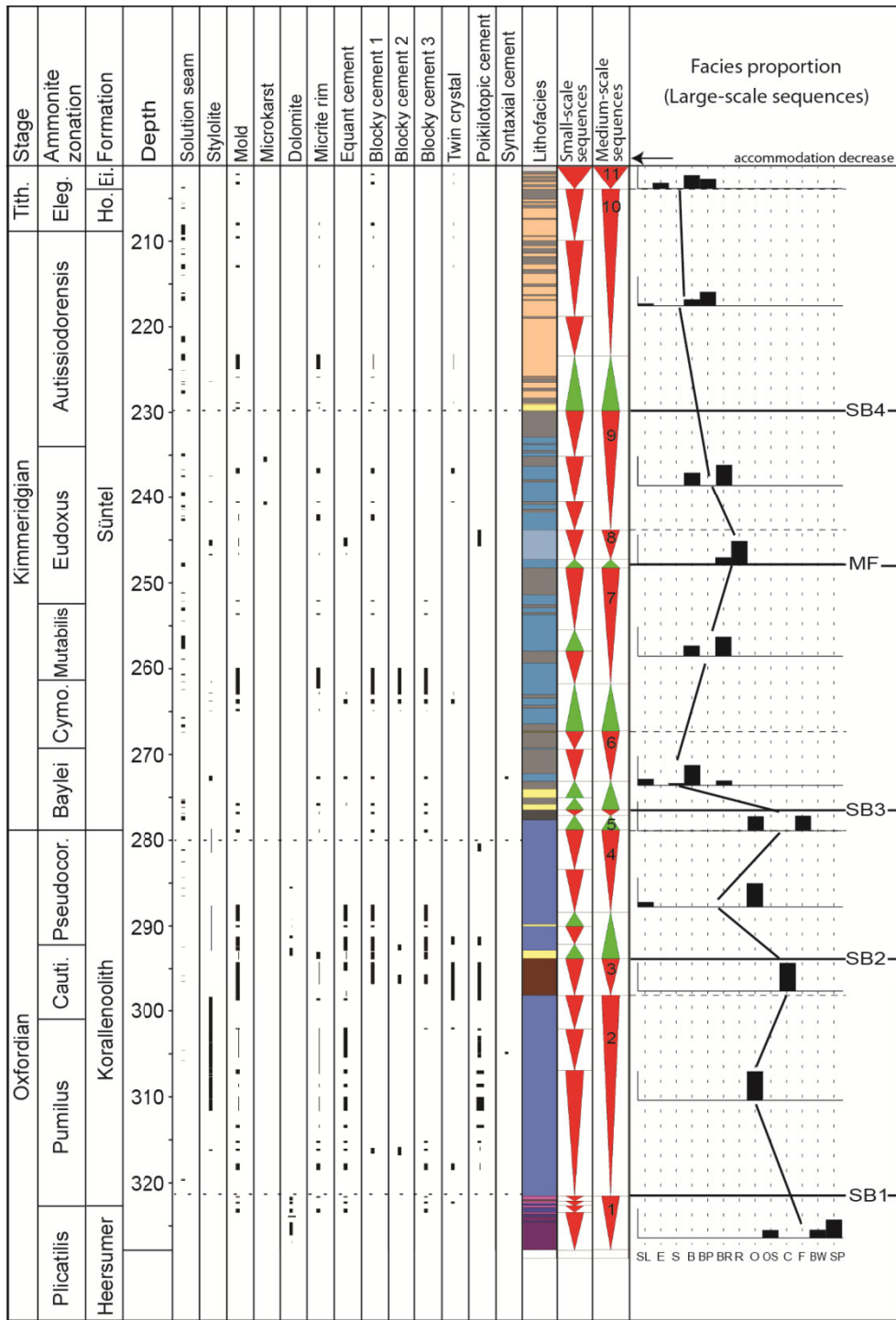


**Fig. 4.3** Logs of different diagenesis elements and oxygen isotope date in the Eulenflucht-1 core from 201.00 to 328.00 m. Facies divisions are from Bai et al. (2017). Horizontal dashed lines mark the boundaries of the four diagenetic zones

#### 4.4 Results

Thirteen elements are found in different lithofacies, which are produced by different diagenetic processes (Fig. 4.3). These elements are solution seams and stylolites due to physical or chemical compactions, moldic pores, and microkarsts resulting from dissolution, euhedral and subeuhedral dolomite formed by dolomitization, and eight types of cement formed by precipitation, recrystallization, and syntaxial overgrowth. Different generations of the cement with homogenous features under the polarized microscope are recognized aided by their luminescent features under the CL microscope.

Solution seams resulting from compactions are common throughout the researched core. Stylolites have a narrow down distribution depth range between 240.00 and 320.00 m, and are constrained in facies Ooid packstone and grainstone and Radial ooid packstone and grainstone (Fig. 4.4a).

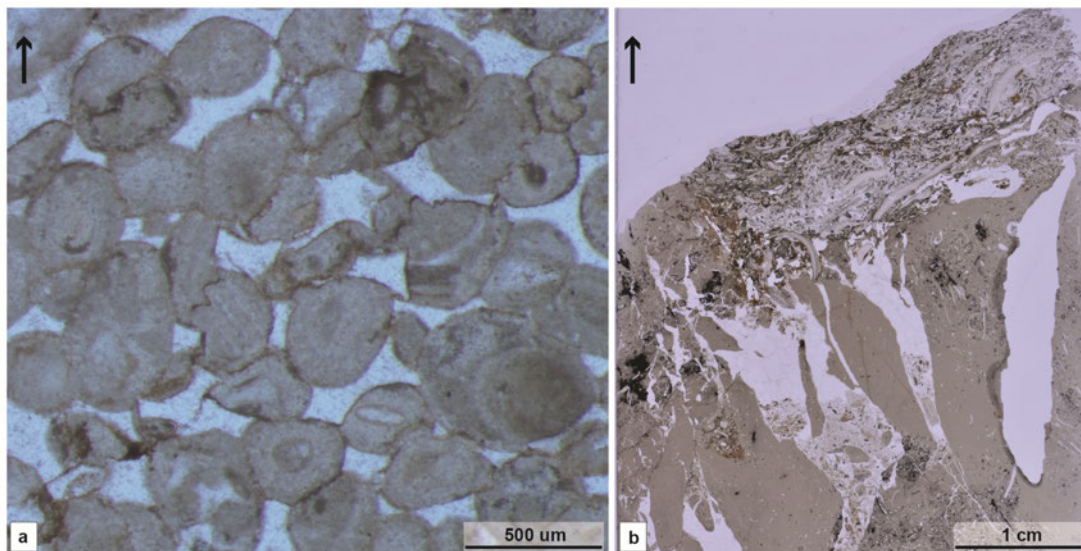


**Fig. 4.4** a Stylolites in the radial ooid grainstone, at 245.15 m; b Microkarst refilled by calcite and sediments fallen down from the overlying layer, at 240.52 m. Black arrow points to the top of the thin-section

Moldic pores resulting from solution are wide spread in the Eulenflucht-1 core, and most of them are occluded either by blocky calcite or micrite. Grain components dissolved consist of corals, some other bioclastic skeletons, and ooid layers. Another element results from solution process is microkarst. It is found at 235.20 and 240.52 m, with the collapsed sediment of the overlying layer falling down in the bottom of the paleokarst (Fig. 4.4b).



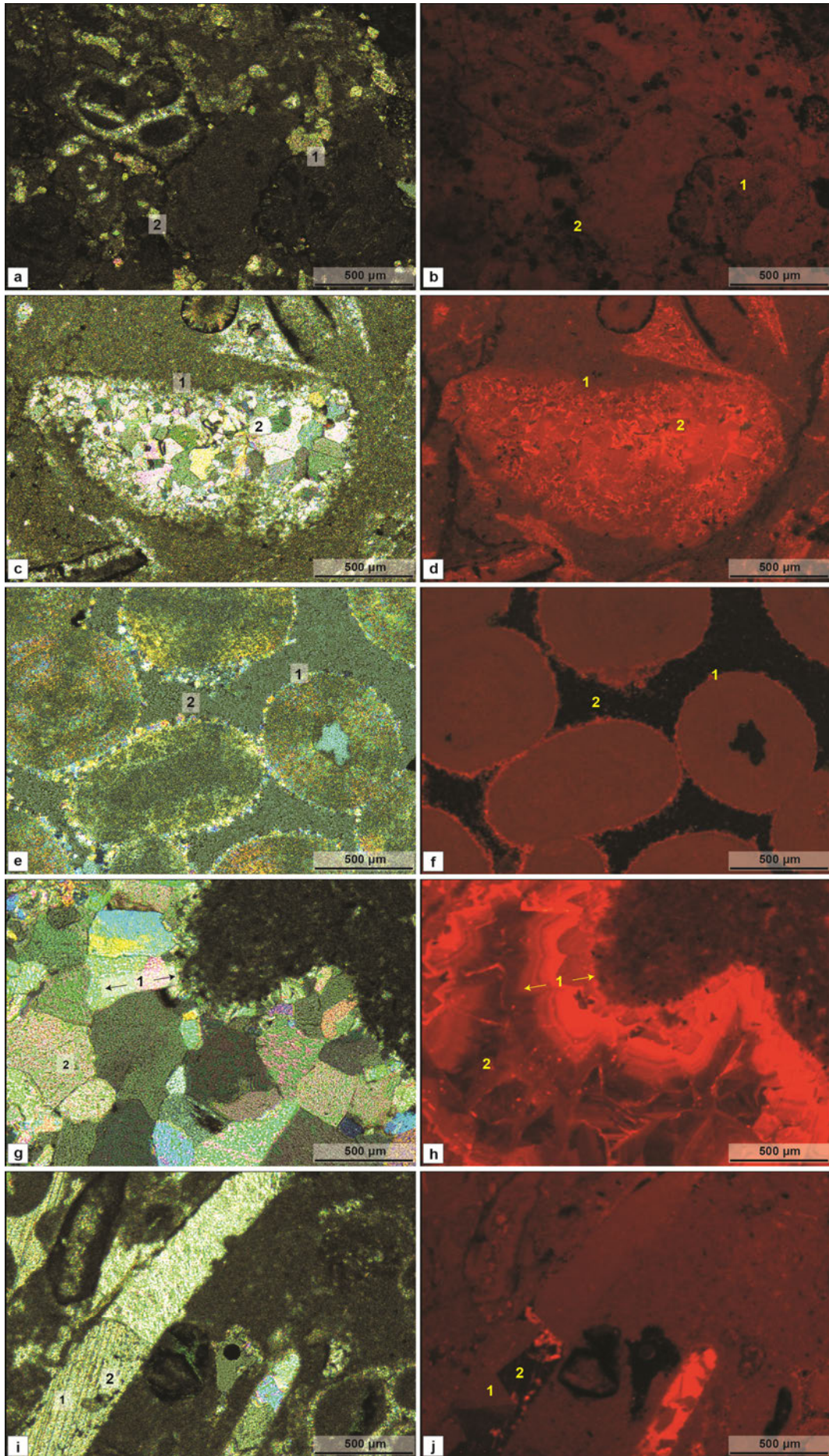


**Fig. 4.5** Cement properties und polarized microscope and CL microscope. **a, b** Dolomite rhombs with dull luminescence (1) and non luminescence (2), at 292.54 m; **c, d** Micrite rim with dull luminescence (1) and blocky cement with sub-bright luminescence in the central and bright luminescence at the edge (2), at 208.05 m; **e, f** Equant cement with bright luminescence (1) and the poikilotopic cement with no luminescence (2), at 310.20 m; **g, h** Blocky cement with a spectrum of luminescence (1) and no luminescence (2), at 295.86 m; **i, f** Twin crystal with sub-bright luminescence (1) and no luminescence (2), at 263.85 m

Dolomite with euhedral to subeuhedral morphology is linked to facies Ooid packstone and grainstone, Bioturbated sponge spicule limestone, Bioturbated bioclastic wackestone, and Oyster-serpulid rudstone (Fig. 4.3). In bioturbated sediment, dolomite is concentrated in burrows. This is similar as dolomitization in Korallenoolith Fm described by Betzler et al. (2007) in Lauensteiner Pass. Some of the dolomite rhombs are cut by solution seams. Dull to non-luminescence is detected in dolomite (Figs. 4.5a and 4.5b).

The eight types of cement formed by precipitation, recrystallization, and syntaxial overgrowth are described below.

Micrite rims spread pervasively across the researched core and play an important role in delineating the original shape of grains, especially between 209.45 and 229.29 m, where skeleton grains were leached and refilled by calcite cement. Weak red CL is shown in the micrite rims (Figs. 4.5c and 4.5d).

Equant cement prefers to encrust on grain surfaces. They occurred predominantly between the base of the core and 243.88 m, in facies which have minor matrix and grain supported structure, such as Ooid packstone and grainstone, Bioclastic floatstone and rudstone, and Coral boundstone (Fig. 4.3). Bright luminescence is observed in this type of cement (Figs. 4.5e and 4.5f).

Blocky cement has nearly equant morphology and occludes most of the leached pores, interparticle and intraparticle spaces. This type of cement can be divided into three generations according to their different performances under the CL microscope. Generation 1 (Blocky cement 1) is common through the Eulenflucht-1 core. Single crystal of this type of cement exhibits homogenously optical properties under plane-polarized light, but is zoned under CL microscope. The large central part of the crystal is sub-bright luminescent compared to bright luminescent edge of the crystal (Figs. 4.5c and 4.5d). Generation 2 (Blocky cement 2) is found between 260.00 and 320.00 m and shows a preference to occur in sediments having large interparticle spaces with grain supported structures, such as facies Bioclastic floatstone and rudstone, Coral boundstone, and Ooid packstone and grainstone (Fig. 4.3). Under polarized microscope, this type of cement grow layer by layer from the grain surfaces into large interparticle or moldic pores with the increase in single crystal size.

Under CL microscope, they cover a series of luminescent zones changing gradually from sub-bright to bright then to sub-bright again (Figs. 4.5g and 4.5h). As the luminescence intensity decreases continuously, the Generation 3 (Blocky cement 3) cement with dull to non-luminescence developed (Figs. 4.5g and 4.5h). They have larger crystal size and similar occurrence depth range compared with that of Generation 2.

Cement with twin crystals is commonly constrained in facies Coral boundstone between 293.92-298.48 m with some scattered in other part in facies Bioclastic rudstone and Ooid grainstone. They show dull to non-luminescent features under CL microscope (Figs. 4.5i and 4.5j)

Poikilotopic cements is concentrated between 280.00 and 320.00 m in facies Ooid packstone and grainstone, and Coral boundstone, and between 243.88 and 247.32 m in facies Radial ooid packstone and grainstone, where grain supported structure is dominating. Most of them are inclusion-free. No luminescence is detected in poikilotopic cement (Figs. 4.5e and 4.5f).

Cement resulting from syntaxial overgrowth is minor in Eulenflucht-1 core, and commonly is syntaxial overgrowth of echinoids in facies Bioclastic floatstone and rudstone.

## **4.5 Discussion**

### **4.5.1 Diagenetic processes**

Assemblages of diagenetic elements delineate different diagenetic processes. Cement morphologies and their luminescent features provide information to reveal their forming environments. Cross-cutting relationships between the diagenetic elements, e.g., between compaction structures and dolomite, helps to assign them to specific diagenetic processes and to depict their paragenetic sequence. Marine to early burial, meteoric phreatic, and deep burial diagenesis are recognized in the Eulenflucht-1 core. Vadose diagenetic products is only recognized at around 240.52 m with the occurrence of microkarst (Fig. 4.4b).

CL features have been used as an efficient supplement for diagenetic analysis (Bruckschen et al., 1992; Godet et al., 2016; Korngreen and Benjamini, 2001). Twenty-six factors can cause luminescence have been recognized according to Machel (2000), and a consensus that  $Mn^{2+}$  is the most important activator and  $Fe^{2+}$  the most important quencher in diagenetic calcites has been arrived. The content of precipitated  $Mn^{2+}$  and  $Fe^{2+}$  depend commonly on



the fluctuations in redox conditions in pore water. Based on this concept, it is possible to use CL features to help the analysis of the diagenetic process.

Micrite rims composed by microcrystalline magnesium calcite, which are the dominating cement precipitated during marine diagenesis (Melim et al., 2001), are common in shallow marine environment. The weak luminescent feature indicates a little incorporation of  $Mn^{2+}$  content. According to Frank et al. (1982) and Pierson (1981),  $Mn^{2+}$  content in the calcite precipitated from sea water varies between 0.3 and 100 ppm which is below the  $Mn^{2+}$  content window for causing luminescence in natural calcite. It is thus believed that these micrite rims were formed in marine and early burial diagenesis stage, where early burial environment with reducing conditions provided enough  $Mn^{2+}$  in the solution to be incorporated in calcite. This type of cement is comparable to the submarine Mg calcite with blotchy luminescence described by Bruckschen et al. (1992).

Equant fabric is typical for cement developed in phreatic diagenesis (Scholle and Ulmer-Scholle, 2003). Equant cement with low magnesium calcite is generally formed in meteoric pore waters with low salinity (Folk and Land, 1975; Lahann, 1978). But factors such as temperature, saturation state, and fluid flow rate, may also affect crystal morphologies and control the formation of the equant cement (Given and Wilkinson, 1985). Therefore marine phreatic and burial phreatic can not be excluded solely on equant cement morphology. The homogenous bright luminescence phenomenon manifests the overprint of early burial diagenesis and rules out the marine phreatic diagenesis, as calcite precipitated from marine water does not have enough  $Mn^{2+}$  to cause luminescence (Frank et al., 1982; Pierson, 1981). Deep burial diagenesis is also ruled out because high  $Fe^{2+}$  in calcite can quench the luminescence activated by  $Mn^{2+}$ . According to Machel (2000),  $Mn^{2+}$  and  $Fe^{2+}$  take place during transition from eogenetic diagenesis to burial diagenesis, but reducing environment for  $Fe^{2+}$  formation is more strict than that for  $Mn^{2+}$ . So at first,  $Mn^{2+}$  is removed from solutions into calcite firstly, and cause bright luminescence. As burial diagenesis goes further,  $Fe^{2+}$  availability and incorporation into calcite will be more and exceed  $Mn^{2+}$  (Scholle and Ulmer-Scholle, 2003), so CL intensity decrease until quenched non-luminescent cement appears. Thus this cement type is formed in meteoric phreatic to early burial diagenesis stage.

Blocky cement 1 also has equant fabric, but the zoned luminescence feature in each single crystal makes it different from the equant cement mentioned above. The bright to sub-bright luminescence shows it probably formed during the meteoric phreatic and early burial diagenesis. Two assumptions are assigned to the formation mechanisms of this cement. One

is that the cement with homogeneous sub-bright luminescence was firstly precipitated in a certain environment with stable pore water chemical compositions and full-filled a moldic pore. Then as the burial depth increase, more reducing environment appears, fluid with more  $Mn^{2+}$  content went through the inter-crystal spaces and recrystallized the edge of the crystals, making a bright luminescent rim occurred. The other one is that they are formed due to the original crystal growth mechanism. The incorporation of the luminescence activator  $Mn^{2+}$  is a function of  $D_{Mn}$  and  $(aMn^{2+}/aCa^{2+})$  according to formation:

$$D_{Mn} = (Mn^{2+}/Ca^{2+})_{calcite}/(aMn^{2+}/aCa^{2+})$$

where  $D_{Mn}$ ,  $(Mn^{2+}/Ca^{2+})_{calcite}$ ,  $aMn^{2+}/aCa^{2+}$  represent distribution coefficient, Mn/Ca molar ratio in calcite, and Mn/Ca molar activity ratio in solution, respectively. The activity coefficient "a" is 1 for fresh water, and 0.2 for brine water (Kharaka et al., 1988). This means in a certain diagenetic stage, when the pore water chemical composition is stable, factor  $aMn^{2+}/aCa^{2+}$  is invariant, and the  $(Mn^{2+}/Ca^{2+})_{calcite}$  is a function of  $D_{Mn}$ . In connected water filled pores, fluid always flow faster in the central part of pores and slower near grain surfaces due to friction. As crystals keep growing, the decline in the rock permeability results in a decrease in fluid flowing velocity. Growth of crystals fed by the pore fluid are therefore decreased. Thus crystals have the biggest growth rate in the central part of crystal and lowest rate around grain interfaces. As  $D_{Mn}$  decreases with the increase in growth rate (Dromgoole and Walter, 1990; Lorens, 1978, 1981; Mucci, 1988; Pingitore et al., 1988), more  $Mn^{2+}$  are incorporated in the cement contact part with low growth rate and lead to a high luminescent intensity. So the difference in CL intensity in Blocky cement 1 is caused by change of growth rate rather than change in redox conditions of different diagenesis phase. Both of the two mechanisms require relative stable chemical properties of the solution, and is believed to occur in meteoric phreatic to early burial diagenesis phase.

Blocky cement 2 also has a equant fabric, but covers a spectrum of luminescence. For continuous change of brightness in cement, two models have been established. In closed system, the trace element concentration in the solid changes continuously as the solution concentration changes with crystal growth. Trace element concentrations in solid decrease (increase) from initial value to final value, when distribution coefficient  $D$  is greater (smaller) than one (McIntire, 1963). Because  $D_{Mn}$  varies approximately from 2.5 to 20 both in field observations and laboratory measurements (Bodine et al., 1965; Ichikumi, 1973; Kumagai, 1978; Michard, 1968; Pingitore et al., 1988), which are larger than 1, concentration of  $Mn^{2+}$  in calcite will decrease along the grow direction. But the firstly increase in CL intensity in Blocky cement 2 countered the expected phenomenon according

to this model. Another model is established in an open system, continuous chemical composition change induced the change of incorporation of  $\text{Fe}^{2+}$  and  $\text{Mn}^{2+}$  into calcite then result in CL zonation. During transition from eogenetic diagenesis to burial diagenesis, reducing environment emerged and  $\text{Mn}^{2+}$  and  $\text{Fe}^{2+}$  take place, but reducing environment for  $\text{Fe}^{2+}$  formation is more strict than that for  $\text{Mn}^{2+}$ . So at first, because  $D_{\text{Mn}}$  is larger than  $D_{\text{Fe}}$ ,  $\text{Mn}^{2+}$  is much easier to be removed from solutions into calcite (Machel, 2000). Thus CL intensity increase temporally in this stage. As burial diagenesis goes further,  $\text{Fe}^{2+}$  availability and incorporation into calcite will be more and exceed  $\text{Mn}^{2+}$  (Scholle and Ulmer-Scholle, 2003), so CL intensity decrease until quenched non-luminescent cement (Blocky cement 3) formed in intermediate or late stage of burial diagenesis. Therefore, Blocky cement 2 and 3 represent the cement formed during the switch from the meteoric phreatic or early burial diagenesis to late burial diagenesis with continuous changes in the chemical properties of the pore water.

Twin crystals are interpreted to be formed during deep burial diagenesis. Because intense twinning commonly involves dissolution as well as crystal dislocation and is typically a result of burial loading or tectonic deformation (Simonsen and Friedman, 1992). The dull to non-luminescent blocky calcite with twin crystals is believed to result from partial or total quenching by too much incorporation of  $\text{Fe}^{2+}$  as the burial diagenesis went further.

Cement with poikilotopic texture and its clear, inclusion-free feature is common in cements formed during burial diagenesis (Druckman and Moore, 1985). The non-luminescent feature is probably caused by  $\text{Fe}^{2+}$  quenching in deep burial environment. All these features show this type of cement is a product of late burial diagenesis.

Syntaxial cement, e.g., overgrowth of echinoids, is not a diagnostic cement that can infer certain diagenetic process. They have been reported from marine, meteoric, and burial diagenesis (Melim et al., 2001; Walker et al., 1989). As there is no other features to narrow it down to a specific diagenesis process, overgrowth here can be formed in any diagenesis processes.

Moldic pores are caused by dissolution, to which modification of sea water is necessary. Change of sea water properties can be caused by meteoric water influx in shallow water or by oxidation of organic matter producing  $\text{H}_2\text{S}$  in deep water (Melim et al., 2001). Dissolution in Bioclastic floatstone and rudstone, and Bioclastic wackestone and mudstone is tied to meteoric diagenesis, because fenestrate and microkarst structure (Fig. 4.4b) exhibit possible existence of subaerial exposure and meteoric water. Leaching in coral boundstone and parts of ooid grainstone can be caused by disintegration of coral residues during marine-

early burial diagenesis, because microbially induced decay of organic matter and elevated CO<sub>2</sub> could initiate aragonite dissolution and trigger the mechanism of marine-early burial diagenesis (Melim et al., 2002). Most of the moldic pores are occupied by blocky cement without clastic infillings and moldic pore collapse, indicating there is no long time gap between these dissolution and the precipitation of blocky cement. Preservation of the outline of the leached grains delineated by micrite calcite suggests that the dissolution postdates formation of micrite rims.

Structures such as solution seams and stylolites are caused by physical and chemical compaction during burial diagenesis, and stylolites is commonly formed in late-burial stage according to Scholle and Ulmer-Scholle (2003).

Dolomitization predates deep burial diagenesis is suggested by the dolomite cut by solution seams. An unconformity boundary defined on top of Oyster-serpulid rudstone at 321.73 m, where dolomite are common, favors the interpretation of dolomitization occurring during marine and early burial diagenesis, because a deposition break on sea floor can provide long time influx of marine water into deposits and trigger the dolomitization. The dull to no luminescence features indicate a gradual change from early burial to deep burial diagenesis.

Element	Meteoric	Marine	Burial
Microkarst	—————		
Mold	—————	—————	
Syntaxial cement	— — — — —	—————	—————
Micrite rim		—————	
Equant cement		—————	—————
Blocky cement 1		—————	—————
Dolomite			—————
Solution seam			—————
Blocky cement 2			—————
Blocky cement 3			—————
Stylolite			—————
Twin crystal			—————
Poikilotopic cement			—————

**Fig. 4.6** Paragenetic sequences of different diagenetic elements

Based on the above interpretation, diagenetic elements result from marine to early burial, meteoric phreatic, and deep burial diagenesis are recognized. A paragenesis sketch is established to show the corresponding diagenetic process of each diagenetic element (Fig. 4.6).

#### 4.5.2 Diagenetic zones

Four zones with different assemblages of diagenetic elements are recognized. Zone 1 ( 201.00 - 229.80 m) consists of elements resulting from meteoric phreatic diagenesis to dissolve the grain components and refill the molds with blocky cement. Some marine diagenesis is detected represented by micrite rims, and deep burial diagenesis is very rare to absent. In zone 2 (229.80 - 280.00 m), meteoric phreatic and marine diagenetic elements are common, represented by the occurrence of micrite rims and equant cement. Early to deep burial diagenetic products, such as blocky cement 2 and 3, take place. In zone 3 (294.00 - 321.74 m), the deep burial diagenetic elements, such as blocky cement 3, twin crystals, poikilotopic cement, and stylolites, become prevailing. This indicates zone 3 experienced severe burial diagenesis. Zone 4 (321.74 - 328.00 m) is dominated by marine and early burial diagenesis. Dolomite induced by these diagenetic processes is common in this zone. According to Bai et al., (2017), zone 1 covers the facies formed in restricted-lagoon setting with matrix-supported texture. Zone 2 and 3 covers the facies formed in the open-lagoon and the shoal area, respectively. Zone 4 covers the facies formed below storm wave base with fine grain components. Burial diagenetic elements increase as the proportion of the shoal facies with grain-supported texture increases from zone 2 to zone 3, and they are rare in the matrix-supported facies in zone 1 and 4. Thus, it is proposed that the facies with grain-supported texture, such as Ooid packstone and grainstone and Coral boundstone, can resist severe compactions and provide favorable water circulation to form cements during deep burial diagenesis. Dolomite is common both in the ooid shoals in zone 3, and in the wackestone and mudstone in the outer ramp facies in zone 4. The dolomite constrained in ooid grainstone and oyster-serpulid rudstone near sequence boundary is supposed to be precipitated from the mixed meteoric and marine water, whereas the dolomite concentrated in the wackestone and mudstone is comparable to that discovered in Maryville Limestone interpreted as neomorphic products of early formed dolomite, associated with bacterial reduction of sulfate in fine grained lithofacies (Srinivasan, 1993). Except the microkarst at around 235.25 and 240.54 m, element reflecting meteoric vadose diagenesis related to sequence boundary was not detected.

#### 4.6 Conclusions

Thirteen diagenetic elements reflecting physical or chemical compaction, component dissolution, cement precipitation and recrystallization, and dolomitization during the diagenetic processes are recognized based on the thin-section observation. Eight of them are cement types differentiated by their morphology and CL characteristics.

Paragenetic sequence of different diagenetic elements is established. Micrite rims, composed of microcrystalline calcite with dull luminescence, represent the products of marine to early diagenesis. Equant cement and blocky cement 1, 2 with equant fabric and sub-bright to bright luminescence indicate meteoric phreatic or early burial diagenesis. Non-luminescent dolomite and cement with twin crystals or poikilotopic fabrics and non-luminescence imply the late burial diagenesis. Solution seams and stylolites represent physical and chemical compactions during the early and late burial diagenesis respectively.

Four depth zones with different assemblage of diagenetic elements are recognized. Zone 1 (201.00 - 229.80 m) consists of meteoric phreatic diagenetic elements with some marine diagenetic elements. Zone 2 (229.80 - 280.00 m) is dominated by meteoric phreatic and marine diagenetic elements, with some early to deep burial diagenetic products take place. In zone 3 (294.00 - 321.74 m), the deep burial diagenetic elements are prevailing. Zone 4 (321.74 - 328.00 m) is dominated by marine and early burial diagenesis, whereas some deep burial diagenesis are reflected by dolomite and blocky cement 3. Facies evolution shows great impact on the distribution of diagenetic products. Deep burial diagenesis products prefer facies with grain-supported texture that can provide enough solution for recrystallization or cement precipitation. Dolomite favors wackestone or mudstone, where bacterial induced sulfate induction is common. Sequence stratigraphic associated diagenetic elements are dolomite in the ooid grainstone and oyster-serpulid rudstone, and microkarsts. They are distributed in the vicinity of sequence boundaries.





## Chapter V

### **Conclusions**

This study aims to establish a sequence stratigraphic framework for the Upper Jurassic deposits in the North German Basin, which makes sequence stratigraphic correlation a possible supplement to the limited biostratigraphic correlation in this area. This study also aims to reveal the paleoclimate control on the evolution of the sequences, as well as to decipher how the diagenetic processes were affected by the sequence stratigraphy and facies evolution. For these purposes, the Eulenflucht-1 core drilled in Süntel Mountains and the Wendhausen-6 core drilled in Hildesheimer Wald covering the deposits of the Oxfordian to Tithonian age were studied by core description, microfacies analysis, isotopic and element analysis, and cathodoluminescence imaging.

The following conclusions were obtained:

- (1) Thirteen facies and eight facies were respectively identified in the Eulenflucht-1 core and the Wendhausen-6 core, based on their lithology, components, and microscopic texture.
- (2) The facies succession in the Eulenflucht-1 core was interpreted to be deposited in a carbonate ramp ranging from the outer ramp into the restricted lagoon, whereas the succession of the Wendhausen-6 core were considered to be deposited in a transition area between a delta setting and a carbonate ramp.
- (3) A sequence stratigraphy of three hierarchies has been established in the Eulenflucht-1 core and the Wendhausen-6 core. They are the short-, medium-, and large-scale sequences. Sequence stratigraphic correlation was constructed and three medium-scale sequence boundaries were correlated across the North German Basin.
- (4) Sea-level fluctuations show potential control on the development of the sequence stratigraphy from the late Callovian to the middle Oxfordian age. From the Late Oxfordian to the Kimmeridgian age, the impact of the uplifting tectonic movement outpaced that of the sea-level rise, and induced the continuous decrease in the accommodation/sediment supply (A/S) ratio from the Late Oxfordian to Kimmeridgian time.
- (5) The warm period during the Middle Oxfordian and Late Kimmeridgian was recorded by the development of the ooid grainstone and coral boundstone facies, as well as by the increase in Mg/Ca ratio.
- (6) Paleoclimate had a great control on the evolution of large-scale sequences. This is recorded by the carbon isotopic correlation across different European Basins, and by the Mg/Ca data in the Eulenflucht-1 core and in the Wendhausen-6 core.

(7) Early diagenetic cement was pervasively altered by burial diagenetic processes, making correlation of diagenetic products to certain sequence stratigraphic position and specific facies difficult. Only dolomite in the ooid grainstone and oyster-serpulid rudstone, and microkarsts can be linked to sequence boundaries. Facies with grain-supported texture formed in settings with high water energy, e.g., ooid grainstone and coral boundstone, favors the development of deep burial diagenetic cement, such as the poikilotopic cement and twin crystals.

The new sequence stratigraphy framework established in this study covers a larger time interval than any previous works in this area. The sequence stratigraphy for the Oxfordian to the Early Tithonian age can be used as a reference for the correlation with other sequences in the North German Basin. The paleoclimate control on the sequence stratigraphic evolution provides the base for its correlation with the sequences in other European Basins.



## References

- Abbink, O.**, 2001. Late Jurassic to earliest Cretaceous palaeoclimatic evolution of the southern North Sea: *Global and Planetary Change*, 30, p. 231–256.
- Abbink, O.A., Mijlief, H.F., Munsterman, D.K., and Verreussel, R.**, 2006. New stratigraphic insights in the 'Late Jurassic' of the Southern Central North Sea Graben and Terschelling Basin (Dutch Offshore) and related exploration potential: *Geologie en Mijnbouw*, 85, p. 221–238.
- Abbink, O., Targarona, J., Brinkhuis, H., and Visscher, H.**, 2001. Late Jurassic to earliest Cretaceous palaeoclimatic evolution of the southern North Sea: *Global and Planetary Change*, 30, p. 231–256.
- Adegoke, O.S., Omatsola, N.E., and Salami, N.B.**, 1976. Benthonic foraminiferal biofacies of the Niger Delta: First International Symposium on Benthonic Foraminifera of Continental Margins. Halifax, Canada, Part A, p. 273-292.
- Aguirre-Urreta, M.B., Price, G.D., Ruffell, A.H., Lazo, D.G., Kalin, R.M., Ogle, N., Rawson, P.F.**, 2008. Southern Hemisphere Early Cretaceous (Valanginian-Early Barremian) carbon and oxygen isotope curves from the Neuquén Basin, Argentina. *Cretaceous Research*, 29, p. 87–99.
- Bai, H.Q., Betzler, C., Erbacher, J., Reolid, J., and Zuo, F.F.**, 2017. Sequence stratigraphy of Upper Jurassic deposits in the North German Basin (Lower Saxony, Süntel Mountains): *Facies*, 63.
- Bailey, T.R., Rosenthal, Y., McArthur, J.M., van de Schootbrugge, B., and Thirlwall, M.F.**, 2003. Paleooceanographic changes of the Late Pliensbachian-Early Toarcian interval: a possible link to the genesis of an Oceanic Anoxic Event: *Earth and Planetary Science Letters*, 212, p. 307–320.
- Barnard, T., Cordey, W.G., and Shipp, D.J.**, 1981. Foraminifera from the Oxford Clay (Callovian-Oxfordian of England): *Revista Espanola d Micropaleontologia*, 13, p. 383-462.
- Bartolini, A., Pittet, B., Mattioli, E., and Hunziker, J.C.**, 2003. Shallow-platform palaeoenvironmental conditions recorded in deep-shelf sediments: C and O stable isotopes in Upper Jurassic sections of southern Germany (Oxfordian–Kimmeridgian): *Sedimentary Geology*, 160, p. 107–130.
- Betz, D., Führer, F., Greiner, G., and Plein, E.**, 1987. Evolution of the Lower Saxony Basin: *Tectonophysics*, 137, p. 127–170.
- Betzler, C., Pawellek, T., Abdullah, M., and Kossler, A.**, 2007. Facies and stratigraphic architecture of the Korallenoolith Formation in North Germany (Lauensteiner Pass, Ith Mountains): *Sedimentary Geology*, 194, p. 61–75.
- Betzler, C., Pawellek, T.**, 2014. Facies, stratigraphic architecture and high-resolution sequence stratigraphy of the Zechstein anhydrite (Werra Anhydrite) in Menslage area (Lower Saxony, N Germany): *Zeitschrift der Deutschen Gesellschaft für Geowissenschaften*, 165, p. 331-344.
- Brand, U., and Veizer, J.**, 1981. Chemical diagenesis of a multicomponent carbonate system; 2, Stable isotopes: *Journal of Sedimentary Research*, 51(3), p. 987-997.
- Bruckschen, P., Neuser, R.D., and Richter, D.K.**, 1992. Cement stratigraphy in Triassic and Jurassic limestones of the Weserbergland (northwestern Germany): *Sedimentary Geology*, 81, p. 195-214.

- Bodine, M.W., Holland, H.D., and Borcsik, M.,** 1965. Coprecipitation of manganese and strontium with calcite. In: Problems of Post magmatic Ore Deposition. Proc. Symp., Prague, 2:401-405.
- Boggs, S., Krinsley, D.H.,** 2006. Application of cathodoluminescence imaging to the study of sedimentary rocks. Cambridge University Press, Cambridge, p. 1-165.
- Bougeois, L., de Rafélis, M., Reichart, G.J., de Nooijer, L.J., Dupont-Nivet, G.,** 2016. Mg/Ca in fossil oyster shells as palaeotemperature proxy, an example from the Palaeogene of Central Asia: Palaeogeography, Palaeoclimatology, Palaeoecology, 441, p. 611–626.
- Bruckschen, P., Neuser, R.D., and Richter, D.K.,** 1992. Cement stratigraphy in Triassic and Jurassic limestones of the Weserbergland (northwestern Germany): Sedimentary Geology, 81, p. 195–214.
- Carpentier, C., Lathuilière, B., Ferry, S., and Sausse, J.,** 2007. Sequence stratigraphy and tectonosedimentary history of the Upper Jurassic of the Eastern Paris Basin (Lower and Middle Oxfordian, Northeastern France): Sedimentary Geology, 197, p. 235–266.
- Cäsar, S.,** 2012. Sedimentologie und Sequenzstratigraphie oberjurassischer Karbonate von Norddeutschland (Oxfordium/Kimmeridium, Niedersächsisches Becken). Dissertation, University of Hamburg, p. 1-235.
- Christensen, J.N., Halliday, A.N., Lee, D-C., Hall, C.M.,** 1995. In situ Sr isotopic analysis by laser ablation: Earth and Planetary Science Letters, 136, p. 79-85.
- Cross, T.A., Baker, M.R., Chapin, M.A., Clark, M.S., Gardner, M.H., Hanson, M.S., Lessenger, M.A., Little, L.D., Mcdonough, K-J., Sonnenfeld, M.D., Valasek, D.W., Williams, M.R., and Witter, D.N.,** 1993. Applications of high-resolution sequence stratigraphy to reservoir analysis. In: Subsurface Reservoir Characterization from Outcrop Observations. (Eschard, R., and Doligez, B., eds.) Éditions Technip, Paris, p. 11-34.
- Cross, T.A., and Lessenger, M.A.,** 1998. Sediment volume partitioning: rationale for stratigraphic model evaluation and high-resolution stratigraphic correlation. In: Sequence stratigraphy-Concepts and Applications (Gradstein, F.M., Sandvik, K.O., and Milton, N.J., eds.). Elsevier Science B. V, Amsterdam, p. 171-195.
- Davies, P.J., Bubelab, B., and Ferguson, J.,** 1978. The formation of ooids: Sedimentology, 25, p. 703-730.
- Dromgoole, E.L., and Walter, L.M.,** 1990. Iron and manganese incorporation into calcite: Effects of growth kinetics, temperature and solution chemistry: Chemical Geology, 81, p. 311–336.
- Druckman, Y., Moore, C.H.,** 1985. Late Subsurface Secondary Porosity in a Jurassic Grainstone Reservoir, Smackover Formation, Mt. Vernon Field, Southern Arkansas. In: Carbonate Petroleum Reservoirs (Roehl, P.O., Choquette, P.W., eds) Springer New York, New York, NY, p. 369–383.
- Dunham, R.J.,** 1962. Classification of carbonate rocks according to depositional texture: AAPG Memoir, 1, p. 108-121.
- Dupraz, C., and Strasser, A.,** 2002. Nutritional modes in coral--microbialite reefs (Jurassic, Oxfordian, Switzerland): evolution of trophic structure as a response to environmental change: PALAIOS, 17, p. 449–471.

- Embry, A.F., and Klovan, J.E.,** 1971. A Late Devonian reef tract on northeastern Banks Island, N.W.T.: *Bulletin of Canadian Petroleum Geology*, 19, p. 730-781.
- Ferdani, M.,** 2006. Oil and Gas in Germany. TU Bergakademie Freiberg, p.1-10.
- Folk, R.L., and Land, S.L.,** 1975. Mg/Ca Ratio and Salinity: Two Controls over Crystallization of Dolomite: *AAPG Bulletin*, 59, p. 60-68.
- Frank, J.R., Carpenter, A.B. and Oglesby, T.W.,** 1982. Cathodoluminescence and composition of calcite cement in the Taum Sauk Limestone (Upper Cambrian), Southeast Missouri: *Journal of Sedimentary Research*, 52, p. 631-638.
- Frank, T.D., Lohmann, K.C., and Meyers, W.J.,** 1996. Chronostratigraphic significance of cathodoluminescence zoning in syntaxial cement: Mississippian Lake Valley Formation, New Mexico: *Sedimentary Geology*, 105, p. 29–50.
- Freytet, P., Plaziat, J.C.,** 1982. Continental carbonate sedimentation and pedogenesis-Late Cretaceous and Early Tertiary of Southern France: *Contributions to Sedimentary Geology*, Stuttgart
- Füchtbauer, H.** 1968. Carbonate sedimentation and subsidence in the Zechstein Basin (Northern Germany). – In: *Recent developments in carbonate sedimentology in Central Europe*(Müller, G. &Friedman, G.M. eds.) Springer Berlin Heidelberg, Berlin, Heidelberg, p. 196–203.
- Gillhaus, A., Richter, D.K., Meijer, J., Neuser, R.D., and Stephan, A.,** 2001. Quantitative high resolution cathodoluminescence spectroscopy of diagenetic and hydrothermal dolomites: *Sedimentary Geology*, 140, p. 191–199.
- Given, R.K., and Wilkinson, B.H.,** 1985. Kinetic Control of Morphology, Composition, and Mineralogy of Abiotic Sedimentary Carbonates: *Journal of Sedimentary Research*, 55, p. 109-119.
- Godet, A., Durlet, C, Spangenberg, J.E., and Föllmi, K.B.,** 2016. Estimating the impact of early diagenesis on isotope records in shallow-marine carbonates: A case study from the Urgonian Platform in western Swiss Jura: *Palaeogeography, Palaeoclimatology, Palaeoecology*, 454, p. 125–138.
- Gramann, F., Heunish, C., Klassen, H., Kockel, F., Dulce, G., Harms, F.J., Katschorek, T., Mönnig, E., Schudack, M., Schudack, U., Thies, D., and Weiss, M.,** 1997. Das Niedersächsische Oberjura-Becken ---- Ergebnisse interdisziplinärer Zusammenarbeit: *Zeitschrift der Deutschen Geologischen Gesellschaft*, 148, p. 165-236.
- Gygi, R.A.,** 2000. Integrated stratigraphy of the Oxfordian and Kimmeridgian (Late Jurassic) in northern Switzerland and adjacent southern Germany: *Memoirs of the Swiss Academy of Sciences*, 104, p. 1–152.
- Gygi, R.A., Coe, A.L., and Vail, P.R.,** 1998. Sequence stratigraphy of the Oxfordian and Kimmeridgian stages (Late Jurassic) in northern Switzerland: *Special Publications of Society for sedimentary Geology*, 60, p. 527–544.
- Haq, B.U., Hardenbol, J., and Vail, P.R.,** 1987. Chronology of Fluctuating Sea Levels Since the Triassic: *Science*, 235, p.1156–1167.
- Hardenbol, J., Thierry, J., Farley, M.B., Jacquin, T., Graciansky, P.C, and Vail, P.,** 1998. Mesozoic and Cenozoic sequence chronostratigraphic framework of European basins. In: *Mesozoic*



- and Cenozoic Sequence Stratigraphy of European Basins (Graciansky, P.C., Hardenbol, J., Jacquin, T., Vail, P.R., eds.) Society for sedimentary Geology, Special Publication, 60, p. 3-13.
- Haslett, S.K.**, 1992. Rhaxellid sponge microscleres from the Portlandian of Dorset, UK: *Geological Journal*, 27, p. 339–347.
- Helm, C.**, 1998. Palaeokarst-Erscheinungen im Oberjura (Oxfordium, Dachfläche der florigemma-Bank, Korallenoolith, Hauptdiskontinuität) von NW-Deutschland (Süntel). *Ber. Naturhist. Ges. Hannover*, 140, p. 99-120.
- Helm, C.**, 2005. Riffe und fazielle Entwicklung der florigemma-Bank (Korallenoolith, Oxfordium) im Süntel und östlichen Wesergebirge (NW-Deutschland). Dissertation, Universität Hannover, p. 1-302.
- Helm, C., Reuter, and M., Schülke, I.**, 2003. Der Korallenoolith (Oberjura) im Osterwald (NW-Deutschland, Niedersächsisches Becken): Fazielle Entwicklung und Ablagerungsdynamik. *Zeitschrift der Deutschen Geologischen Gesellschaft*, 153, p. 159-186.
- Helm, C., and Schülke, I.**, 2006. Patch reef development in the florigemma-Bank Member (Oxfordian) from the Deister Mts (NW Germany): a type example for Late Jurassic coral thrombolite thickets: *Facies*, 52, p. 441–467.
- Heunisch, C., and Luppold, F.W.**, 2015. Mitteljura bis Unterkreide in den Bohrungen Eulenflucht 1 und Wendhausen 6-litho- und biostratigraphische Ergebnisse. In: *Neue Erkenntnisse zu Quartär, Jura und Unterkreide in Niedersachsen* (Fischer, K., Herrendorf, G., Heunisch, C., Luppold, F.W., Meinsen, J., Possin, W., Schwarz, C., and Thomas, M., eds). Landesamt für Bergbau, Energie und Geologie, Hannover, p. 40–69.
- Hofmann, H.J.**, 1976. Stromatoid morphometrics: *Developments in Sedimentology*, 20, p. 45-54.
- Homewood, P.W., Mauriaud, P., and Lafont, F.**, 2000. Best practices in sequence stratigraphy for explorationists and reservoir engineers: *Vade-mecum de stratigraphie séquentielle: pour géologues, géophysiciens et ingénieurs réservoir*. Elf EP-Éditions, Pau, France.
- Hoyer, P.**, 1965. Facies, Paläogeographie und Tektonik des Malm in Deister, Osterwald und Süntel: *Geol. Jb., Beih.* 61, p. 263.
- Hönig, M.R., John, C.M., and Manning, C.**, 2017. Development of an equatorial carbonate platform across the Triassic-Jurassic boundary and links to global palaeoenvironmental changes (Musandam Peninsula, UAE/Oman): *Gondwana Research*, 45, p. 100–117.
- Hughes, G.W.**, 2004. Middle to Upper Jurassic Saudi Arabian carbonate petroleum reservoirs: biostratigraphy, micropaleontology and palaeoenvironments: *GeoArabia*, 9, p. 79–114.
- Hyam, S.D., and Kamal, H.K.**, 2010. Stromatolites in the Barsarin formation, Barzinja area: *Iraqi Bulletin of Geology and Mining*, 6, p. 47-57.
- Ichikuni, M.**, 1973. Partition of strontium between calcite and solution: Effect of substitution by manganese: *Chemical Geology*, 11, p. 315–319.
- Jacquin, T., Dardeau, G., Durllet, C., de Graciansky, P.C., and Hantzpergue, P.**, 1998. The North Sea cycle: an overview of 2nd-order transgressive facies cycles in Western Europe. In: *Mesozoic and Cenozoic Sequence Stratigraphy of European Basins*(de Graciansky, P.C., Hardenbol,

J., Jacquin, T., Vail, P.R., eds.) Special Publications, Society for Sedimentary Geology, 60, p. 445–466.

**James, N. P., and Choquette, P. W.,** 1983. Diagenesis 6. Limestones — The sea floor diagenetic environment: *Geoscience Canada*, 10, p. 162-179.

**Jank, M., Meyer, C.A., and Wetzel, A.,** 2006. Late Oxfordian to Late Kimmeridgian carbonate deposits of NW Switzerland (Swiss Jura): Stratigraphical and palaeogeographical implications in the transition area between the Paris Basin and the Tethys: *Sedimentary Geology*, 186, p. 237–263.

**Kästner, M., Schülke, I., and Winsemann, J.,** 2008. Facies architecture of a Late Jurassic carbonate ramp: the Korallenoolith of the Lower Saxony Basin: *International Journal of Earth Sciences*, 97, p. 991–1011.

**Kästner, M., Schülke, I., Winsemann, J., and Böttcher, J.,** 2010. High-resolution sequence stratigraphy of a Late Jurassic mixed carbonate-siliciclastic ramp, Lower Saxony Basin, Northwestern Germany: *Zeitschrift der Deutschen Gesellschaft für Geowissenschaften*, 161, p. 263–283.

**Kerans, C., and Tinker, S.W.,** 1997. Sequence Stratigraphy and Characterization of Carbonate Reservoirs: *Society for Sedimentary Geology*, 40, p. 1-123.

**Ketzer, J.M.M.,** 2002. Diagenesis and Sequence stratigraphy. Dissertation, Uppsala University, p. 1-29.

**Kharaka, Y.K., Gunter, W.D., Aggarwal, P.K., Perkins, E.H., and Debraal, J.D.,** 1988. SOLMINEQ.88. A computer program for geochemical modeling of water-rock interactions: U.S.G.S. Water Resources Investigations Report, p. 88-4227.

**Klassen, H.,** 2003. Zur Entwicklungsgeschichte des nördlichen Osnabrücker Berglandes: *Osnabrücker Naturwissenschaftliche Mitteilungen*, 29, p. 13-44.

**Klein, R.T., Lohmann, K.C., and Thayer, C.W.,** 1996. Bivalve skeletons record sea-surface temperature and  $\delta^{18}\text{O}$  via Mg/Ca and  $^{18}\text{O}/^{16}\text{O}$  ratios: *Geology*, 24, p. 415-418.

**Kockel, F., Baldschuhn, R., and Frisch, U.,** 1996. Tectonic Atlas of NW-Germany: Federal Institute for Geosciences and Natural Resources, Hannover.

**Korngreen, D., and Benjamini, C.,** 2001. Upper Triassic reef facies in the Asher-Atlit-1 borehole, Northern Israel: Microfacies, cement stratigraphy and paleogeographic implications: *Facies* 45, p. 1–23.

**Kreisa, R.D., and Bambach, R.K.,** 1982. The Role of Storm Processes in Generating Shell Beds in Paleozoic Shelf Environments. In: *Cyclic and Event Stratification* (Einsele, G., and Seilacher, A., eds.) Springer Berlin Heidelberg, Berlin, Heidelberg, p. 200–207.

**Kumagai, T.,** 1978. Coprecipitation of manganese with calcium carbonate. *Bulletin of the Institute for Chemical Research, Kyoto University*, 56, p. 280-285.

**Lahann, R.W.,** 1978. A Chemical Model for Calcite Crystal Growth and Morphology Control. *Journal of Sedimentary Research*, 48, p. 337-344.

**Lathuiliere, B., Gaillard, C., Habrant, N., Bodeur, Y., Boullier, A., Enay, R., Hanzo, M., Marchand D., Thierry, J., and Werner, W.,** 2005. Coral zonation of an Oxfordian reef tract in the northern French Jura: *Facies*, 50, p. 545–559.

- Lear, C.H., Rosenthal, Y., and Slowey, N.,** 2002. Benthic foraminiferal Mg/Ca-paleothermometry: a revised core-top calibration: *Geochimica et Cosmochimica Acta*, 66, p. 3375–3387.
- Leinfelder, R.R., Nose, M., Schmid, D.U., and Werner, W.,** 1993. Microbial crusts of the late jurassic: Composition, palaeoecological significance and importance in reef construction: *Facies*, 29, p. 195–229.
- Leinfelder, R.R., Werner, W., Nose, M., Schmid, D.U., Krautter, M., Laternser, R., Takacs, M., and Hartmann, D.,** 1996. Paleoecology, Growth Parameters and Dynamics of Coral, Sponge and Microbiolite Reefs from the Late Jurassic: *Göttinger Arb. Geolo.Paläont*, p. 227-248.
- Lorens, R.B.,** 1978. A study of biological and physical controls on the trace metal content of calcite and aragonite. Dissertation, University of Rhode Island, Kingston, R.I., p. 405.
- Lorens, R.B.,** 1981. Sr, Cd, Mn and Co distribution coefficients in calcite as a function of calcite precipitation rate: *Geochimica et Cosmochimica Acta*, 45, p. 553–561.
- Lutze, G.F., and Wolf, R.,** 1976. Persian gulf foraminifera, depth distribution and sea-level change: First International Symposium on Benthonic Foraminifera of Continental Margins. Halifax, Canada, Part B, p. 425-429.
- Machel, H.G.,** 2000. Application of cathodoluminescence to carbonate diagenesis. In: *Cathodoluminescence in Geosciences* (Pagel, M., Barbin, V., Blanc, P., Ohnenstetter, D., eds.), Springer Berlin Heidelberg, Berlin, Heidelberg, p. 271-302.
- McIntire, W.L.,** 1963. Trace element partition coefficients—a review of theory and applications to geology: *Geochimica et Cosmochimica Acta*, 27, p. 1209–1264.
- Medwedeff, D.A., and Wilkinson, B.H.,** 1983. Cortical fabrics in calcite and aragonite ooids. In: *Coated Grains*(Peryt, T.M., ed) Springer Berlin Heidelberg, Berlin, Heidelberg, p. 109-115.
- Melim, L.A., Swart, P.K., and Maliva, R.G.,** 2001. Meteoric and marine burial diagenesis in the subsurface of the Great Bahama Bank. In: *Subsurface Geology of a Prograding Carbonate Platform margin, Great Bahama Bank*(Ginsburg, R.N., Ed.) Special Publications, 70, p. 137-162.
- Melim, L.A., Westphal, H., Swart, P.K., Eberli, G.P., and Munnecke, A.,** 2002. Questioning carbonate diagenetic paradigms: evidence from the Neogene of the Bahamas: *Marine Geology*, 185, p. 27–53.
- Meyers, W.J.,** 1974. Carbonate Cement Stratigraphy of the Lake Valley Formation (Mississippian) Sacramento Mountains, New Mexico: *Journal of Sedimentary Research*, 44, p. 837-861.
- Michard, C.D.,** 1968, Coprecipitation de L'ion maganeux avec le carbonate de calcium: *Comptes Rendus Acad. Sci. Paris, ser. D*, 267, p. 1685-1688.
- Mönnig, E.,** 2005. Der Jura von Norddeutschland in der Stratigraphischen Tabelle von Deutschland 2002: *Newsletters on Stratigraphy*, 41, p. 253–261.
- Morad, S., Ketzer, J.M., and De Ros, L.F.,** 2000. Spatial and temporal distribution of diagenetic alterations in siliciclastic rocks: implications for mass transfer in sedimentary basins: *Sedimentology*, 47, p. 95–120.
- Morad, S., Ketzer, J.M., and De Ros, L.F.,** 2012. Linking diagenesis to sequence stratigraphy: An Integrated Tool for Understanding and Predicting Reservoir Quality Distribution. *International Association of Sedimentologists, Special Publication*, 45, p. 1-36.

- Mouchi, V., de Rafélis, M., Lartaud, F., Fialin, M., and Verrecchia, E.P.,** 2013. Chemical labelling of oyster shells used for time-calibrated high-resolution Mg/Ca ratios: A tool for estimation of past seasonal temperature variations: *Palaeogeography, Palaeoclimatology, Palaeoecology*, 373, p. 66–74.
- Mucci, A.,** 1988. Manganese uptake during calcite precipitation from seawater: Conditions leading to the formation of a pseudokutnahorite: *Geochimica et Cosmochimica Acta*, 52, p. 1859–1868.
- Nagy, J., Dypvik, H., and Bjaerke, T.,** 1984. Sedimentological and paleontological analysis of Jurassic north sea deposits from deltaic environments: *Journal of Petroleum Geology*, 7:169–187.
- Nagy, J., Hess, S., and Alve, E.,** 2010. Environmental significance of foraminiferal assemblages dominated by small-sized *Ammodiscus* and *Trochammina* in Triassic and Jurassic delta-influenced deposits: *Earth-Science Reviews*, 99, p. 31–49.
- Neuser, R.D.,** 1988. Zementstratigraphie und Kathodolumineszenz des Korallenooliths (Malm) im Siidnieders~ichsischen Bergland. *Bochumer Geol. Geotechn. Arb.*, 32, p. 172.
- Nunn, E.V., and Price, G.D.,** 2010. Late Jurassic (Kimmeridgian–Tithonian) stable isotopes ( $\delta^{18}\text{O}$ ,  $\delta^{13}\text{C}$ ) and Mg/Ca ratios: New palaeoclimate data from Helmsdale, northeast Scotland: *Palaeogeography, Palaeoclimatology, Palaeoecology*, 292, p. 325–335.
- Nunn, E.V., Price, G.D., Hart, M.B., Page, K.N., and Leng, M.J.,** 2009. Isotopic signals from Callovian–Kimmeridgian (Middle–Upper Jurassic) belemnites and bulk organic carbon, Staffin Bay, Isle of Skye, Scotland: *Journal of the Geological Society*, 166, p. 633–641.
- O'Brien, G.W., Milnes, A.R., and Veeh, H.H., Heggie, D. T., Riggs, S. R., Cullen, D. J., Marshall, J. F., and Cook, P. J.,** 2011. Sedimentation dynamics and redox iron-cycling: controlling factors for the apatite-glaucconite association on the East Australian continental margin. In: *Phosphorite Research and Development*(Notholt, A. J. G., and Jarvis, I., eds.) special publications, Geology society, London, 52, p. 61-86.
- Ogg, J.G., and Hinnov, L.A., and Huang, C.,** 2012. Jurassic. In: *The Geologic Time Scale* (Gradstein, F.M., Ogg, J.G., Schmitz, M.D., and Ogg, G.M., eds.) Oxford, 1, p. 731–791.
- Opdyke, B.N., and Wilkinson, B.H.,** 1990. Paleolatitude distribution of Phanerozoic marine ooids and cements: *Palaeogeography, Palaeoclimatology, Palaeoecology*, 78, p. 135–148.
- O'Reilly, S.S., Mariotti, G., Winter, A.R., Newman, S.A., Matys, E.D., McDermott, F., Pruss, S.B., Bosak, T., Summons, R.E., and Klepac-Ceraj, V.,** 2017. Molecular biosignatures reveal common benthic microbial sources of organic matter in ooids and grapestones from Pigeon Cay, The Bahamas: *Geobiology*, 15, p. 112–130.
- Padden, M., Weissert, H., and Rafelis, M.,** 2001. Evidence for Late Jurassic release of methane from gas hydrate: *Geology*, 29, p. 223-226.
- Pierson, B.J.,** 1981. The control of cathodoluminescence in dolomite by iron and manganese: *Sedimentology*, 28, p. 601–610.
- Pieńkowski, G., Schudack, M.E., and Bosák, P., Enay, R., Feldman-Olszewska, A., Golonka, J., Gutowski, J., Hengreen, G. F. W., Jordan, P., Krobicki, M., Lathuiliere, B., Leinfelder, R. R., Michalík, J., Mönnig, E., Noe-Nygaard, N., Pálffy, J., Pint, A., Rasser, M. W., Reisdorf, A G., Schmid, D.U., Schweigert, G., Surlyk, F., Wetzell, A., Wong, T. E.,** 2008. Jurassic. In: *The*

geology of central Europe volume 2: Mesozoic and Cenozoic (McCann, T., ed). Geological Society, London, p. 823-922.

**Pingitore, N.E., Eastman, M.P., Sandidge, M., Oden, K., and Freiha, B.,** 1988. The coprecipitation of manganese(II) with calcite: an experimental study: *Marine Chemistry*, 25, p. 107–120.

**Pisera, A.,** 1997. Upper Jurassic siliceous sponges from the Swabian Alb: taxonomy and paleoecology: *Palaeotologia Polonica*, 57, p. 1-216.

**Pittet, B., and Strasser, A.,** 1998. Long-distance correlations by sequence stratigraphy and cyclostratigraphy: examples and implications (Oxfordian from the Swiss Jura, Spain, and Normandy): *Geologische Rundschau*, 86, p. 852–874.

**Pittet, B., Strasser, A., and Mattioli, E.,** 2000. Depositional Sequences in Deep-Shelf Environments: A Response to Sea-Level Changes and Shallow-Platform Carbonate Productivity (Oxfordian, Germany and Spain): *Journal of Sedimentary Research*, 70, p. 392–407.

**Price, G.D., and Rogov, M.A.,** 2009. An isotopic appraisal of the Late Jurassic greenhouse phase in the Russian Platform: *Palaeogeography, Palaeoclimatology, Palaeoecology*, 273, p. 41–49.

**Podlaha, O.G., Mutterlose, J., and Veizer, J.,** 1998. Preservation of delta 18 O and delta 13 C in belemnite rostra from the Jurassic/Early Cretaceous successions: *American Journal of Science*, 298, p. 324–347.

**Pomoni-Papaioannou, F.,** 2008. Facies analysis of Lofer cycles (Upper Triassic), in the Argolis Peninsula (Greece): *Sedimentary Geology*, 208, p. 79–87.

**Rais, P., Louis-Schmid, B., Bernasconi, S.M., and Weissert, H.,** 2007. Palaeoceanographic and palaeoclimatic reorganization around the Middle–Late Jurassic transition: *Palaeogeography, Palaeoclimatology, Palaeoecology*, 251, p. 527–546.

**Reid, R.E.H.,** 1968. Bathymetric distributions of *Calcarea* and *Hexactinellida* in the Present and in the past: *Geological Magazine*, 105, p. 546-559.

**Riboulleau, A., Baudin, F., Daux, V., Hantzpergue, P., Renard, M., and Zakharov, V.,** 1998. Sea surface paleotemperature evolution of the Russian platform during the Upper Jurassic. *Comptes Rendus de la Academie des Sciences Serie II Fascicule A—Sciences de la Terre et des Planetes*, 326, p. 239–246.

**Richter-Bernburg, G.,** 1985. Zechstein-Anhydrite–Fazies und Genese. *Geologisches Jahrbuch Reihe A*, 85, p. 3–82.

**Roller, R.A., and Stickle, W.B.,** 1985. Effects of salinity on larval tolerance and early developmental rates of four species of echinoderms: *Canadian Journal of Zoology*, 63, p.1531–1538.

**Ruf, M., Link, E., Pross, J., and Aigner, T.,** 2005a. Integrated sequence stratigraphy: Facies, stable isotope and palynofacies analysis in a deeper epicontinental carbonate ramp (Late Jurassic, SW Germany): *Sedimentary Geology*, 175, p. 391-414.

**Ruf, M., Link, E., Pross, J., and Aigner, T.,** 2005b. A multi-proxy study of deeper-water carbonates (Upper Jurassic, southern Germany): combining sedimentology, chemostratigraphy and palynofacies: *Facies*, 51, p. 327–349.

- Samankassou, E., Di Gioia, E., Strasser, A.,** 2003. High-resolution record of lateral facies variations on a shallow carbonate platform (Upper Oxfordian, Swiss Jura Mountains): *Eclogae Geologicae Helvetiae*, 96, p. 425-440.
- Scholle, P.A., and Ulmer-Scholle, D.S.,** 2003. A color guide to the petrography of carbonate rocks: grains, textures, porosity, diagenesis. American Association of Petroleum Geologists, Tulsa, 77, p. 1-486.
- Schmid, D.U.,** 1996. Marine Mikrobolithe und Mikroinkrustierer aus dem Oberjura. Dissertation, University of Stuttgart, p. 101-251.
- Schudack, U.,** 1994. Revision, Dokumentation und Stratigraphie der Ostracoden des Nordwestdeutschen Oberjura und Unter-Berriasium. Selbstverlag Fachbereich Geowissenschaften, FU , Berlin, p. 1-192.
- Schulze, K-H.,** 1975. Mikrofazielle, geochemische und technologische Eigenschaften von Gesteinen der Heersumer Schichten und des Korallenoolith (Mittleres und Oberes OxfordianNWDdeutschlands) zwischen Weser und Leine. *Geol. Jb, D 11*,p. 3–102.
- Shen, J., and Kawamura, T.,** 2001. Guadalupian algae-sponge reefs in siliciclastic environments—the reefs at Lengwu (South China) compared with the reef at Iwaizaki (Japan): *Facies*, 45, p. 137–156.
- Simonsen, J.M., and Friedman, G.M.,** 1992. Closely spaced twin lamellae in limestones as an indicator of deep-burial diagenesis: *Carbonates Evaporites*, 7, p. 38–47.
- Sneider, J.S., Clarens, P., and de, Vail, P.R.,** 1995. Sequence stratigraphy of the middle to upper jurassic, viking graben, north sea. In: *Norwegian Petroleum Society Special Publications*, 5, p. 167–197.
- South, D.L. and Talbot, M.R.** 2000. The sequence stratigraphic framework of carbonate diagenesis within transgressive fan-delta deposits: Sant Llorenç del Munt fandelata complex, SE Ebro Basin, NE Spain: *Sedimentary Geology*, 138, p. 179–198.
- Srinivasan, K.,** 1993. Depositional History, Sequence Stratigraphy and Diagenesis of the Maryville Limestone (Middle Cambrian) Southern Appalachians. Dissertation, University of Tennessee, p. 1-166.
- Strasser, A.,** 1986. Ooids in Purbeck limestones (lowermost Cretaceous) of the Swiss and French Jura: *Sedimentology*, 33, p. 711-727.
- Strasser, A., Pittet, B., Hillgärtner, H., and Pasquier, J.-B.,** 1999. Depositional sequences in shallow carbonate-dominated sedimentary systems: concepts for a high-resolution analysis: *Sedimentary Geology*, 128, p. 201–221.
- Strasser, A., Hillgartner, H., Hug, W., and Pittet, B.,** 2000. Third-order depositional sequences reflecting Milankovitch cyclicity: *Terra Nova*, 12, p. 303–311.
- Strohmenger, C., and Strauss, C.,** 1996. Sedimentology and palynofacies of the Zechstein 2 Carbonate (Upper Permian, Northwest Germany): implications for sequence stratigraphic subdivision: *Sedimentary Geology*, 102, p. 55–77.
- Suess, E., and Fütterer, D.,** 1972. Aragonitic ooids: experimental precipitation from seawater in the presence of humic acid: *Sedimentology*, 19, p. 129-139.

- Swart, P.K.**, 2015. The geochemistry of carbonate diagenesis: The past, present and future: *Sedimentology*, 62, p. 1233–1304.
- Thierry, J.**, 2000. Early Kimmeridgian. Map 10. In: *Atlas Peri-Tethys. Palaeogeographical Maps*, Leeds, p. Palaeogeographical Maps (Dercourt J, Gaetani M, Vrielynck B, Barrier E, Biju-Duval B, Brunet MF, Cadet JP, Crasquin S, Sandulescu M eds)
- Townson, W.G.**, 1975. Lithostratigraphy and deposition of the type Portlandian: *Journal of the Geological Society*, 131, p. 619 - 638.
- Tucker, M.E.** 1993. Carbonate diagenesis in a sequence stratigraphic framework. In: *Sedimentology Review* (Wright. V.P., Ed.), Blackwell, Oxford, p. 51- 72.
- Vackiner, A.A., and Kukla, P.A.**, 2013. Sedimentary facies reconstruction and kinematic restoration of tight gas fields. Springer Berlin Heidelberg, Berlin, Heidelberg, p. 1-123.
- Walker, G., Abumere, O.E., and Kamaluddin, B.**, 1989. Luminescence spectroscopy of Mn<sup>2+</sup> centres in rock forming carbonates: *Mineralogical Magazine*, 53, p. 201-211.
- Weiss, M.**, 1995. Stratigraphie und Mikrofauna im Kimmeridge SE-Niedersachsens unter besonderer Berücksichtigung der Ostracoden. Dissertation, Technischen Universität Clausthal, p. 1-239.
- Weissert, H.**, 2011. Mesozoic Pelagic Sediments: Archives for Ocean and Climate History during Green-House Conditions: *Developments in Sedimentology*, 63, p. 765-792.
- Weissert, H., and Mohr, H.**, 1996. Late Jurassic climate and its impact on carbon cycling: *Palaeogeography, Palaeoclimatology, Palaeoecology*, 122, p. 27–43.
- Wierzbowski, H.**, 2002. Detailed oxygen and carbon isotope stratigraphy of the Oxfordian in Central Poland: *International Journal of Earth Sciences*, 91, p. 304-314.
- Wierzbowski, H.**, 2004. Carbon and oxygen isotope composition of Oxfordian–Early Kimmeridgian belemnite rostra: palaeoenvironmental implications for Late Jurassic seas: *Palaeogeography, Palaeoclimatology, Palaeoecology*, 203, p. 153–168.
- Wierzbowski, A., Coe, A.L., Hounslow, M.W., Matyja, A.M., Ogg, J.G., Page, K.N., Wierzbowski, H., and Wright, J.K.**, 2006. A potential stratotype for the Oxfordian/Kimmeridgian boundary: Staffin Bay, Isle of Skye UK. *Volumina Jurassica*, 4, p. 17–33.
- Wierzbowski, H., Rogov, M.A., Matyja, B.A., Kiselev, D., and Ippolitov, A.**, 2013. Middle–Upper Jurassic (Upper Callovian–Lower Kimmeridgian) stable isotope and elemental records of the Russian Platform: Indices of oceanographic and climatic changes. *Global and Planetary Change*, 107, p. 196–212.
- Wilson, J.I.**, 1975. *Carbonate Facies in Geological History*: Springer New York, p. 1-471.
- Worden, R.H., and Morad, S.**, 2003. Clay minerals in sandstones: controls on formation, distribution and evolution, In: *Clay Mineral Cements in Sandstones* (Worden, R.H., and Morad, S., Eds) International Association of Sedimentologists, Special Publication, 34, p. 1–41.
- Worden, R.H., Ruffell, A.H. and Cornford, C.** 2000. Paleoclimate, sequence stratigraphy and diagenesis: *Journal of Geochemical Exploration*, 69–70, p. 453–457.

**Wong, T.E., Batjes, D.A.J., Jager, J. de., (eds)** 2007. Geology of the Netherlands. Edita-KNAW, Amsterdam.

**Yang, Y.H., Wu, F.Y., Wilde, S.A., Liu, X.M., Zhang, Y.B., Xie, L.W., and Yang, J.H.,** 2009. In situ perovskite Sr–Nd isotopic constraints on the petrogenesis of the Ordovician Mengyin kimberlites in the North China Craton: *Chemical Geology*, 264, p. 24-42.

**Yang, Y.H., Wu, F.Y., Yang, J.H., Chew, D.M., Xie, L.W., Chu, Z.Y., Zhang, Y.B., and Huang, C.,** 2014. Sr and Nd isotopic compositions of apatite reference materials used in U–Th–Pb geochronology: *Chemical Geology*, 385, p. 35-55.

**Ziegler, P.A.,** 1990. Geological atlas of Western and Central Europe. In: Shell Internationale Petroleum Maatschappij B.V, Geological Society of London.